8-2007

Novel Approaches to Metal Ion Sensing

Nathan Allen Carrington
University of Tennessee - Knoxville

To the Graduate Council:

I am submitting herewith a dissertation written by Nathan Allen Carrington entitled "Novel Approaches to Metal Ion Sensing." I have examined the final electronic copy of this dissertation for form and content and recommend that it be accepted in partial fulfillment of the requirements for the degree of Doctor of Philosophy, with a major in Chemistry.

<div align="right">Ziling Xue, Major Professor</div>

We have read this dissertation and recommend its acceptance:

Jamie L. Adcock, Michael J. Sepaniak, Vincent A. Anfara, Jr.

<div align="right">Accepted for the Council:</div>

<div align="right">Carolyn R. Hodges</div>

<div align="right">Vice Provost and Dean of the Graduate School</div>

(Original signatures are on file with official student records.)

To the Graduate Council:

I am submitting herewith a dissertation written by Nathan Allen Carrington entitled "Novel Approaches to Metal Ion Sensing." I have examined the final electronic copy of this dissertation for form and content and recommend that it be accepted in partial fulfillment of the requirements for the degree of Doctor of Philosophy, with a major in Chemistry.

<div style="text-align:right">

Ziling (Ben) Xue
Major Professor

</div>

We have read this dissertation
and recommend its acceptance:

Jamie L. Adcock

Michael J. Sepaniak

Vincent A. Anfara, Jr.

<div style="text-align:center">

Accepted for the Council:

Carolyn R. Hodges
Vice Provost and Dean of the
Graduate School

(Original Signatures are on file with official student records)

</div>

NOVEL APPROACHES TO METAL ION SENSING

A Dissertation

Presented for the

Doctor of Philosophy Degree

The University of Tennessee, Knoxville

Nathan Allen Carrington

August 2007

DEDICATION

This dissertation is dedicated to my wife

and parents, who have lovingly supported

and guided me throughout the years.

ACKNOWLEDGEMENTS

willingness to help and for not wearing Ohio State and Cleveland Brown sweatshirts too much.

In addition, I have made several friends in the department here that have made my time at UT very worthwhile. They include but are not limited to: Peter Chapman, Kasey Hill, Amber Wellman, Maggie Connatser, Jenny Oran, Pampa Dutta, Joe Long, Fabrice Gritti, Khaled, Josh Abbott, MP, AP, Caleb Dyer, Brent Magnusson, Clarissa Tatum, Brian Bachner, Peter Yaron, Sami Channaa, Jeremiah Harden, and Matt Smith. I also need to thank Marco DeJesus and Kathleen Giesfeldt for exposing me to their instrumental operator positions and the early training they provided on many of the departmental instruments.

Finally, I owe an enormous debt to my family. My parents have always believed in me and challenged me to do my best, and any portion of my success can be directly attributed to their positive influence. They have always been there for me, and I cannot thank them enough. My sister, Natalie, has also been a great encouragement during my graduate school career, and I am thankful for her. Lastly, my wife, Sara, has made this entire journey possible. She has been devoted to me since before I even came here to UT, and I can never thank her enough for her love and support. She has encouraged and been there for me during the difficult and trying times, and anything that I have accomplished has taken place because she is by my side. I could devote an endless amount of pages in her honor, but I hope it is sufficient to say that I love her and that she has made this entire process worthwhile.

ABSTRACT

The primary focus of this dissertation is the development of new chemical analyses for metal ions. Approaches combining electrochemical, spectroscopic, analytical, inorganic, and materials chemistry have been used to investigate novel methods for metal ion sensing. Topics discussed in this dissertation include pyridinium-functionalized sol-gel films for the enhanced electrochemical analysis of Cr(VI), pyridinium-functionalized sol-gel monoliths for the optical determination of Cr(VI), the use of the electrochemical quartz crystal microbalance for the determination of Pd(II), novel electrochemical and spectroscopic approaches to Fe(III) sensing, and the electrochemical quartz crystal microbalance investigation of the Cr(III)-DTPA complex.

TABLE OF CONTENTS

LIST OF TABLES

LIST OF FIGURES

NOMENCLATURE AND ABBREVIATIONS

A	absorbance, surface area of the electrode
A	amps
a	absorptivity
Å	angstrom
AA	atomic absorption
AE	atomic emission
AOP	Advanced Oxidation Process
b	path length
BET	Brunauer-Emmett-Teller
°C	degrees Celcius
c	concentration
C_f	collective term for quartz crystal properties
cm	centimeter
CV	cyclic voltammetry
DI	deionized
DTPA	diethylenetriaminepentaacetic acid
e^-	electron
E_b	binding energy of an electron
E_k	kinetic energy of a displaced electron
ESCA	electron spectroscopy for chemical analysis
EQCM	electrochemical quartz crystal microbalance

eV	electron Volt
F	Faraday's constant
f_0	resonant frequency of the fundamental mode of the crystal
g	gram
h	hour
$h\upsilon$	incident photon energy
Hz	hertz
ICP-MS	inductively coupled plasma mass spectrometry
ITO	indium-tin oxide
L	liter
m	meter
mm	millimeter
mM	millimolar
M	molar
M^+	metal ion
MΩ	megohm
mA	milliamps
min	minute
mg	milligram
MHz	megahertz
min	minute
mL	milliliter
mtorr	millitorr

n	number of electrons involved in an electrode reaction
N	number of moles of electrolyzed species
nm	nanometer
ppb	parts per billion
ppm	parts per million
ppt	parts per trillion
Q	amount of charge
QCM	quartz crystal microbalance
R^2	square of correlation coefficient
s	second
SEM	scanning electron microscopy
SWV	square-wave voltammetry
t	time
TIBC	total iron binding capacity
UV-vis	ultraviolet-visible
V	volts
V	volume
w	work function of the spectrometer
XPS	X-ray photoelectron spectroscopy
Δf	measured frequency shift
Δm	mass change
μ	shear modulus of quartz
μA	microamps

μg	microgram
μL	microliter
μm	micrometer
ρ	density of quartz

Part 1

Introduction and Background

1.1. Foreword

Chemical sensors are of intense current interest.[1] Whether relying on optical, electrochemical, mass-sensitive, or spectroelectrochemical modes of operation, sensors have been developed to monitor everything from halitosis[2] to halogenated hydrocarbons.[3,4] Our research has focused on the development of sensors for the monitoring of metals in complex sample matrices. Preliminary work[5] in this area involved the Advanced Oxidation Process (AOP), a sample pre-treatment method that uses a combination of hydrogen peroxide and UV light to decompose organic ligands in metal complexes that interfere with measurements. Such studies showed that, through the use of AOP, metals in complex matrices, such as catalytic waste and blood, could be measured. While AOP is effective in removing organic interferents from sample matrices, new methods of detecting the metals, often present at low concentrations, were necessary. This dissertation outlines new methods for the determination of various metal ions. These methods can either be coupled with the Advanced Oxidation Process for the analysis of metals in complex sample matrices, or they can be used alone as methods for metal analyses in aqueous solutions.

1.2. Analysis Techniques Used in the Research Studies

1.2.1. Electrochemical Techniques

Cyclic voltammetry (CV) and square-wave voltammetry (SWV) are two electrochemical techniques often used in the research presented in this

dissertation. In cyclic voltammetry, a potential is first varied linearly until it reaches a set potential, known as the switching potential, whereupon the scan is reversed until the potential returns to its original value. Switching potentials are often chosen so that the oxidation or reduction of one or many of the analytes present takes place within their range. The direction of the initial scan can either be in the negative or positive directions, and often times several cycle scans are repeated in sequence. Cyclic voltammetry is primarily used as a tool in fundamental and diagnostic studies to provide qualitative information about various electrochemical processes.[6]

Square-wave voltammetry is a type of pulse voltammetry that offers high sensitivity. In this method, the current generated from a short (usually around 5 ms) reverse pulse is subtracted from the current generated by an equally short forward pulse. A series of these pulses is collected throughout the desired potential range, and the differences in the currents are plotted to give the voltammogram. When electroactive species are present, the potential of the peak generated corresponds to the half-wave potential, and the peak height is proportional to the concentration of the analyte. Besides a sensitivity enhancement, SWV also is advantageous in that it is a fast technique and is not affected by dissolved species that may interfere with the analytical signal.[6,7]

1.2.2. Absorption Spectroscopy

Two forms of absorption spectroscopy used in the presented research are UV-visible spectroscopy and atomic absorption spectroscopy. Both of these

techniques rely on Beer's law (Eq. 1.1) for quantitative measurements of concentration.

$$A = abc \qquad\qquad \text{(Eq. 1.1)}$$

where A is absorbance, a is a proportionality constant called the absorptivity, b is the path length through the medium, and c is the concentration of the absorbing species.

Beer's law shows that there is a linear relationship between absorbance and concentration. This allows for the constructing of calibration plots so that unknown analyte concentrations can be determined. Deviations from Beer's law occur when high concentrations are analyzed and when stray radiation is present.[6,8]

For experiments involving UV-vis, two different types of instruments, a dual beam scanning and a diode array, were used. The diode array instrument was advantageous in that it could obtain scans from 200 to 800 nm in less than one second. The scanning instrument was used when improved sensitivity was needed, as it is capable of providing higher resolution measurements than the diode array spectrometer due to the fact that its scan speed can be adjusted. Atomic absorption measurements were collected when the concentration of ppm levels of metals in solutions needed to be determined.

1.2.3. The Quartz Crystal Microbalance

The Quartz Crystal Microbalance (QCM) is a variant of acoustic wave microsensors that are capable of ultra-sensitive measurements. The crystal oscillates in a shear mode under the influence of a high frequency AC electric field which is applied across the thickness of the crystal. The crystal undergoes distortion, and oscillates at a set frequency. Upon sorption or electrodeposition of an analyte, there is a frequency drop. This frequency drop can be directly correlated to the mass deposited on the crystal, using the Sauerbrey equation (Eq. 1.2).[7,9]

$$\Delta f = \frac{-2 f_0^2}{A \sqrt{\mu \rho}} \Delta m \qquad\qquad \text{(Eq. 1.2)}$$

where Δf = measured frequency shift, f_0 = resonant frequency of the fundamental mode of the crystal, Δm = mass change (g), A = surface area of the electrode (cm^2), ρ = density of quartz (2.648 g cm^{-3}), and μ = shear modulus of quartz (2.947 $\times$ 10^{11} g cm^{-1} s^{-2}).

In this equation, the direct correlation between change in mass and frequency can be seen. An increase in mass will give a frequency decrease, and vice versa. The other parameters in this equation are dependent on the crystal itself. Typically, these terms are collected together as C_f.[7,9]

5

When an electrochemical quartz crystal microbalance (EQCM) is employed, an analyte reaches the surface of the quartz crystal by electrodeposition. In these experiments, the crystal serves as the working electrode. Figure 1.1 shows a schematic of the operation of an EQCM. Initially, a negative potential is applied. Electrons flow from the working electrode, and reduce the species to a metal. It plates out on the surface of the crystal, giving a negative change in frequency. In order to remove the metal from the crystal, a reverse potential is applied, and the species can be stripped back off, giving a positive change in frequency. This method is well-suited for applications in sensing trace metals, since regenerating the sensor is quite easy and requires little time. However, it can also be used to monitor the growth of other species, such as sol-gels.

1.2.4. Scanning Electron Microscopy

Scanning electron mictroscopy (SEM) is an imaging technique used to characterize the sol-gels prepared and reported in this dissertation. This technique is capable of providing magnifications of 10 to 100,000x and can resolve features down to the nanometer scale.[10] The method operates by scanning the electron probe across the surface of a specimen in synchronism with the electron beam produced from a separate cathode-ray tube. The image results from the modulation of the cathode-ray tube intensity by one of the signals recorded. Scan coils are used to control the electron beam, and the scan coil current can be increased or decreased to control the magnification while
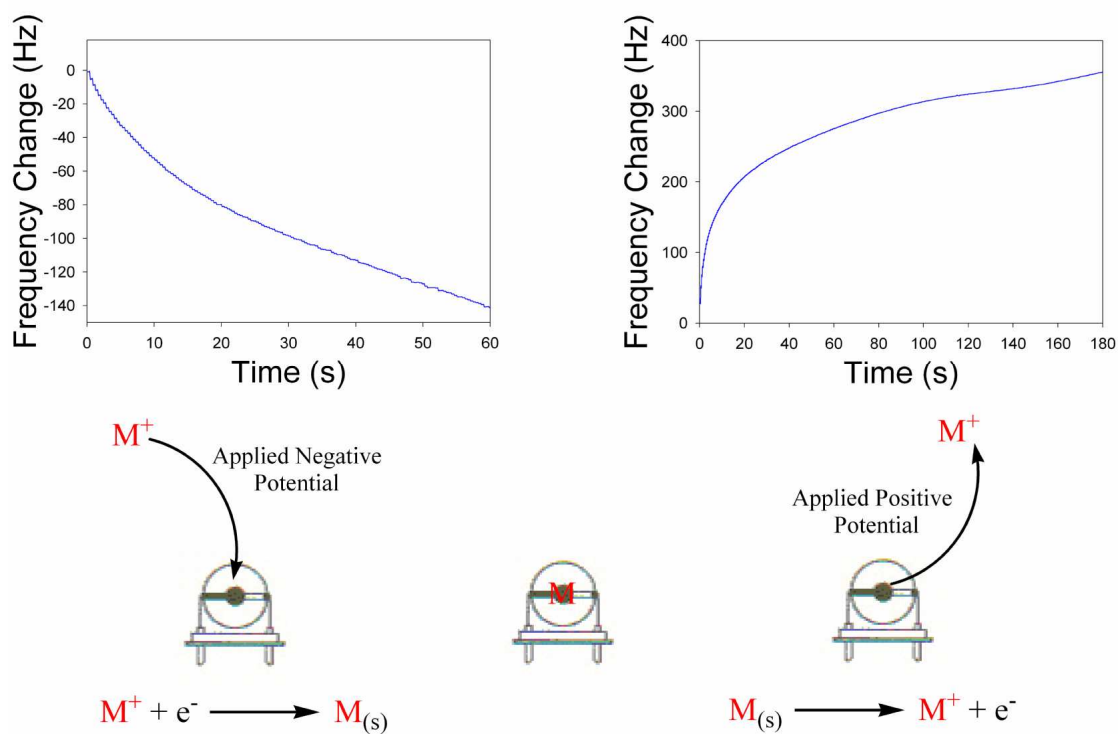
Figure 1.1. Schematic of the operation of the electrochemical quartz crystal microbalance.

keeping the image size on the cathode-ray tube constant. It is also possible to control the penetration depth of the electrons by choosing the electron energy.[11]

1.2.5. X-ray Photoelectron Spectroscopy

X-ray Photoelectron Spectroscopy (XPS) is a technique that provides information about atomic composition, structure, and oxidation state. Also known as electron spectroscopy for chemical analysis (ESCA), this method has a variety of applications, although its most important contributions involve the analysis of surfaces.[6,7,12,13] In XPS, a photon of a monochromatic X-ray beam is absorbed typically by a K or L inner electron of a sample atom (K corresponds to n=1, L corresponds to n=2), although, in principal, all electrons can be studied. This electron is then displaced, and it has an identifiable kinetic energy. This energy can be measured by an electron spectrometer. From Eq. 1.3, the binding energy of the electron (E_b) can be calculated using the known values of the incident photon energy (hν), the kinetic energy of the displaced electron (E_k), and the work function (w) of the spectrometer, a factor that accounts for the electrostatic environment of the electron. This binding energy is characteristic of the atom and orbital from which it was emitted, and, as a result, it can be used to determine the identity of the sample.[6,7,13]

$$E_b = h\nu - E_k - w \qquad \text{(Eq. 1.3)}$$

1.2.6. Brunauer-Emmett-Teller Gas Adsorption Analysis

The Brunauer-Emmett-Teller (BET) method is a commonly used procedure for the determination of the surface area, pore volume, and pore size distribution of solid materials. By using a series of BET equations based on the amount of N_2 vapor that is adsorbed by a sample, the total pore volume can be calculated. Based upon this pore volume, the average pore size can be determined, and the pore size distribution is determined by the pore size with respect to the disbursement of the pore volume. A sharp peak in a plot of pore volume versus average pore diameter indicates a narrow pore size distribution, indicating relatively uniform pore sizes throughout the bulk of the material. Pores can be categorized based on their diameters, with micropores being less than 20 Å, mesopores between 20 and 500 Å, and macropores greater than 500 Å. In addition, BET measurements can produce an isotherm plot, a plot of the total volume adsorbed versus the relative pressure. There are six distinct types of isotherm plots, and these are used to classify samples based on their porosity, surface area, and other surface features.[14]

1.3. *Sol-gels and Their Use in Sensing*

First reported some 150 years ago, the sol-gel process refers to a multitude of reactions using alkoxide precursors to prepare solid products such as glasses and ceramic oxides.[15-17] In this process, an alkoxide precursor, such as $Si(OR)_4$, is hydrolyzed. The resulting silanols undergo condensation to form a cross-linked inorganic matrix that is subsequently dried to form a three-

dimensional porous glass. These sol-gel reactions, summarized in Figure 1.2, are profoundly affected by many factors, such as the size of the alkoxide ligand, solution pH, types and concentrations of solvents, temperature, and catalysts.[15-18] These factors drastically impact the structure development and subsequent properties of the gels and thus may be adjusted to tailor materials for specific needs. For example, surfactants are used to reduce surface tension, increase the specific surface area, prevent fracture, and stabilize smaller particles. By incorporating cross-linking agents, specific areas of the gels are increased.[19] Catalysts are often used in sol-gel reactions to enhance the hydrolysis rate. Acid-catalyzed reactions result in dense gels with low pore volume and small pore size, while base-catalyzed reactions give low-density gels with high pore volume and large pore size.[15,20] Aging is also a critical step, as it ensures complete polycondensation and increases the gel strength. By carefully tailoring these variables, sol-gel materials have been produced for numerous applications, including electronics, optics, separation technology, catalysis, and sensing.[15,20]

There are many properties of sol-gels that make them particularly attractive for use in sensing applications. Sol-gels are compatible with numerous chemical agents, making possible the incorporation of sensing elements onto sol-gel substrates. Since little or no heating is required during the sol-gel process, thermally sensitive organic molecules have been encapsulated within the gel interiors without degradation.[21] This encapsulation is usually accomplished using either doping or grafting processes to give organofunctional sol-gel materials. Doping involves the physical entrapment of a reagent inside the substrate, while

Hydrolysis

$$\equiv\text{Si}-\text{OR} \quad + \quad \text{H}_2\text{O} \quad \rightleftharpoons \quad \equiv\text{Si}-\text{OH} \quad + \quad \text{ROH}$$

Condensation

$$\equiv\text{Si}-\text{OR} \quad + \quad \text{HO}-\text{Si}\equiv \quad \rightleftharpoons \quad \equiv\text{Si}-\text{O}-\text{Si}\equiv \quad + \quad \text{ROH}$$

$$\equiv\text{Si}-\text{OH} \quad + \quad \text{HO}-\text{Si}\equiv \quad \rightleftharpoons \quad \equiv\text{Si}-\text{O}-\text{Si}\equiv \quad + \quad \text{H}_2\text{O}$$

Figure 1.2. A summary of the basic sol-gel reactions.

grafting involves the anchoring of a reagent through covalent bonding. These techniques have distinct advantages and disadvantages.[21-23] Doping techniques are simple and applicable to many organic compounds, but the pore size must be carefully tailored, as dopant leaching is often a problem. Grafting techniques yield highly reproducible, stable products, but the overall process can be tedious. The reagents need to contain a –Si(OR)$_3$ group, and this limits the selection of reagents suitable for the grafting processes. The porous nature of sol-gels allows for the delivery of analytes to the encapsulated reagent, resulting in the interactions required for sensing applications. Sol-gels have found particular use in optical sensing, as they are transparent in the visible region.[24] Such sensors have been developed for monitoring pH,[16,18,22,25-27] metal ions,[28,29] and a variety of other analytes.[30] Sol-gels have also been used in electrochemical[31-34] and spectroelectrochemical[35] sensing applications. Proteins encapsulated in sol-gels retain their activities, and such proteins have been used for chemical and biochemical sensing.[30a-d] The depth and breadth with which sol-gels have been used in chemical sensing expands over an enormous area, and there are many reviews available describing such work.[17,20,23,24,30a-d,36]

1.4. *Summary of Dissertation Parts*

1.4.1. Part Two

The application of electrodeposited sol-gels for enhanced Cr(VI) determination is reported in Part 2 of this dissertation. In this work, a pyridine-

functionalized sol–gel film has been formed by electrodeposition at a glassy

carbon electrode surface. When this protonated film is exposed to a Cr(VI)

solution, the Cr(VI) anions are preconcentrated at the electrode surface. Using

square wave voltammetry, the Cr(VI) species are reduced to Cr(III), and a peak

current corresponding to this reduction is generated at 0.17 V. The peak currents

can be correlated with the Cr(VI) concentration. The functionalized sol–gel films

demonstrated an enhanced sensitivity for Cr(VI) in aqueous solutions, providing

a limit of detection at the low ppb level. Interference studies also displayed the

high selectivity of the films for Cr(VI), and the system was able to tolerate a large

excess of Cr(III) with no adverse affects. The growth of the sol–gel films was

monitored using an electrochemical quartz crystal microbalance (EQCM), and

they were characterized by X-ray photoelectron spectroscopy (XPS) and

scanning electron microscopy (SEM). In addition to glassy carbon electrodes,

studies involving gold and indium-tin oxide (ITO) electrodes were carried out as

well. Two articles containing the results discussed in this section have been

published.[37,38]

1.4.2. Part Three

Part 3 of this dissertation reports work on the optical determination of

Cr(VI) using regenerable, functionalized sol-gel monoliths. In these studies,

transparent, pyridine-functionalized sol–gel monoliths have been formed and

their use in Cr(VI) sensing applications is demonstrated. The monoliths were

immersed in acidic Cr(VI)-containing solutions, and the Cr(VI) uptake was

monitored using UV–vis and atomic absorption spectroscopies. At concentrations

at the ppm level, the monoliths exhibit a yellow color change characteristic of

Cr(VI) uptake, and this can be measured by monitoring the absorption change at

about 350 nm using UV–vis spectroscopy. Concentrations at the ppb level are

below the limit of detection using this wavelength of 350 nm for measurement.

However, by adding a diphenylcarbazide solution to monoliths that have been

previously immersed in ppb-level Cr(VI) solutions, a distinct color change takes

place within the gels that can be measured at about 540 nm using UV–vis

spectroscopy. Concentrations as low as 10 ppb Cr(VI) can be measured using

this method. The monoliths can then be regenerated for subsequent sensing

cycles by thorough washing with 6.0 M HCl. The factors affecting monolith

uptake of Cr(VI) have been explored. In addition, the gels have been

characterized using X-ray photoelectron spectroscopy (XPS), scanning electron

microscopy (SEM), and Brunauer–Emmett–Teller (BET) measurements. An

article detailing this work has been published.[39]

1.4.3. Part Four

A new method for the quantitative determination of palladium(II) by the

electrochemical quartz crystal microbalance (EQCM) technique is reported in

Part 4. Using a bare carbon-coated quartz crystal, Pd(II) ions are directly

deposited from aqueous solution as palladium metal onto the crystal surface, and

the Pd(II) concentration is determined with a detection limit of 0.0156 mM, or

1.66 ppm. No complexing agent or preconcentration of palladium is required for

the analysis. The palladium is stripped from the crystal through its electrochemical oxidation, regenerating the crystal for subsequent multi-cycle palladium analyses. A conventional gold-coated quartz crystal was incapable of carrying out the same measurements. The EQCM technique presented is simple, sensitive, and reproducible for the detection of this widely used precious metal. The results from this work have been published in an article.[40]

1.4.4. Part Five

Part 5 of this dissertation reports some work involving novel approaches to iron sensing. In this work, calcein, a well-known fluorophore that undergoes fluorescence quenching in the presence of iron, was doped into sol-gel thin films deposited on glass slides. When such slides were exposed to Fe(III), a noticeable drop in their fluorescence occurred, indicating their potential for use in iron sensing applications. In addition, electrochemical techniques for the enhanced determination of Fe(III) were investigated. Carbon paste electrodes modified with 1,10-phenanthroline or calcein were prepared for enhanced determination of Fe(III). Bismuth film electrodes were also investigated for the determination of Fe(III) using a catalytic voltammetry method, and this method was found to detect the analyte species quickly and reproducibly at the low ppb level. Using the bismuth film technique, attempts were made at detecting iron levels present in hog blood samples.

1.4.5. Part Six

Preliminary work investigating the interaction between Cr(III) and DTPA at a bismuth film electrode using EQCM is discussed in Part 6. Early studies show the adsorption of the Cr(III)-DTPA complex onto the bismuth film surface as a negative potential is applied. Possible future studies involving this work are also discussed.

References

1. A SciFinder (Chemical Abstracts) search in November 2006 using the term "sensors" and refined by the year "2005" yielded 12,776 hits.

2. Mitsubayashi, K.; Minamide, T.; Otsuka, K.; Kudo, H.; Saito, H. *Anal. Chim. Acta* **2006**, *573*, 80.

3. Rodman, D.L.; Carrington, N.A.; Qiu, H.; Goswami, K.; Xue, Z.-L. *Anal. Chim. Acta* **2005**, *548*, 143.

4. Carrington, N.A.; Rodman, D.L.; Goswami, K.; Xue, Z.-L. *J. Appl. Polym. Sci.* **2007**, *104*, 1043.

5. (a) Rodman, D.L.; Carrington, N.A.; Xue, Z.-L. *Talanta* **2006**, *70*, 426. (b) Rodman, D.L.; Carrington, N.A.; Xue, Z.-L. *Talanta* **2006**, *70*, 668. (c) Yong, L.; Armstrong, K.C.; Dansby-Sparks, R.N.; Carrington, N.A.; Chambers, J.Q.; Xue, Z.-L. *Anal. Chem.* **2006**, *78*, 7582.

6. Skoog, D.A.; West, D.M.; Holler, F.J. *Analytical Chemistry an Introduction*, 5th ed.; Harcourt Brace & Company: Philadelphia, 1998.

7. Bard, A.J.; Faulkner, L.R. *Electrochemical Methods Fundamentals and Applications,* 2nd ed.; John Wiley & Sons, Inc.: New York, 2001.

8. Christian, G.D. *Analytical Chemistry*, 4th ed.; John Wiley & Sons, Inc.: New York, 1986.

9. (a) Buttry, D.A.; Ward, M.D. *Chem. Rev.* **1992**, *92*, 1355. (b) Sauerbrey, G.Z. *Phys.* **1959**, *155*, 206. (c) Ullevlg, D.M.; Evans, J.F.; Albrecht, M.G. *Anal. Chem.* **1982**, *54*, 2341.

10. Whan, R.E. *Metals Handbook – Materials Characterization*, 9th ed.; American Society for Metals: Ohio, 1986, Vol. 10.

11. (a) Reimer, L. *Scanning Electron Microscopy*; Springer-Verlag: New York, 1985. (b) Chescoe, D.; Goodhew, P. *The Operation of Transmission and Scanning Electron Microscopes;* Royal Microscopical Society, Oxford University Press: 1990.

12. (a) Turner, N.H.; Schreifels. *Anal. Chem.* **1994**, *66*, 163R. (b) Johansson, L.-S. *Mikrochim. Acta* **2002**, *138*, 217.

13. Hollander, J.M.; Jolly, W.L. *Acc. Chem. Res.* **1970**, *3*, 193.

14. (a) Brunauer, S.; Emmett, P.; Teller, E. *J. Am. Chem. Soc.* **1938**, *60*, 309. (b) Brunauer, S.; Deming, L.S.; Deming, W.S.; Teller, E. *J. Am. Chem. Soc.* **1940**, *62*, 1723. (c) Dubinin, M.M. *J. Col. Interfac. Sci.* **1967**, *2*, 487. (d) Dollimore, D.; Spooner, P.; Turner, A. *Surf. Technol.* **1976**, *4*, 121.

15. Brinker C. J.; Scherer, G. W. *Sol-Gel Science*, Academic Press: San Diego, 1990.

16. (a) Allain, L. R.; Sorasaenee, K.; Xue, Z. *Anal. Chem.* **1997**, *69*, 3076. (b) Allain, L. R.; Xue, Z. *Anal. Chem.* **2000**, *72*, 1078. (c) Allain, L. R.; Xue, Z. *Anal. Chim. Acta* **2001**, *433*, 97.

17. Schubert, U. *Chem. Mater.* **1995**, *7*, 2010.

18. (a) Carey, W. P.; Jorgensen, B. S. *Appl. Spectrosc.* **1991**, *45*, 834. (b) Carey, W. P.; DeGrandpre, M. D.; Jorgensen, B. S. *Anal. Chem.* **1989**, *61*, 1674.

19. Lev, O.; Tsionsky, M.; Rabinovich, L.; Glezer, V.; Sampath, S.; Pankratov, I.; Gun, J. *Anal. Chem.* **1995**, *67*, 22A.

20.   (a) Klein, L. C. Solgel coatings, in Coatings Technology Handbook, 3rd Ed.; Tracton, A. A. Ed.; CRC Press: Boca Raton, Florida 2006, pp. 96/1-96/4. (b) Sanchez, C.; Julian, B.; Belleville, P.; Popall, M. *J. Mater. Chem.* **2005**, *15*, 3559. (c) McDonagh, C.; MacCraith, B. D.; McEvoy, A. K. *Anal. Chem.* **1998**, *70*, 45.

21.   Lin, J.; Brown, C. W. *Trends Anal. Chem.* **1997**, *16*, 200.

22.   MacCraith, B. D.; Ruddy, V.; Potter, C.; O'Kelly, B.; McGilp, J. F. *Electron. Lett.* **1991**, *27*, 1247. (b) Lobnik, A.; Oehme, I.; Murkovic, I.; Wolfbeis, O. S. *Anal. Chim. Acta.* **1998**, *367*, 159.

23.   Avnir, D. *Acc. Chem. Res.* **1995**, *28*, 328.

24.   (a) Dunn, B.; Zink, J. I. *J. Mater. Chem.* **1991**, 1, 903. (b) Lev, O. *Analusis* **1992**, *20*, 543.

25.   (a) Allain, L. R.; Canada, T. A.; Xue, Z. *Anal. Chem.* **2001**, *73*, 4592. (b) Canada, T. A.; Allain, L. R.; Beach, D. B.; Xue, Z. *Anal. Chem.* **2002**, *74*, 2535.

26.   (a) Shamsipur, M.; Gholamhassan, A. *Anal. Lett.* **2001**, *34*, 1603. (b) Wang, E.; Chow, K.-F.; Wang, W.; Wong, C.; Yee, C.; Persad, A.; Mann, J.; Bocarsly, A. **2005**, *534*, 301.

27.   (a) Canada, T. A.; Xue, Z. *Anal. Chem.* **2002**, *74*, 6073. (b) Canada, T. A.; Beach, D. B.; Xue, Z. *Anal. Chem.* **2005**, *77*, 2842.

28.   (a) Rodman, D. L.; Pan, H.; Clavier, C. W.; Feng, X.; Xue, Z. *Anal. Chem.* **2005**, *77*, 3231. (b) Clavier, C. W.; Rodman, D. L.; Sinski, J. F.; Allain, L.

R.; Im, H.-J.; Yang, Y.; Clark, J. C.; Xue, Z. *J. Mater. Chem.* **2005**, *15*, 2356.

29.   (a) Zevin, M.; Reisfeld, R.; Oehme, I.; Wolfbeis, O. S. *Sensor Actuat. B-Chem.* **1997**, *B39,* 235. (b) Oehme, I.; Wolfbeis, O. S. *Mikrochim. Acta* **1997**, *126*, 177.

30.   See, e.g., (a) Lan, E. H.; Dave, B. C.; Fukuto, J. M.; Dunn, B.; Zink, J. I.; Valentine, J. S. *J. Mater. Chem.* **1999**, *9*, 45. (b) Avnir, D.; Braun, S.; Lev, O.; Ottolenghi, M. *Chem. Mater.* **1994**, *6*, 1605. (c) Narang, U.; Prasad, P. N.; Bright, F. V.; Ramanathan, K.; Kumar, N. D.; Malhotra, B. D.; Kamalasanan, M. N.; Chandra, S. *Anal. Chem.* **1994**, *66*, 3139. (d) Wang, J. *Anal. Chim. Acta* **1999**, *399*, 21. (e) Rao, M. S.; Dave, B. C. *Adv. Mater.* **2002**, *14*, 443. (f) McGaughey, O.; Ros-Lis, J. V.; Guckian, A.; McEvoy, A. K.; McDonagh, C.; MacCraith, B. D. *Anal. Chim. Acta* **2006**, *570*, 15. (g) Rupcich, N.; Nutiu, R.; Li, Y.; Brennan, J. D. *Anal. Chem.* **2005**, *77*, 4300.

31.   Deepa, P. N.; Kanungo, M.; Claycomb, G.; Sherwood, P. M. A.; Collinson, M.M. *Anal. Chem.* **2003**, *75*, 5399.

32.   Walcarius, A.; Sibottier, E. *Electroanal.* **2005**, *17*, 1716.

33.   Shacham, R.; Avnir, D.; Mandler, D. Electrodeposition of methylated sol-gel films on conducting surfaces. *Adv. Mater.* **1999**, *11*, 384.

34.   (a) Walcarius, A.; Mandler, D.; Cox, J. A.; Collinson, M.; Lev, O. *J. Mater. Chem.* **2005**, *15*, 3663. (b) Lev, O.; Wu, Z.; Bharathi, S.; Glezer, V.;

Modestov, A.; Gun, J.; Rabinovich, L.; Sampath, S. *Chem. Mater.* **1997**, *9*, 2354. (c) Alber, K. S.; Cox, J. A. *Mikrochim. Acta* **1997**, *127*, 131.

35.   Shi, Y.; Slaterbeck, A. F.; Seliskar, C.J.; Heineman, W. R. *Anal. Chem.* **1997**, *69*, 3679.

36.   Carrington, N.A.; Xue, Z.-L. *Acc. Chem. Res.* **2007**, *in press.*

37.   Carrington, N.A.; Yong, L.; Xue, Z.-L. *Anal. Chim. Acta* **2006**, *572*, 17.

38.   Carrington, N.A.; Qiu, H.; Xue, Z.-L. *Am. Lab.* **2007**, in press.

39.   Carrington, N.A.; Thomas, G.H.; Rodman, D.L.; Beach, D.B.; Xue, Z.-L. *Anal. Chim. Acta* **2007**, *581*, 232.

40.   Carrington, N.A.; Rodman, D.L.; Xue, Z.-L. *Anal. Chim. Acta* **2006**, *572*, 303.

Part 2

Electrochemical Deposition of Sol-gel Films for Enhanced Chromium(VI) Determination in Aqueous Solutions

2.1. Introduction

As a suspected carcinogenic agent and toxic pollutant, Cr(VI) poses a threat when present even at trace levels. Several methods have been reported for the successful determination and quantification of Cr(VI) in solution.[1-16] Some of these techniques rely on spectroscopic methods[1-4] while others depend on mass-sensitive devices.[5-8] Electrochemical detection of Cr(VI) species has attracted much interest[9-16] due to its high sensitivity, portability, and ability to distinguish Cr(VI) from Cr(III). Cox and Kulesza investigated Cr(VI) determination at a poly(4-vinylpryidine)-coated platinum electrode. They were able to demonstrate the preconcentration of Cr(VI) in the polymer film and show the lack of interference by metal cations.[9] Using diphenylcarbazide, Paniagua and coworkers showed the potential of their modified carbon paste electrode for enhanced Cr(VI) determination.[10] Svancara and coworkers also investigated Cr(VI) determination at a carbon paste electrode modified with quarternary ammonium salts.[11] More recently, Compton and coworkers have probed Cr(VI) detection at bare gold, glassy carbon, and boron-doped diamond electrodes.[12] Detection limits at the low ppt level using electrochemical methods have been reported. Yang and Huang have used a polyaniline/polystyrene composite electrode as a detector in a flow injection analysis system that provides a Cr(VI) detection limit of 4 ppt,[13] while Wang and coworkers have developed a novel method of Cr(VI) determination at a bismuth film electrode using catalytic adsorptive stripping voltammetry.[14] Turyan and Mandler have also investigated the determination of Cr(VI) at a self-assembled monolayer electrode, achieving a

24

detection limit of about 1 ppt and a high degree of selectivity over other metal ions.[15]

One attractive method for analytical sensing is the use of sol-gel materials in conjunction with electrochemistry.[17-28] Typically, sol-gels have been deposited on electrode surfaces using spin-coating techniques.[17,21,25,26] Films formed in this manner are usually acid-catalyzed and, as a result, have a compact structure with low porosity.[17,19] Base-catalyzed sol-gels, formed by the reactions shown in Eq. 2.1-2.3, are usually of higher porosity,[28,29] a critical issue in many sol-gel sensing applications.

Based-Catalyzed Hydrolysis:

$$OH^- + \quad RO-\underset{\underset{RO}{|}}{\overset{\overset{RO}{|}}{Si}}-OR \quad \rightleftharpoons \quad \overset{RO}{\underset{\overset{|}{OR}}{HO}}\overset{OR}{\underset{}{\cdots\cdots Si\cdots\cdots OR}} \quad \rightleftharpoons \quad HO-\underset{\underset{RO}{|}}{\overset{\overset{RO}{|}}{Si}}-OR \quad + \quad OR^- \qquad (Eq.\ 2.1)$$
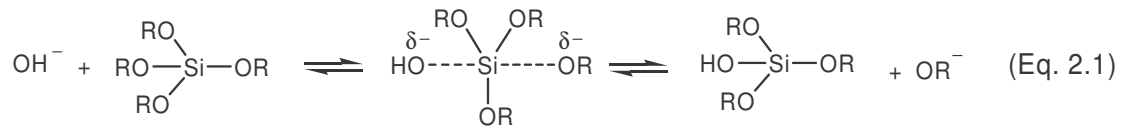
Base-Catalyzed Condensation:

$$RO-Si(OH)_3 + OH^- \quad \overset{fast}{\rightleftharpoons} \quad RO-\underset{\overset{|}{O^-}}{Si(OH)_2} + H_2O \qquad (Eq.\ 2.2)$$

$$RO-Si(OH)_3 + RO-\underset{\overset{|}{O^-}}{Si(OH)_2} \quad \overset{slow}{\rightleftharpoons} \quad RO-\underset{\overset{|}{OH}}{\overset{\overset{OH}{|}}{Si}}-O-\underset{\overset{|}{OH}}{\overset{\overset{OH}{|}}{Si}}-OR + OH^- \qquad (Eq.\ 2.3)$$
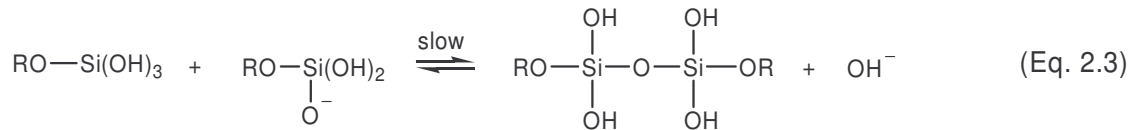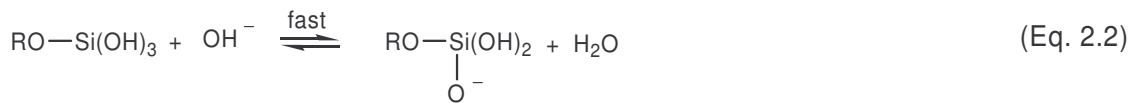
A very promising method that has recently emerged for the formation of sol-gel films of high porosity is the electrodeposition of sol-gels at electrode surfaces.[18-20,22,23] Initially investigated by Shacham et al.[23] and later elaborated on by Collinson et al.[18,19] and Walcarius and coworkers,[20,22] this method of sol-

gel formation relies on the application of a negative potential to increase the pH at the electrode surface, causing the immediate condensation of the sol-gel. The unique aspect of this procedure is that gelation and drying proceed independently of each other, allowing for the formation of films with greater porosity.[19]

In this work, the electrodeposition technique is used to form a functionalized sol-gel film at the surface of a glassy carbon electrode for the enhanced determination of Cr(VI) anions. Most metal ions are cations. Chromium at its highest, VI oxidation state, however, exists mainly as anions ($HCrO_4^-$, $Cr_2O_7^{2-}$ and $HCr_2O_7^-$ in acidic and CrO_4^{2-} in basic solutions[30]), providing a unique opportunity for Cr(VI) preconcentration and detection.[31] Previous reports have demonstrated the use of sol-gels for the detection and separation of Cr(VI) from aqueous solutions.[1,32] We have designed and deposited a sol-gel thin film containing grafted pyridinium on a glassy carbon electrode, and the thin film was found to preconcentrate Cr(VI) anions, leading to Cr(VI) detection with enhanced sensitivity and selectivity (Figure 2.1). This approach is based on the electrostatic interaction between the positively charged pyridinium groups in the sol-gel matrix and the negatively charged Cr(VI) anions.[15,33-37] Reduction of the preconcentrated Cr(VI) anions converts them into Cr^{3+} cations, regenerating the electrode surface for subsequent preconcentration and analysis. Our studies are reported here.
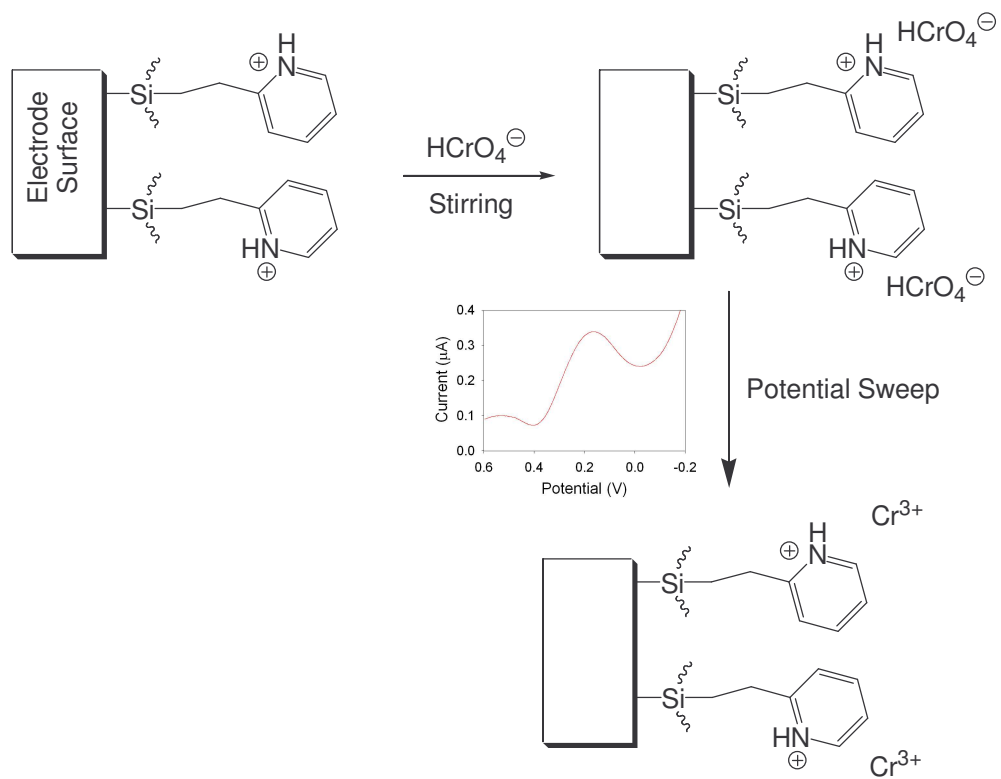
Figure 2.1. Schematic of the electroanalysis process at a pyridinium-functionalized electrode. $HCrO_4^-$ is used to represent the Cr(VI) anionic species.

2.2. Experimental

2.2.1. Chemical Reagents and Materials

Tetramethyl orthosilicate (TMOS, $Si(OMe)_4$, 98%, Sigma-Aldrich), 2-[2-(trimethoxysilyl)ethyl]-pyridine (Gelest), hydrochloric acid (HCl, certified A.C.S., Fisher), ethanol (EtOH, 95%, Fisher), and potassium chloride (KCl, certified A.C.S., Mallinckrodt) were used as received. Standard solutions of Cr(VI) were prepared by serial dilution of a 1017 µg/mL AA standard (Sigma-Aldrich). All compounds used for interference studies were of the highest purity available. Solutions and standards were prepared using deionized (DI) water (18 MΩ-cm) from a Barnstead International E-pure 4-holder deionization system. The working electrodes typically used during the experiments were glass-encased glassy carbon electrodes (3 mm diameter, Cypress Systems, Inc.). Before each coating process, these electrodes were polished using 0.05 micron alumina powder. Each electrode was then rinsed with water and sonnicated for 20 minutes, followed by soaking in piranha solution for an additional 15 minutes (**Caution:** piranha solution will react violently with organics and proper caution should be taken when handling). For the electrodeposition experiments, a Ag/AgCl wire electrode, prepared by soaking Ag wire in bleach, was used. For all other applications, a typical, fritted reference Ag/AgCl electrode was employed. Platinum wire was used as an auxiliary electrode. For the electrochemical quartz crystal microbalance (EQCM) experiments, a Teflon cell was used to house the crystals. Polished, mounted, and bonded gold-coated

quartz crystals (International Crystal Manufacturing Company, Inc.) were used as received. Each crystal had a fundamental frequency of approximately 7.995 MHz and an electrode diameter of 0.546 cm, consisting of a 1000 Å film of gold deposited on a 100 Å layer of chromium.

2.2.2. Instrumentation

A CH Instruments model 400A potentiostat with electrochemcial quartz crystal microbalance (EQCM) capability and corresponding software were used for the electrochemical studies. X-ray photoelectron spectroscopy (XPS) was carried out using a Phi 5100LS spectrometer with an Al K_α source at 300 W. Scanning electron microscopy (SEM) images were obtained using a Hitachi S4300-E SEM with the field-emission gun operating at 3 kV.

2.2.3. Coating Procedure

A sol solution typically consisting of 2 mL of 0.2 M KCl, 2 mL of EtOH, 250 µL of TMOS, and 250 µL of 2-[2-(trimethoxysilyl)ethyl]-pyridine was prepared and stirred thoroughly for several minutes to ensure a homogeneous mixture. After mixing, the working electrode was exposed to the sol solution, and a potential of -0.9 V was applied for 60 s. The working electrode was then rinsed with several aliquots of a 50:50 mixture of EtOH and DI water. It was then placed in an oven at 68 °C for 12 h and subsequently cured further at room temperature for an additional 12 h.

2.2.4. Analysis Procedure

Before each analysis procedure, the sol-gel coated electrode was placed in 0.1 M HCl (pH = 1) for 10 min to ensure protonation of the pyridinium[38] and silanol[29] groups within the film. The electrodes were then exposed to a solution consisting of 0.1 M KCl, 0.1 M HCl, and a variable amount of Cr(VI). After 10 min of solution stirring, a square wave voltammogram was collected, typically from 0.6 V to -0.2 V with a frequency of 15 Hz, amplitude of 0.025 V, and incremental potential of 0.004 V. The electrodes were then rinsed with electrolyte solution consisting of 0.1 M KCl and 0.1 M HCl, and several CV scans were run in only electrolyte solution to ensure that any residual Cr(VI) present was eliminated. Subsequent analyses of various Cr(VI) concentrations could then be carried out.

2.3. Results and Discussion

2.3.1. Film Electrodeposition and Characterization

The electrodeposition process is similar to those reported previously.[18,19] Briefly, a negative potential applied to the working electrode creates an increase in pH at the electrode surface due to the generation of hydroxide ions (Eq. 2.4-2.6). When TMOS and 2-[2-(trimethoxysilyl)ethyl]-pyridine are present, the increase in OH^- concentration base catalyzes the hydrolysis and condensation (Eq. 2.1-2.3) of the sol at the electrode surface and produces a film functionalized with pyridine. Exposing the glassy carbon electrode to piranha solution prior to carrying out the electrodeposition process is expected to produce

numerous surface oxides that allow for greater film adhesion to the electrode. The applied time and magnitude of the electrodeposition potential and the ratio of TMOS to 2-[2-(trimethoxysilyl)ethyl]-pyridine all affect the thickness and porosity of the film.[37]

$$2H_2O + 2e^- \longrightarrow 2OH^- + H_2 \qquad \text{(Eq. 2.4)}$$

$$O_2 + 2H_2O + 4e^- \longrightarrow 4OH^- \qquad \text{(Eq. 2.5)}$$

$$O_2 + 2H_2O + 2e^- \longrightarrow H_2O_2 + 2OH^- \qquad \text{(Eq. 2.6)}$$
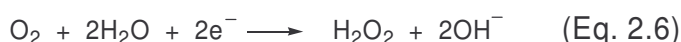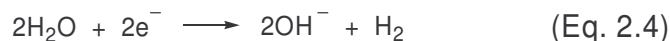
2.3.1.1. EQCM Study

In order to probe the electrodeposition process and to characterize the functionalized sol-gel films by XPS and SEM, Au-coated quartz crystal microbalance (QCM) crystals were employed to prepare sol-gel films under otherwise identical conditions as those used to coat sol-gel films on glassy carbon electrodes. Measurements using an electrochemical quartz crystal microbalance (EQCM), a device sensitive to minute mass changes at the electrode surface, were carried out to monitor in-situ the sol-gel formation. Figure 2.2 shows the change in current and frequency as a function of time at a Au-coated, 8.0 MHz QCM crystal when a potential of -0.9 V was applied to the standard sol solution (Experimental Section). As expected, the frequency drops as the potential is applied and the sol-gel film forms at the electrode surface. After 60 s of deposition, a relatively thin film is formed on the surface. Longer deposition times were found to result in thick films that eventually prevent the
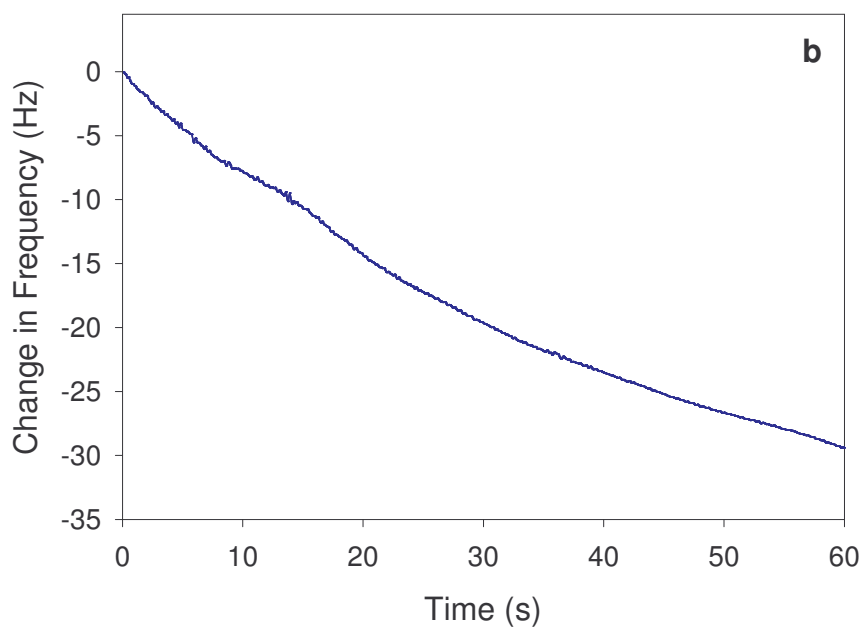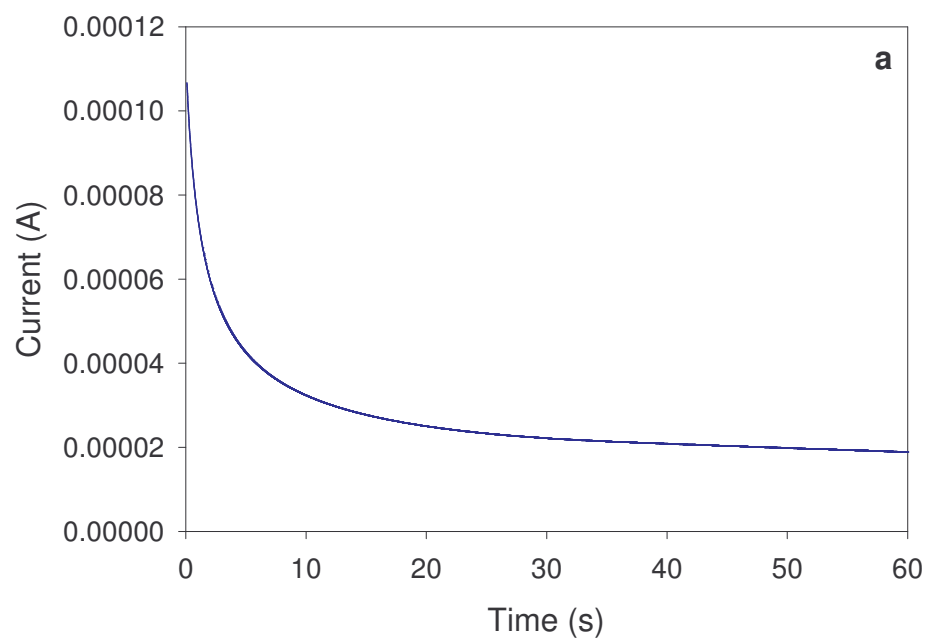
Figure 2.2. (a) Current-time and (b) frequency-time plots at a gold QCM electrode in a TMOS/2-[2-(trimethoxysilyl)ethyl]-pyridine sol solution when a potential of -0.9 V is applied.

32

crystal from further oscillation.[37] In such cases, the deposited sol-gel mass had

become so large that the crystal frequency had drifted significantly from its initial

fundamental frequency and was no longer compatible with the EQCM oscillator.

Increasing the amount of 2-[2-(trimethoxysilyl)ethyl]-pyridine in the sol solution

hindered film formation and produced films with reduced stability that easily

flaked off the electrode surfaces. A deposition time of 60 s was also used to

make sol-gel coatings on glassy carbon electrodes. As discussed below, the

Cr(VI) preconcentration in the pyridium-grafted sol-gel coatings and detection are

likely a mass-transport control process, and the deposition time of 60 s gives

coatings that provide optimum detection limits.[37]

2.3.1.2. Analysis of Films Using SEM

        SEM studies were carried out to reveal the morphology of the sol-gel

coatings electrodeposited on the Au QCM crystals (Figure 2.3). The images

obtained at higher magnifications (Figure 2.3a and 2.3b) show islands of particles

that are likely nucleation centers for film growth.[22] Lower magnifications (Figure

2.3c and 2.3d) show particles on the nanometer scale separated from one

another. The vacant areas between the particles are likely the gold QCM

surface, as Au peaks were observed in some of the XPS spectra that are

discussed below.[37] Such vacancies can likely be attributed to the evolution of

hydrogen gas during the electrodeposition process.[22] Also, considering the short

deposition time of 60 s that provides the optimum detection limit, to be discussed

below, it is perhaps not surprising that there are the vacant areas. Traditional
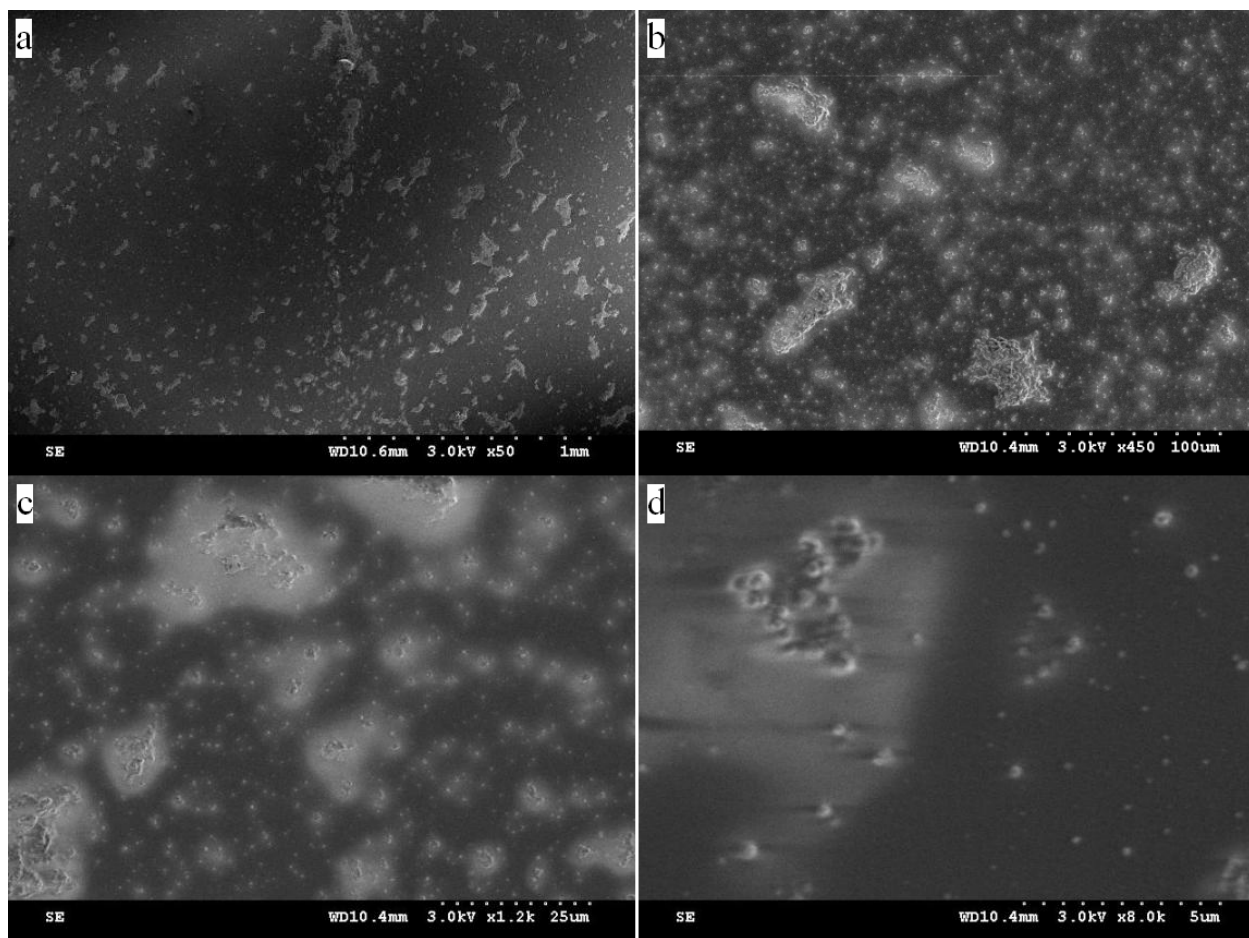
Figure 2.3. SEM images of a pyridine-functionalized sol-gel deposited on a gold QCM surface. Images taken are at magnifications of: (a) 1 mm; (b) 100 μm; (c) 25 μm; (d) 5 μm.

sol-gel deposition processes usually require a much longer reaction time prior to, e.g., spin- or dip-coating on substrates.[29,39] The particulate nature of the films is expected as the sol formations are base-catalyzed,[29] and coated glassy carbon electrodes viewed under an optical microscope revealed an analogous surface morphology. Similar structures of electrodeposited sol-gel films have been reported.[19,22]

2.3.1.3. XPS Film Analysis

XPS spectra were obtained of films deposited on gold QCM crystals.[37] Peaks of Si, C, O, and N as well as Au[37] were observed. Figure 2.4 shows the results obtained when one such film was analyzed. The Si, C, O, and N peaks are consistent with the formation of a sol-gel film functionalized with pyridine on the QCM electrode surface. The Au peaks[37] are likely from the vacant areas between islands of sol-gel particles. Additional studies showed that longer film deposition times led to increased peak intensity, as expected.[37]

2.3.2. Cr(VI) Analysis

The general process occurring at the modified glassy carbon electrode during Cr(VI) analysis is illustrated in Figure 2.1. The pyridinium groups present in the sol-gel are protonated by prior soaking of the film in 0.1 M HCl. The electrode is then exposed to a Cr(VI) solution where the analyte anions are preconcentrated at the electrode surface through the electrostatic interaction between the positively-charged pyridinium groups and the negatively-charged

35
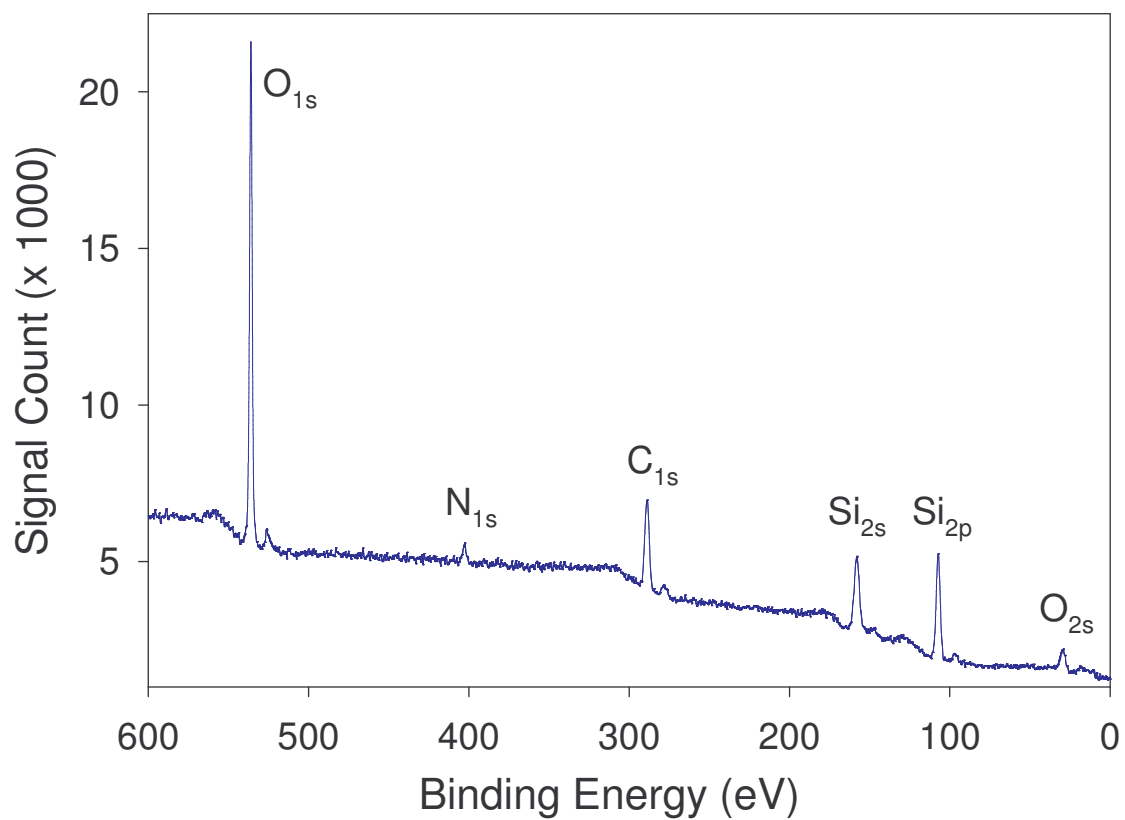
Figure 2.4. XPS spectrum obtained at a functionalized sol-gel film deposited on a QCM crystal.

Cr(VI) ions. After a period of time has passed and the analyte species has had sufficient time to diffuse to the electrode surface, a square wave voltammogram is collected. A peak occurs at approximately 0.17 V corresponding to the reduction of Cr(VI) to Cr(III), as has been reported previously.[9,11,15] The produced Cr(III) cations are then expelled from the sol-gel film containing the pyridinium cations. To ensure that that Cr species are removed, however, the electrodes are rinsed with electrolyte solution and several potential cycles are performed.[40]

Attempts in the current work at electrochemically protonating the pyridinium groups via an applied positive potential, similar to the procedure carried out by Walcarius and Sibottier in which a negative potential was applied for the deprotonation of their amine-functionalized silica film,[22] did not result in an enhanced peak current for the Cr(VI) reduction. It was therefore assumed that prior film exposure to a pH 1 acidic solution provided sufficient protonation of both the pyridinium and silanol groups present in the sol-gel. Given the fact that the isoelectric point of silica sol-gel is close to pH = 2[29] and the pKa value of 2-methylpyridine has been reported as 5.96,[38a] this assumption seems accurate.[38b] It should also be pointed out that most electrodeposited sol-gel films formed using similar procedures have been used for the analysis of cations and neutral species.[18,19,22] None of these films has been used for the analysis of anions, as the negatively charged silicate films have excluded the possibility of doing so.[18,19] However, by carrying our studies out under acidic conditions, it should be possible to analyze negatively-charged Cr(VI) ions.

2.3.3. Fe(CN)$_6^{4-}$ as a Redox Probe

Fe(CN)$_6^{4-}$ was used as a redox probe to investigate the electrodeposited sol-gel film and its anion-exchange capability. It was chosen as a model analyte for its negative charge and the fact that it is a well-established redox system.[41] Previous studies have demonstrated the use of anion-exchange selective layers for the partitioning of the Fe(CN)$_6^{4-}$ couple.[42,43-45] In particular, Heineman, Seliskar, and coworkers have shown that sol-gel-derived poly(dimethyldiallylammonium chloride)–SiO$_2$ composite films have been effective in this task.[43-45] We expect our pyridinium-containing sol-gel films to behave in a similar manner with respect to Fe(CN)$_6^{4-}$ preconcentration. Figure 2.5 shows cyclic votammograms that were collected at a glassy carbon electrode before and after coating with a sol-gel film. There is a small, noticeable decrease (6%) in the peak current of the CV obtained with the sol-gel coated electrode, indicating that there is likely increased resistance to mass transport through the film at the electrode surface. Much thicker films result in larger decreases in peak current when compared to the bare glassy carbon electrode. A CV was also collected after the sol-gel electrode had been preconditioned by soaking in 0.1 M HCl for 10 min followed by stirring in the Fe(CN)$_6^{4-}$ solution for 5 min (Figure 2.5). The resultant peak current showed an increase over that generated at either the coated or uncoated electrodes, indicating that preconcentration of the negatively-charged analyte species in the sol-gel film had taken place. This correlates well with previous reports showing the enhanced sensitivity achieved
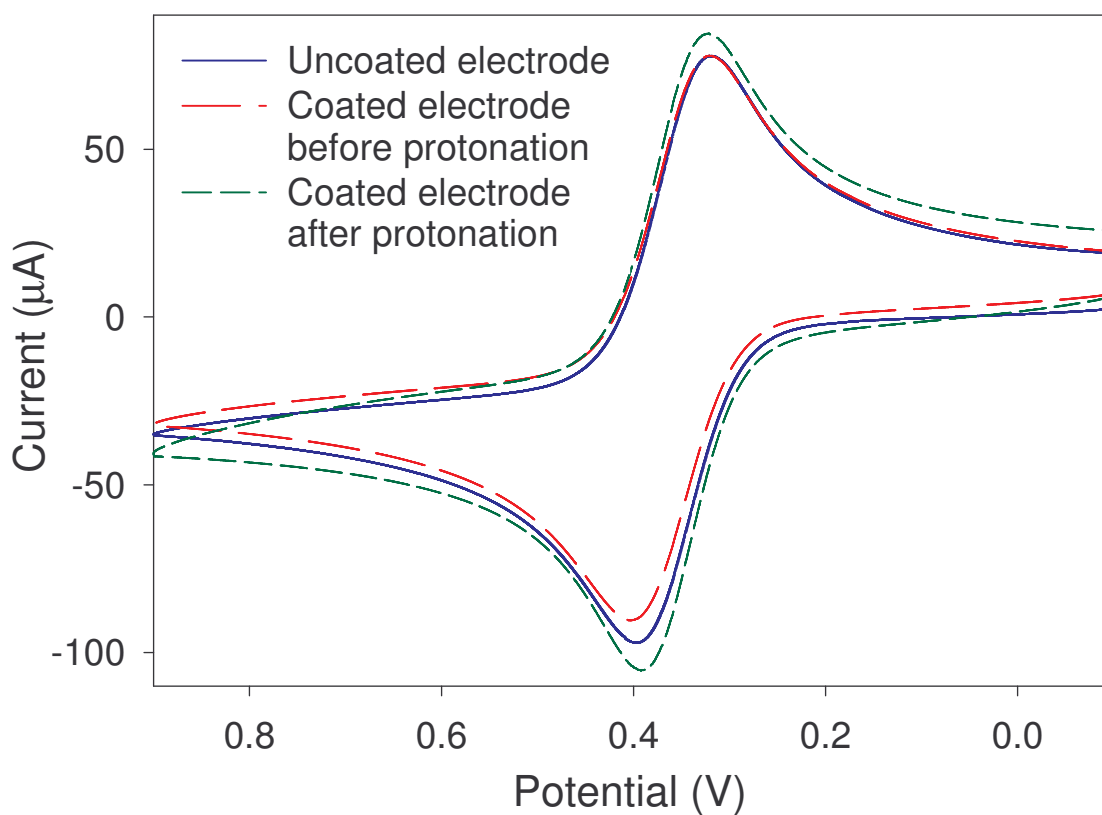
Figure 2.5. Cyclic voltammograms of 5 mM $Fe(CN)_6^{4-}$ at a glassy carbon electrode before and after coating with a pyridium-functionalized sol-gel.

when anionic-exchange films are used for the determination of $Fe(CN)_6^{4-}$.[42,43-45]

These results may suggest that the functionalized sol-gel films are adequate for the preconcentration and analysis of Cr(VI) anions, although the mechanisms of analyte transport for the two systems [mass transport for the irreversible Cr system, diffusion and charge-transport processes for the reversible $Fe(CN)_6^{4-}$ system] are greatly different.

2.3.4. Cr(VI) Quantification

Studies were carried out in which the electrode response was monitored as a function of Cr(VI) concentration. The square wave voltammograms and the corresponding calibration plot are given in Figures 2.6 and 2.7, respectively. There is a linear response ($R^2 = 0.992$) between the concentration of Cr(VI) and the peak current at the electrode, indicating the electrode would be useful for quantifying the concentration of Cr(VI) in an unknown sample.

2.3.5. Reproducibility and Limit of Detection

The reproducibility of the measurements obtained using the pyridinium-functionalized electrode was investigated. Four successive square wave voltammograms of solutions consisting of 53.3 ppb Cr(VI) were carried out (Figure 2.8). The various scans were highly reproducible with an average standard deviation of 1.0×10^{-3} µA for the peak currents from each scan. The detection limit of the proposed system is 4.6 ppb Cr(VI).[46] In addition, over 40 scans were conducted before a substantial decrease in sensitivity, presumably

40
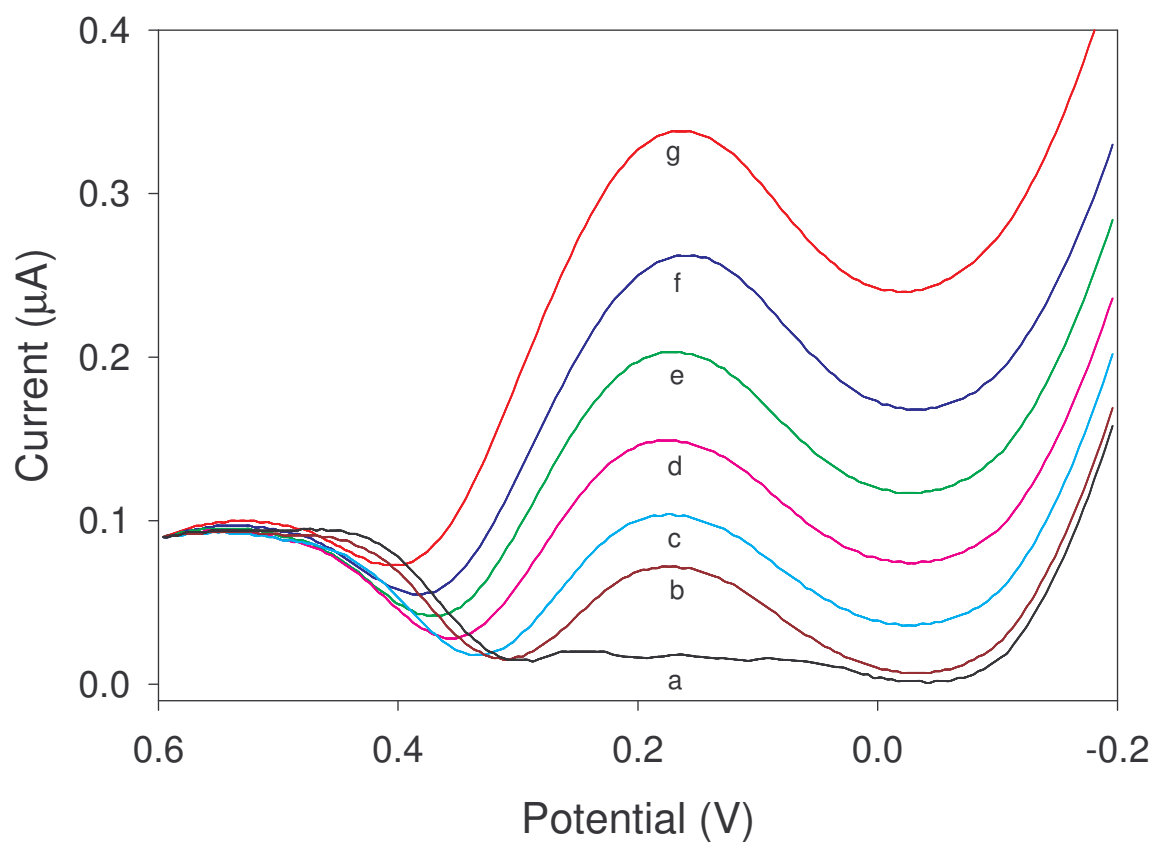
Figure 2.6. Square-wave voltammograms of various Cr(VI) concentrations collected at a pyridine-functionalized sol-gel electrode: (a) 0 ppb; (b) 11.7 ppb; (c) 50.1 ppb; (d) 104 ppb; (e) 203 ppb; (f) 308 ppb; (g) 400 ppb Cr (VI).

$R^2 = 0.992$

Cr(VI) Concentration (ppb)
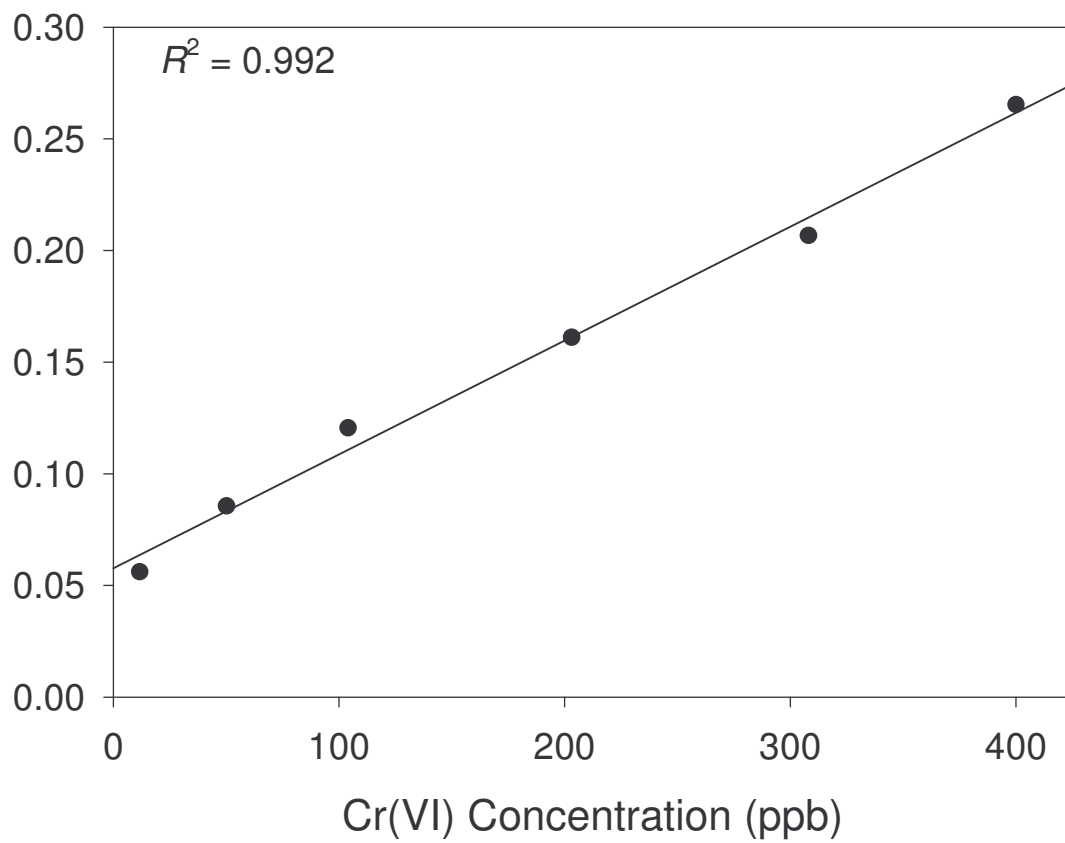
Figure 2.7. Calibration plot for the measurements in Figure 2.6.
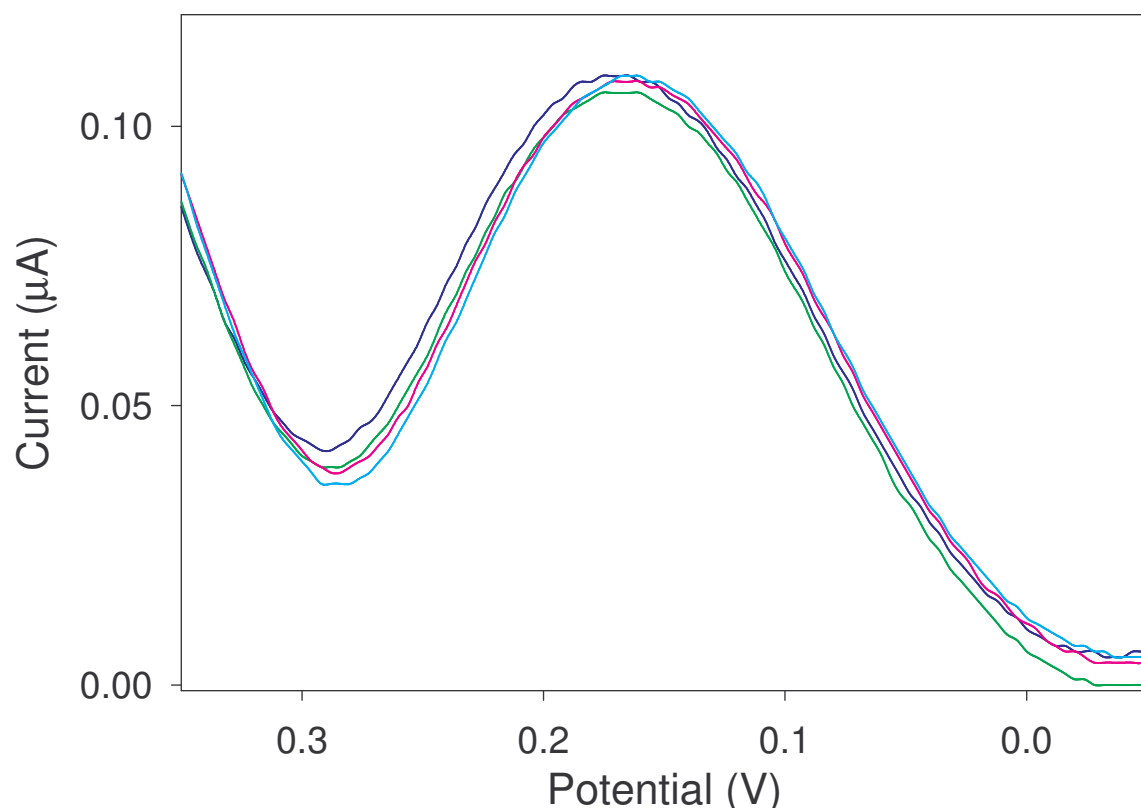
Figure 2.8. Square wave voltammgrams of separate 53.3 ppb Cr(VI) solutions.

Average standard deviation of the peak currents: 1.0×10^{-3} µA.

due to deterioration of the sol-gel film, was noticed.

2.3.6. Effect of Preconcentration Time

In a typical analysis procedure, the functionalized electrode is exposed to the Cr(VI) solution for 10 min while stirring. However, the length of preconcentration time affects the measured peak current. Figure 2.9 shows the relationship between the preconcentration time and the peak current obtained at the electrode surface. Initially, the slope of the plot is rather steep as Cr(VI) anions have more time to diffuse to the vacant pyridinium sites at the electrode surface. Later the slope of the plot begins to flatten out as more pyridinium sites are occupied by Cr(VI) anions. This is an indication that the electrode is becoming saturated with the analyte ions. However, even after 60 min, the peakcurrent is continuing to increase slightly. This continual increase in peak current, even after the long preconcentration, suggest that the mass transport of the Cr(VI) ions inside the sol-gel film is a fairly slow process. Longer preconcentration times may yield improved limits of detection. A 10 min. preconcentration time was chosen in the current studies.

2.3.7. Interference Study

The fact that Cr(VI) is one of few metallic anions makes it very likely that this electrode should be highly selective with regard to Cr(VI) since preconcentration relies on the interaction between the positively-charged pyridinium groups and the negatively-charged anions (Figure 2.1). As a result,
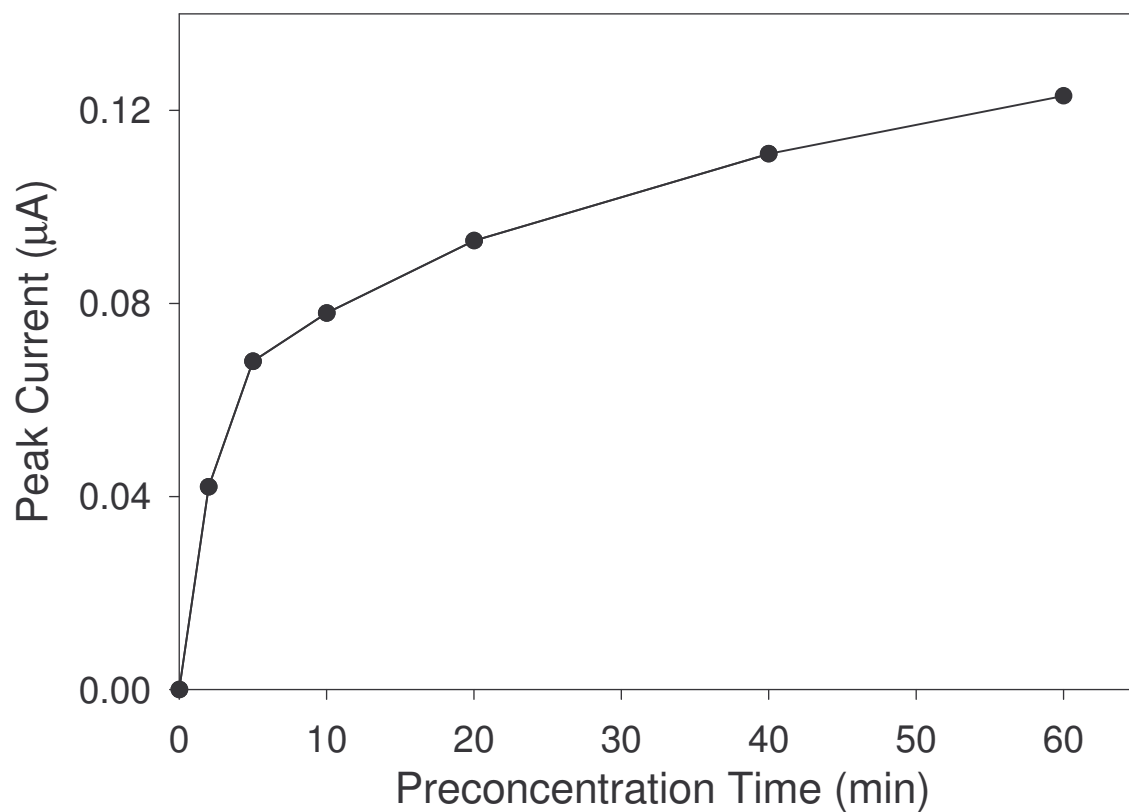
Figure 2.9. Effect of Cr(VI) preconcentration time at the electrode surface on the generated peak current. Analyte solutions consisted of 22.4 ppb Cr(VI), 0.1 M KCl, and 0.1 M HCl.

measurements should suffer little interference from other metallic species. Results from an interference study are shown in Figure 2.10. Even at relatively high interferent concentrations, the peak current associated with the Cr(VI) concentration changes very little. In particular, a 10^5 excess of Cr^{3+} can be tolerated with no adverse affects to the peak current. This is of particular importance, as Cr(III) has been shown to be an essential trace element for mammals[47] while Cr(VI) is a suspected carcinogen and highly toxic to humans. In addition, the relatively small interference of other anions indicates that the interaction between Cr(VI) and pyridine is more than a simple ion-exchange process, as has been shown previously.[15]

2.3.8. Additional Studies

2.3.8.1. Studies Involving Gold Electrodes

In addition to glassy carbon electrodes, studies were carried out involving the electrodeposition of sol-gels onto the surfaces of gold electrodes. Collinson and coworkers have demonstrated that sol-gel films electrodeposited onto gold electrode surfaces show poor adhesion and tend to peel off easily.[18] However, by using a binding agent, such as (3-mercaptopropyl) trimethoxysilane, the sol-gel coatings can be anchored to the electrode surfaces, improving their stability and durability. Figure 2.11 depicts the use of this technique for the sol-gel coating of gold electrodes. Initially, a gold electrode is immersed in an ethanol solution of 21 mM (3-mercaptopropyl) trimethoxysilane for 10 minutes to form a
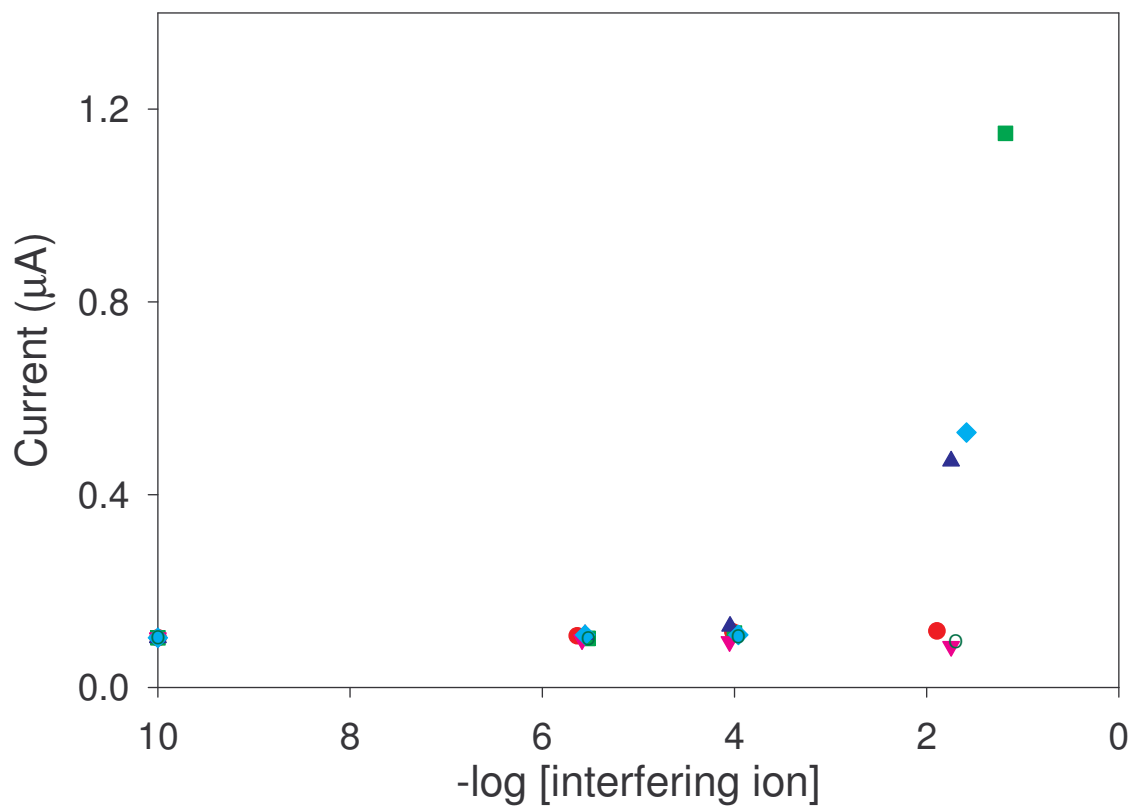
Figure 2.10. Results of the interference study. Peak currents of square wave voltammograms are obtained in solutions consisting of 51.6 ppb Cr(VI) and varying concentrations of the following: (●) Cr^{3+}; (■) Fe^{3+}; (▲) VO_4^{3-}; (▼) CH_3COO^-; (♦) Cu^{2+}; (○) CO_3^{2-}.

Gold Electrode Surface

HS—Si(OMe)(OMe)(OMe)

2-[2-(trimethoxysilyl)ethyl]-pyridine
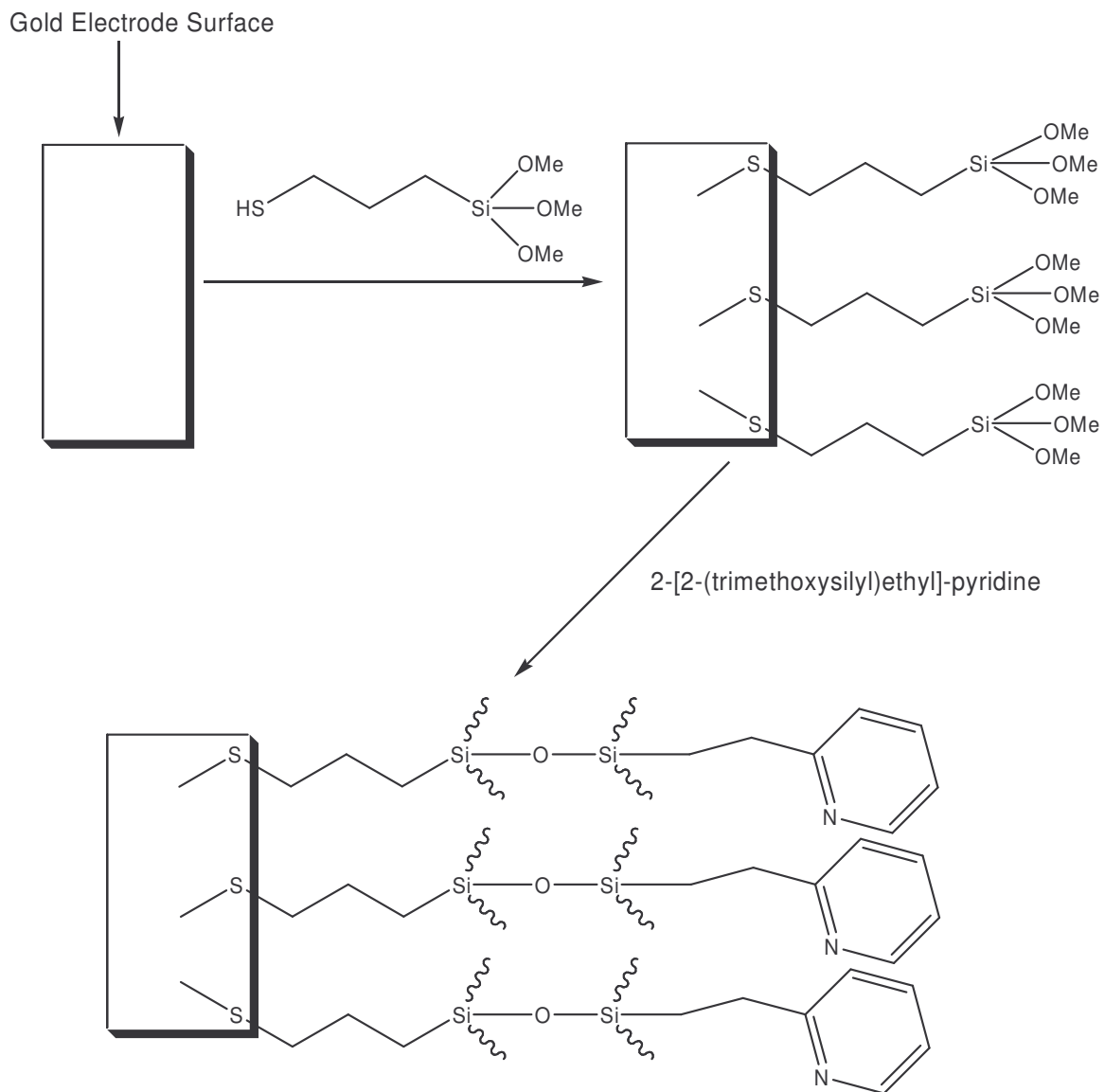
Figure 2.11. Schematic of sol-gel coating at a gold electrode.

self-assembled monolayer at the electrode surface. After rinsing the electrode

with ethanol and water, it is then exposed to a sol solution and coated as

discussed in the Experimental Section.

Figure 2.12 shows cyclic voltammograms collected when a pyridium-

functionalized sol-gel gold electrode is exposed to a solution consisting of 0.1 M

HCl and 5 mM $Fe(CN)_6^{4-}$. Initially, when the electrode is first exposed to the

solution, peak currents occur due to the oxidation and reduction of the $Fe(CN)_6^{4-}$

couple, as was seen in Figure 2.5. These currents increase rather dramatically

after the electrode has been exposed to the redox probe solution for 5 minutes.

This is likely due to the fact that, during the five minutes, preconcentration of the

negatively-charged analyte species in the positively-charged sol-gel film has

taken place, resulting in signal enhancement.

When the sol-gel modified gold electrodes were exposed to Cr(VI)

solutions, they demonstrated a selectivity and sensitivity similar to that exhibited

by the pyridinium-functionalized sol-gel glassy carbon electrodes. Figure 2.13

demonstrates this fact. When a sol-gel modified gold electrode was exposed to a

solution consisting of 68 ppb Cr(VI), 0.1 M HCl, and 0.1 M KCl, a peak current

corresponding to the reduction of Cr(VI) to Cr(III) was generated. The peak

potential is slightly shifted in the positive direction when compared with that

obtained at the glassy carbon modified electrode, and this may possibly be due

to the presence of the self-assembled monolayer at the electrode surface. This

demonstrates that, when (3-mercaptopropyl) trimethoxysilane is employed as a

binding agent, gold electrodes may be a viable alternative to glassy carbon
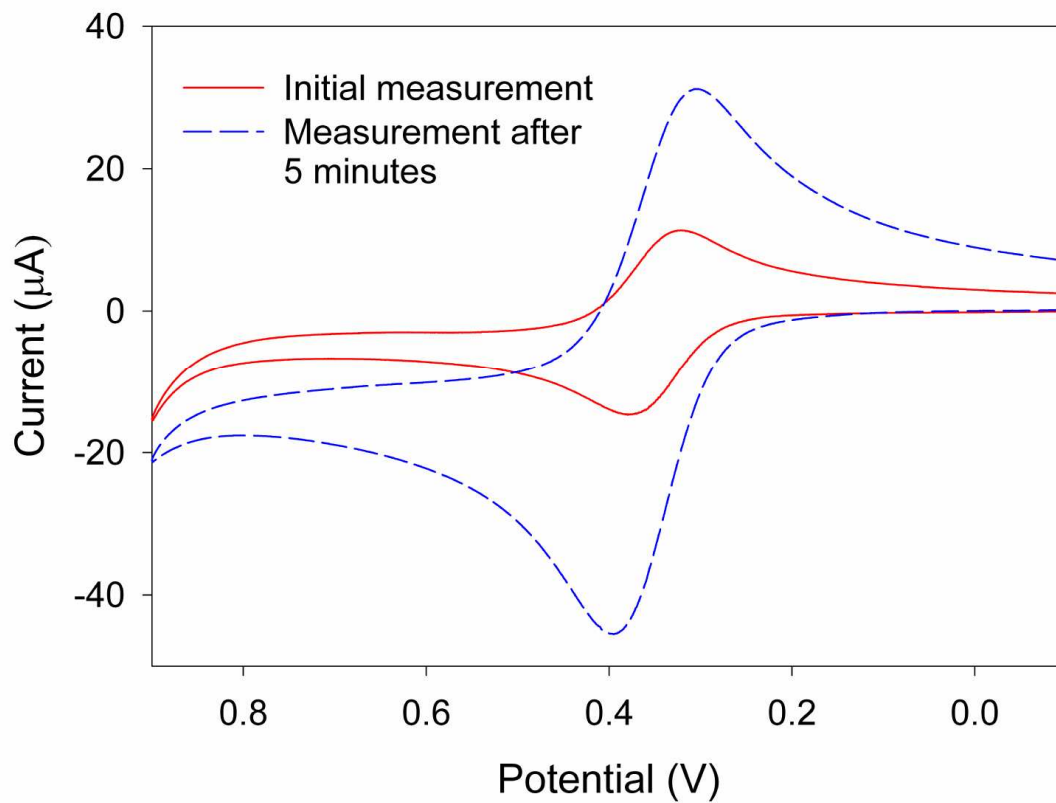
Figure 2.12. Cyclic voltammograms collected at a pyridinium-functionalized sol-gel gold electrode upon exposure to a solution consisting of 5 mM Fe(CN)$_6^{4-}$, 0.1 M HCl, and 0.1 M KCl.
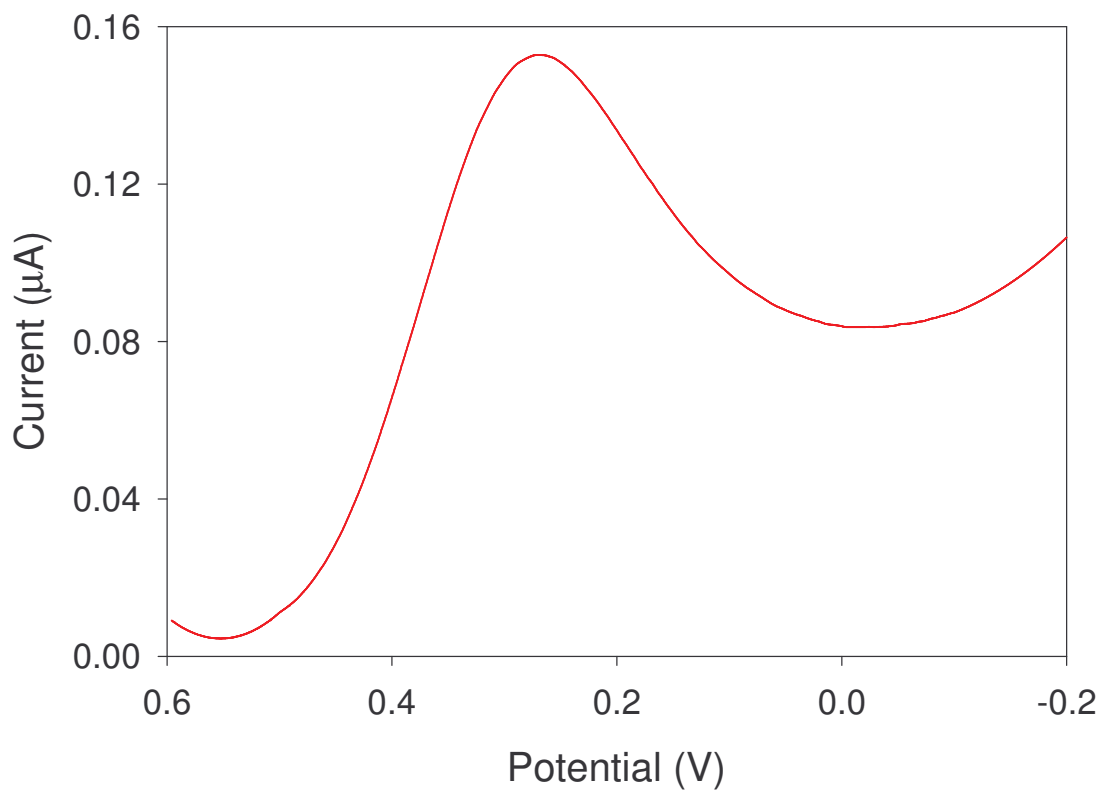
Figure 2.13. A square-wave voltammogram (background subtracted) of 68 ppb

Cr(VI) at a pyrindinium-functionalized sol-gel gold electrode.

electrodes for sol-gel electrodeposition applications.

2.3.8.2. Studies Involving Indium-Tin Oxide Electrodes

A possible use of the electrodeposited pyridinium-functionalized sol-gels is in spectroelectrochemical applications. Spectroelectrochemistry is typically carried out using optically transparent electrodes such as indium-tin oxide (ITO). When a functional film is coated onto the surface of such an electrode, three modes of selectivity (electrochemistry, spectroscopy, and selective partitioning) can take place, greatly enhancing the overall selectivity for the analyte of interest. Heineman, Seliskar, and coworkers have carried out much research in this area,[43-45] and it should be possible to use electrodeposited sol-gels in such applications.

Polished float glass slides with indium-tin oxide coated on the surface (purchased from Delta Technologies, Ltd.) were cut into 1.5 cm x 1.0 cm pieces and washed thoroughly with DI water, acetone, and ethanol. Each slide was then coated using the procedure described in the Experimental Section, except the sol-gel deposition time used was 30 minutes instead of 60 seconds for each electrode. After curing appropriately, one of the pyridinium-functionalized sol-gel ITO electrodes was exposed for 10 minutes to a solution consisting of 19.7 ppm Cr(VI), 0.1 M HCl, and 0.1 M KCl. The electrode was then rinsed with DI water and transferred to pure electrolyte solution, and several CV scans were carried out. The results can be seen in Figure 2.14. Initially, a large peak current occurs at 0.43 V, corresponding to the reduction of a portion of the Cr(VI) partitioned in
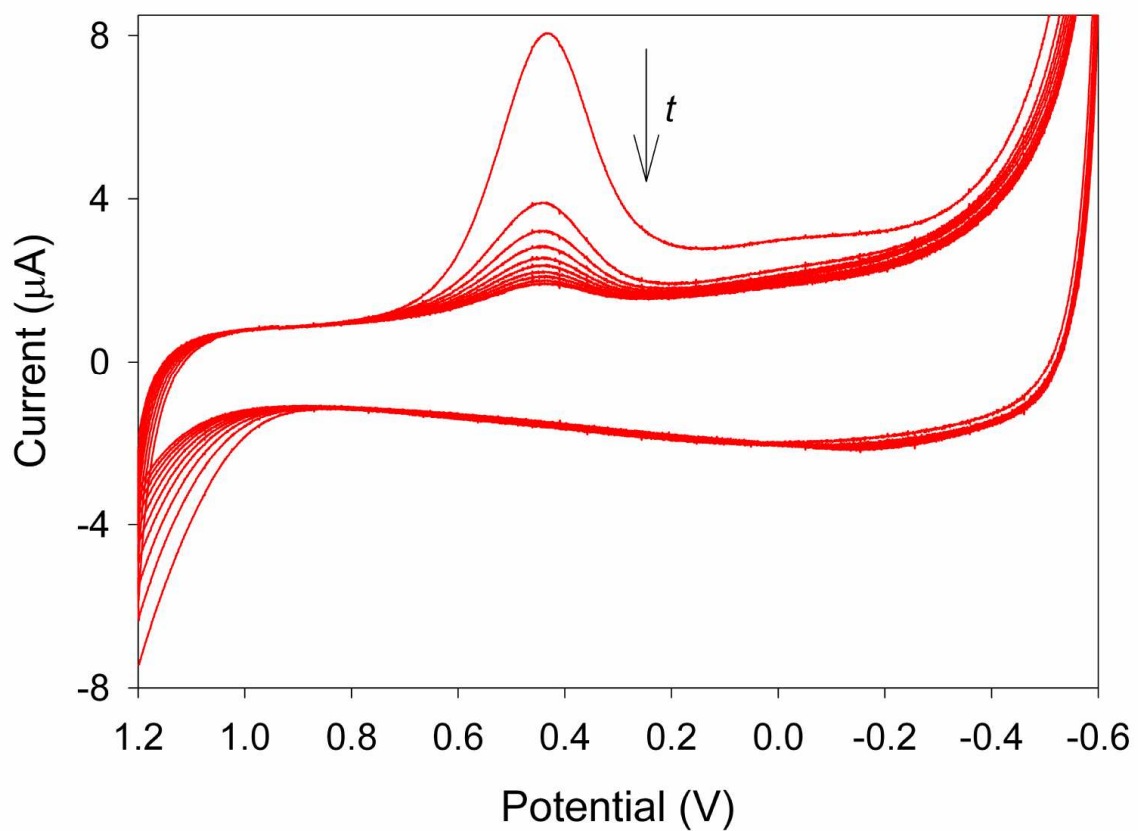
Figure 2.14. Cyclic voltammograms obtained in 0.1 M HCl/0.1 M KCl at a
pyridinium-functionalized sol-gel ITO electrode after immersion in 19.7 ppm
Cr(VI) for 10 minutes.

the film from the immersion of the electrode in the 19.7 ppm Cr(VI) solution. As time goes on and more voltammograms are carried out, the peak current decreases as more and more of the preconcentrated Cr(VI) is reduced to Cr(III). Eventually, the reduction peak becomes indistinguishable from the background, indicating that the majority of the Cr(VI) in the film has been removed.

The successful electrochemical use of these electrodeposited films on ITO electrodes seems to indicate their potential suitability for spectroelectrochemical applications. With the proper instrumentation, the pyridinium-functionalized sol-gel coated ITO electrodes in the current system could be coupled with a transmission or attenuated total reflectance (ATR) spectroscopic techniques. Such a set-up would provide a multi-modal sensing system for Cr(VI). Future work in this area is definitely possible.

2.3.8.3. *Studies Involving 4-[2-(trimethoxysilyl)ethyl]-pyridine-functionalized Electrodes*

Previously, Turyan and Mandler reported a selective electrode for Cr(VI) based on a self-assembled monolayer of 4-(mercapto-n-alkyl)pyridinium on a gold surface. In their study, the researchers investigated both 4-mercaptopyridine and 2-mercaptopyridine and found that the former was able to preconcentrate Cr(VI) to a greater extent than the latter.[15] 2-mercaptopyridine resembles the 2-[2-(trimethoxysilyl)ethyl]-pyridine used thus far in the study, and it was speculated that 4-[2-(trimethoxysilyl)ethyl]-pyridine might improve the overall sensitivity of the technique based on Turyan and Mandler's findings. For

this reason, 4-[2-(trimethoxysilyl)ethyl]-pyridine was synthesized using a previously reported procedure,[48] and its structure was verified using NMR. It was then incorporated into the previously described sol solutions in place of the 2-[2-(trimethoxysilyl)ethyl]-pyridine, and glassy carbon electrodes were coated as described in the Experimental Section.

Figure 2.15 shows the cyclic voltammograms obtained when a 4-[2-(trimethoxysilyl)ethyl]-pyridine-functionalized sol-gel electrode is used to analyze a 5 mM $Fe(CN)_6^{4-}$ solution. As time increases, the peak currents increase, indicating the time-dependent partitioning of $Fe(CN)_6^{4-}$ into the sol-gel film from the aqueous solution by the anion-exchange process. When the partitioned $Fe(CN)_6^{4-}$ permeates through the film to the electrode surface, it is oxidized to $Fe(CN)_6^{3-}$. Eventually, the peak currents become fairly constant, signaling that the sol-gel film has become saturated with the analyte. As mentioned previously, such results suggest that these films should be suitable for the preconcentration of Cr(VI).

When Cr(VI) solutions are analyzed, a peak current is generated at approximately 0.17 V, corresponding to the reduction of Cr(VI) to Cr(III). Square wave voltammograms and a corresponding calibration plot are shown in Figures 2.16 and 2.17, respectively. As can be seen, there is a linear relationship (R^2 = 0.997) between the Cr(VI) concentration and the peak current, and the limit of detection is approximately 1.0 ppb Cr(VI). This is an improvement over the limit of detection provided by the 2-[2-(trimethoxysilyl)ethyl]-pyridine-functionalized sol-gel electrode, previously determined to be approximately 4.6 ppb Cr(VI).
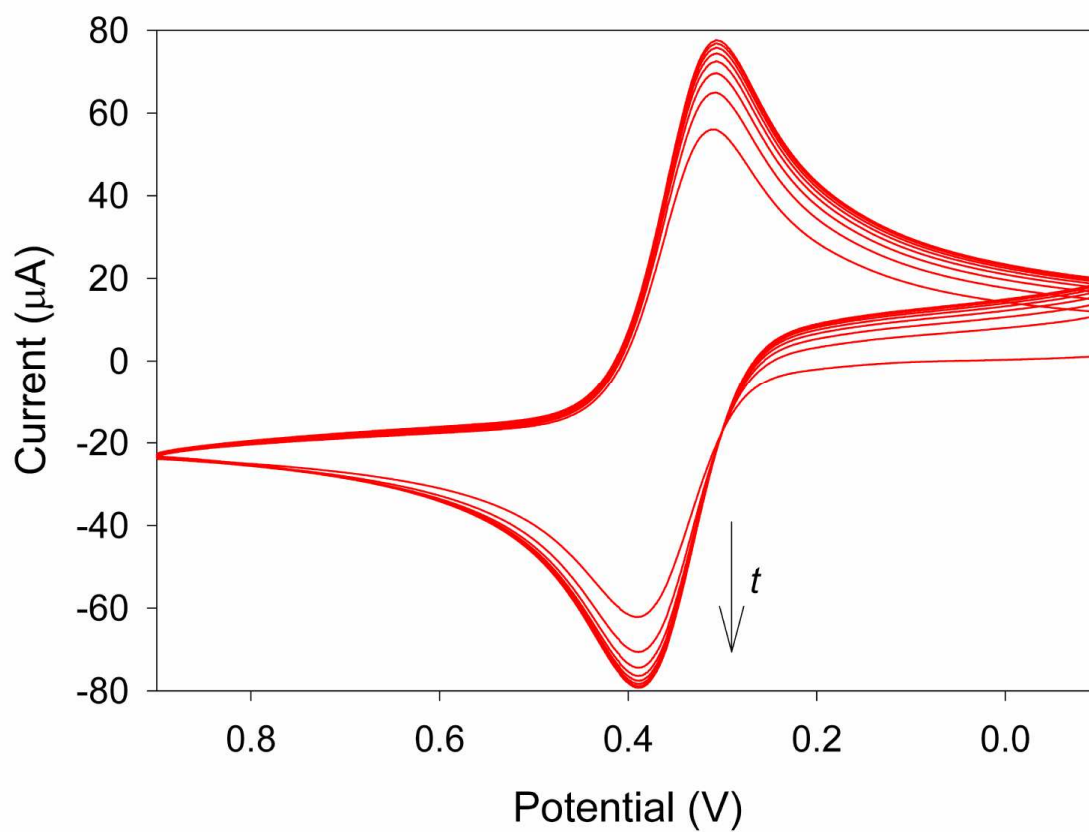
Figure 2.15. Cyclic voltammograms obtained of a solution consisting of 5 mM $Fe(CN)_6^{4-}$, 0.1 M HCl, and 0.1 M KCl using a 4-[2-(trimethoxysilyl)ethyl]-pyridine-functionalized sol-gel electrode.
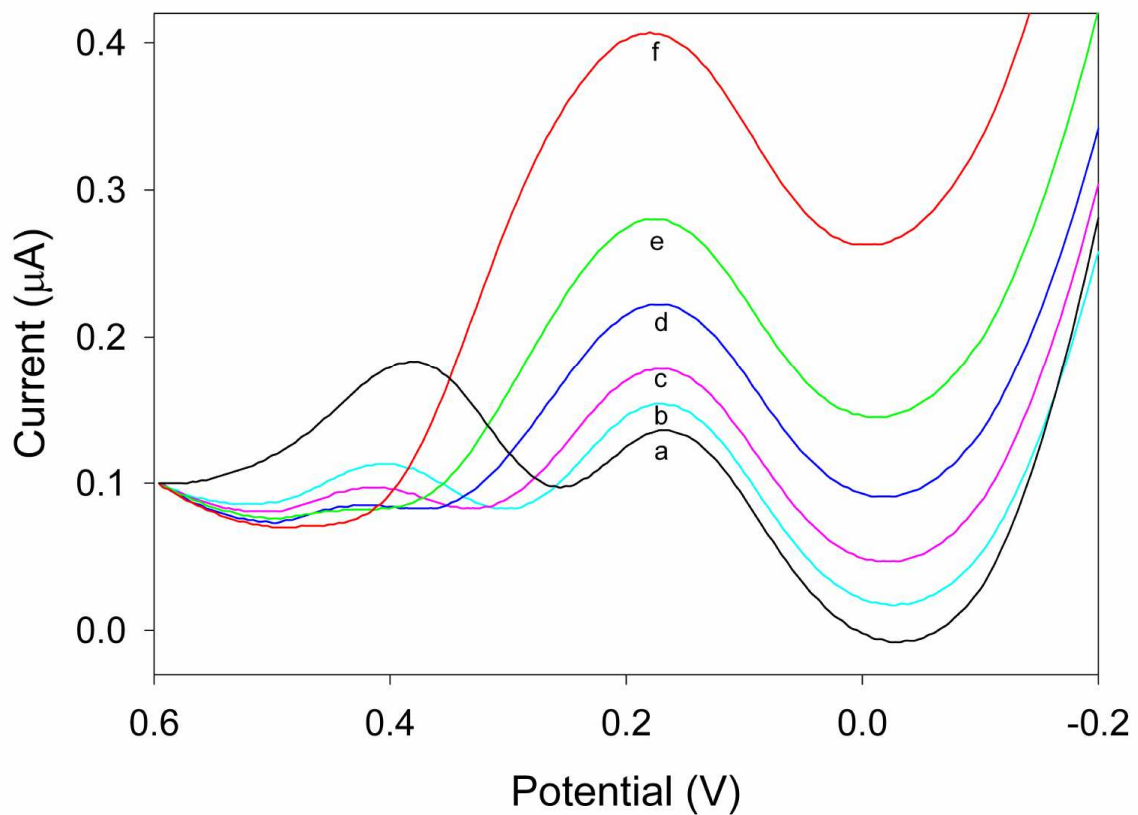
Figure 2.16. Square-wave voltammograms of various Cr(VI) concentrations collected at a 4-[2-(trimethoxysilyl)ethyl]-pyridine-functionalized sol-gel electrode: (a) 0 ppb; (b) 1.1 ppb; (c) 10.7 ppb; (d) 48.4 ppb; (e) 98.5 ppb; (f) 198 ppb.
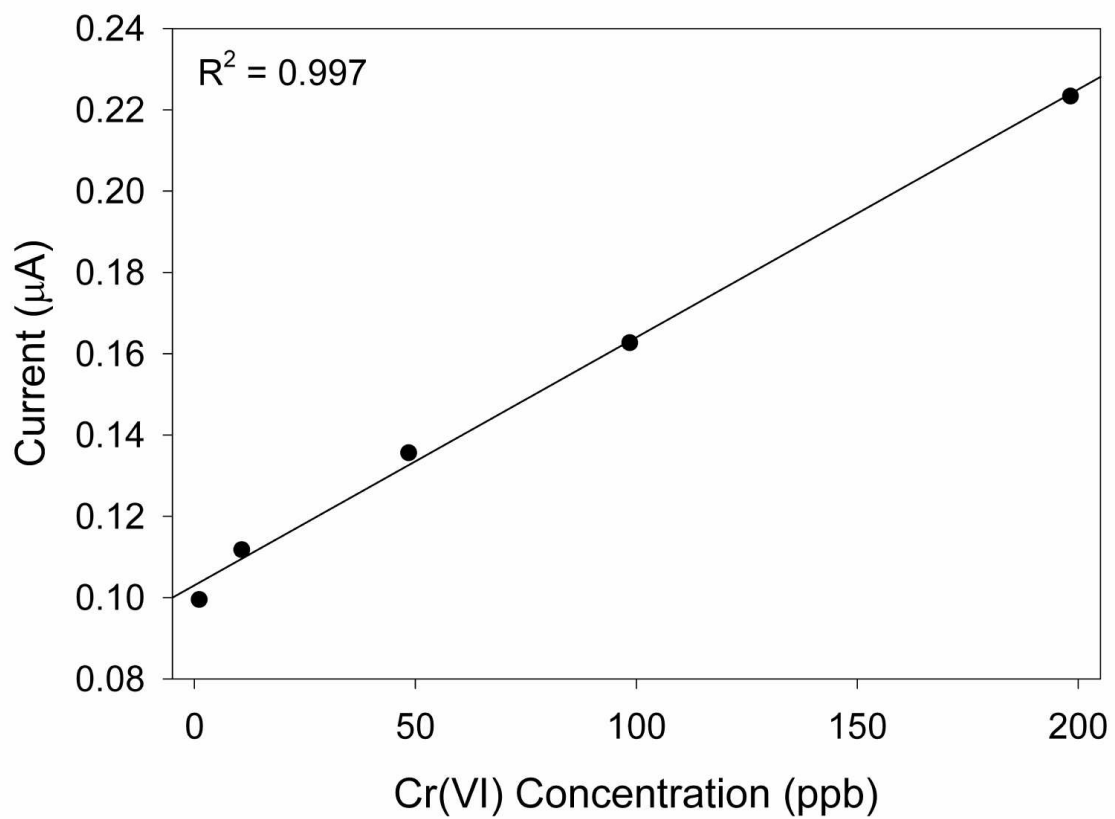
Figure 2.17. Calibration plot of the measurements in Figure 2.16.

2.4. Conclusions

Pyridine-functionalized sol-gel films have been electrodeposited on electrodes for the enhanced determination of Cr(VI). The proposed coating technique typically uses commercially available reagents and can be carried out relatively quickly and reproducibly. Although previously reported sol-gel coatings prepared in this manner have been used for the determination of cations and neutral species, the current work uses the films for enhanced determination of anions. The films were characterized using $Fe(CN)_6^{4-}$ as a redox probe, XPS, and SEM. Interaction of the pyridinium groups in the sol-gel film with Cr(VI) anions in solution results in increased selectivity and sensitivity for the analyte species. The analytical process here tolerates significant concentrations of interferent species, including Cr(III), with little affect on the expected peak current. The calculated limit of detection for the system may be lowered if longer preconcentration times are used. The reported work has demonstrated the success of electrodeposition for the formation of pyridine-functionalized sol-gel films and exhibits their potential in Cr(VI) sensing applications.

References

1. Zevin, M.; Reisfeld, R.; Oehme, I.; Wolfbeis, O.S. *Sens. Actuators* **1997**, *B38-39*, 235.

2. Balasubramanian, S.; Pugalenthi, V. *Talanta* **1999**, *50*, 457.

3. Posta, J.; Berndt, H.; Luo, S.K.; Schaldach, G. *Anal. Chem.* **1993**, *65*, 2590.

4. Scindia, Y.M.; Pandey, A.K.; Reddy, A.V.R.; Manohar, S.B. *Anal. Chim. Acta* **2004**, *515*, 311.

5. Ji, H.-F.; Thundat, T.; Dabestani, R.; Brown, G.M.; Britt, P.F.; Bonnesen, P.V. *Anal. Chem.* **2001**, *73*, 1572.

6. Zhang, Y.; Ji, H.-F.; Brown, G.M.; Thundat, T. *Anal. Chem.* **2003**, *75*, 4773.

7. Pinnaduwage, L.A.; Boiadjiev, V.I.; Brown, G.M.; Thundat, T.; Petersen, S.W. *Sens. Lett.* **2004**, *2*, 25.

8. Tian, F.; Boiadjiev, V.I.; Pinnaduwage, L.A.; Brown, G.M.; Thundat, T. *J. Vac. Sci. Technol. A* **2005**, *23*, 1022.

9. Cox, J.A.; Kulesza, P.J. *Anal. Chim. Acta* **1983**, *154*, 71.

10. Paniagua, A.R.; Vazquez, M.D.; Tascon, M.L.; Sanchez Batanero, P. *Electroanal.* **1993**, *5*, 155.

11. Svancara, I.; Foret, P.; Vytras, K. *Talanta* **2004**, *64*, 844.

12. Welch, M.W.; Nekrassova, O.; Compton, R.G. *Talanta* **2005**, *65*, 74.

13. Yang, Y.-J.; Huang, H.-J. *Anal. Chem.* **2001**, *73*, 1377.

14. Lin, L.; Lawrence, N.S.; Thongngamdee, S.; Wang, J.; Lin, Y. *Talanta* **2005**, *65*, 144.

15. Turyan, I.; Mandler, D. *Anal. Chem.* **1997**, *69*, 894.

16. Ge, H.; Zhang, J.; Wallace, G.G. *Anal. Lett.* **1992**, *25*, 429.

17. Collinson, M.M.; Rausch, C.G.; Voigt, A. *Langmuir* **1997**, *13*, 7245.

18. Collinson, M.M.; Moore, N.; Deepa, P.N.; Kanungo, M. *Langmuir* **2003**, *19*, 7669.

19. Deepa, P.N.; Kanungo, M.; Claycomb, G.; Sherwood, P.M.A.; Collinson, M.M. *Anal. Chem.* **2003**, *75*, 5399.

20. Sayen, S.; Walcarius, A. *Electrochem. Comm.* **2003**, *5*, 341.

21. Etienne, M.; Walcarius, A. *Electrochem. Commun.* **2005**, *7*, 1449.

22. Walcarius, A.; Sibottier, E. *Electroanal.* **2005**, *17*, 1716.

23. Shacham, R.; Avnir, D.; Mandler, D. *Adv. Mater.* **1999**, *11*, 384.

24. Marx, S.; Zaltsman, A.; Turyan, I.; Mandler, D. *Anal. Chem.* **2004**, *76*, 120.

25. Fireman-Shoresh, S.; Turyan, I.; Mandler, D.; Avnir, D.; Marx, S. *Langmuir* **2005**, *21*, 7842.

26. Kane, S.A.; Iwuoha, E.I.; Smyth, M.R. *Analyst* **1998**, *123*, 2001.

27. Walcarius, A.; Mandler, D.; Cox, J.A.; Collinson, M.; Lev, O. *J. Mater. Chem.* **2005**, *15*, 3663.

28. Buckley, A.M.; Greenblat, M. *J. Chem. Ed.* **1994**, *71*, 599.

29. Brinker, C.J.; Scherer, G.W. *Sol-Gel Science*, Academic Press, San Diego, 1990.

30. Greenwood, N.N.; Earnshaw, A. *Chemistry of the Elements*, 2nd Ed.; Pergamon Press: New York, 1997, pp 1002-1040.

31. Bichromate ($HCrO_4^-$) is believed to be the predominant Cr(VI) species in

dilute, acidic solution at pH < 6.5. However, there have been controversies recently about whether bichromate ($HCrO_4^-$) exists. See, e.g. (a) House, D.A. *Adv. Inorg. Chem.* **1997**, *44*, 341. (b) Poulopoulou, V.G.; Vrachnou, E.; Koinis, S.; Katakis, D. *Polyhedron* **1997**, *16*, 521. (c) Ramsey, J.D.; Xia, L.; Kendig, M.W.; McCreery, R.L. *Corrosion Sci.* **2001**, *43*, 1557.

32.   Deshpande, K.; Cheung, S.; Rao, M.S.; Dave, B.C. *J. Mater. Chem.* **2005**, *15*, 2997.

33.   Camelot, M. *Rev. Chim. Miner.* **1969**, *6*, 853.

34.   Corey, E.J.; Schmidt, G. *Tetrahderon Lett.* **1979**, *5*, 399.

35.   Martin-Zarza, P.; Gili, P.; Rodriguez-Romero, F.V.; Ruiz-Perez, C.; Solans, X. *Polyhedron* **1995**, *14*, 2907.

36.   Sisler, H.; Ming, W.Ch.L.; Metter, E.; Hurley, F.R. *J. Am. Chem. Soc.* **1953**, *75*, 446.

37.   See Appendix A.

38.   (a) Gero, A.; Markham, J.J. *J. Org. Chem.* **1951**, *16*, 1835. (b) Given the equilibrium constant $\log K = [Hpy^+] / [H^+] [py] = 5.217(1)$ for the protonation of pyridine (Israeli, M.; Laing, D.K.; Pettit, L.D. *J. Chem. Soc., Dalton Trans.* **1974**, 2194) and stability constant $\log K = [Cr(py)_2^{3+}] / [Cr^{3+}] [py]^2 = 4.88$ for the formation of Cr^{3+}-pyridine complex $Cr(py)_2^{3+}$ (Relan, P.S.; Bhattacharya, P.K. *J. Indian Chem. Soc.* **1969**, *46*, 534), it is unlikely that pyridinium groups in the sol-gel films form a complex with Cr(III) ions. Pre-concentration of Cr(VI) anions on a self-assembled pyridinium

monolayer electrode, followed by the reduction of Cr(VI) anions to Cr(III) cations, was also used to detect chromium.[15]

39. (a) Allain, L.R. Ph.D. Thesis, The University of Tennessee **1999**, Chapter 2. (b) Canada, T.A. Ph.D. Thesis, The University of Tennessee **2002**, Chapter 2.

40. The scans were highly reproducible with an average standard deviation of 1.0×10^{-3} µA for the peak currents (Section 2.3.5), suggesting that, if there are Cr(III) cations left in the film after the washing, they perhaps do not interfere with the Cr(VI) anion uptake and analysis in the subsequent cycles.

41. Pauliukaite, R.; Hocevar, S.B.; Ogorevc, B.; Wang, J. *Electroanal.* **2004**, *16*, 719.

42. Harrison, D.J.; Daube, K.A.; Wrighton, M.S. *J. Electroanal. Chem.* **1984**, *163*, 93.

43. Petit-Dominguez, M.D.; Shen, H.; Heineman, W.R.; Seliskar, C.J. *Anal. Chem.* **1997**, *69*, 703.

44. Shi, Y.; Slaterbeck, A.F.; Seliskar, C.J.; Heineman, W.R. *Anal. Chem.* **1997**, *69*, 3679.

45. Ross, S.E.; Shi, Y.; Seliskar, C.J.; Heineman, W.R. *Electrochim. Acta* **2003**, *48*, 3313.

46. The calculated detection limit here is based on three times the standard deviation of the noise level and the calibration plot established in Figure 2.7.

47.   (a) Schwarz, K.; Mertz, W. *Arch. Biochem. Biophys.* **1959**, *85*, 292. (b) Mertz, W.; Schwartz, K. *J. Physiol.* **1959**, *196*, 614.

48.   Corriu, R.J.P.; Lancelle-Beltran, E.; Mehdi, A.; Reye, C.; Brandes, S.; Guilard, R. *J. Mater. Chem.* **2002**, *12*, 1355.

Part 3

Optical Determination of Cr(VI) Using Regenerable,

Functionalized Sol-gel Monoliths

3.1. Introduction

As discussed previously, Cr(VI) is a suspected carcinogenic agent and toxic pollutant, posing a threat when present even at trace levels. Several methods have been reported for the successful determination and quantification of Cr(VI) in solution.[1-24] Some of these techniques rely on spectroscopic methods[1-12] while others depend on mass-sensitive devices[13-16] and electrochemical detection.[17-25] Of the spectroscopic techniques, many make use of diphenylcarbazide for the colorimetric determination of Cr(VI).[1-7] In this process, Cr(VI) is reduced to Cr(III) while diphenylcarbazide (DPC) is oxidized to diphenylcarbazone (DPCO), and a magenta-colored complex is formed between the reaction products that can be monitored using UV-vis spectroscopy. Using this reagent, detection limits at the low ppb level have been reported.[1,2] One major drawback of techniques using diphenylcarbazide, however, is that the reaction is irreversible, making its incorporation into regenerable sensors a difficult task.

Sol-gels have been commonly used as substrates for optical[1,26-33] and spectroelectrochemical[34] analyses mainly because they are transparent in the visible region. The porosity of the gels can easily be modified, allowing the incorporation of functional groups into the matrix and the fast transport of molecules throughout the gel interior. The two main methods of incorporating organic functional groups into sol-gel glass are doping[1,27-31] and grafting.[32,33,35,36] When doping techniques are employed, SiO_2 substrates doped with organic functional groups are formed, but leaching can often occur due to the fact that

67

the organic molecules are not chemically bound to the gel interior. In the grafting

technique, on the other hand, organic functional groups are covalently bound to

the sol-gel matrix, and leaching is not expected. Our research group has

recently reported a technique for the preparation of transparent porous silica sol-

gel monoliths containing grafted organic functional groups.[33]

In the current work, pyridine-functionalized optically transparent sol-gel

monoliths have been prepared for the optical determination of Cr(VI) in solution.

Most metal ions are cations. Chromium at its highest, VI oxidation state,

however, exists mainly as anions ($HCrO_4^-$, $Cr_2O_7^{2-}$ and $HCr_2O_7^-$ in acidic and

CrO_4^{2-} in basic solutions),[37] providing a unique opportunity for Cr(VI)

preconcentration and detection.[38] Previous studies have demonstrated the

capability of sol-gels for Cr(VI) extraction,[39] and it has been reported that

pyridinium derivatives form strong and stable complexes with Cr(VI)

species.[23,25,40-43] In the present study, 2-[2-(trimethoxysilyl)ethyl]-pyridine is

grafted to sol-gel monoliths and is used for the preconcentration of Cr(VI) inside

the gels. This preconcentration takes place as a result of the electrostatic

interaction between the positively-charged pyridinium groups in the sol-gel matrix

and the negatively-charged Cr(VI) anions in solution. At ppm levels, the

monoliths exhibit a yellow color change characteristic of the Cr(VI) absorption. At

ppb levels, the uptake can be monitored by exposing the monoliths to

diphenylcarbazide and observing the subsequent magenta-colored product

formed by the reaction of the reagent with the Cr(VI) bound inside the gel. Our

studies have shown that concentrations as low as 10 ppb Cr(VI) can be

measured using this method.

Figure 3.1 illustrates the overall sensing cycle for the process. Initially, the pyridine-functionalized sol-gel monolith is exposed to Cr(VI), and a color change occurs. The monolith can then either be partially regenerated through exposure to a basic solution of NaOH or completely regenerated through exposure to diphenylcarbazide and 6.0 M HCl. The resulting clear monolith can then be used for subsequent measurement cycles.

This chapter outlines factors and influences on the monolith preparation and Cr(VI) uptake and sensing. It demonstrates the possible use of pyridine-functionalized sol-gel monoliths as *regenerable* sensors for Cr(VI) determination. In the current approach, pyridinium-functionalized monoliths directly detect chromate (in the ppm range) and preconcentrate chromate (in the ppb range). Diphenylcarbazide is then added *after* ppb-level chromate has been preconcentrated in the monoliths. This diphenylcarbazide plays two roles in that it allows for ppb-level Cr(VI) detection and decomposes chromate for its subsequent removal from the monoliths. An acid wash is then used to regenerate the monoliths for multicycles of Cr(VI) detection. In comparison, in earlier work involving diphenylcarbazide for chromate detection,[1,2] the optodes for chromate sensing are usually for *one time use*.
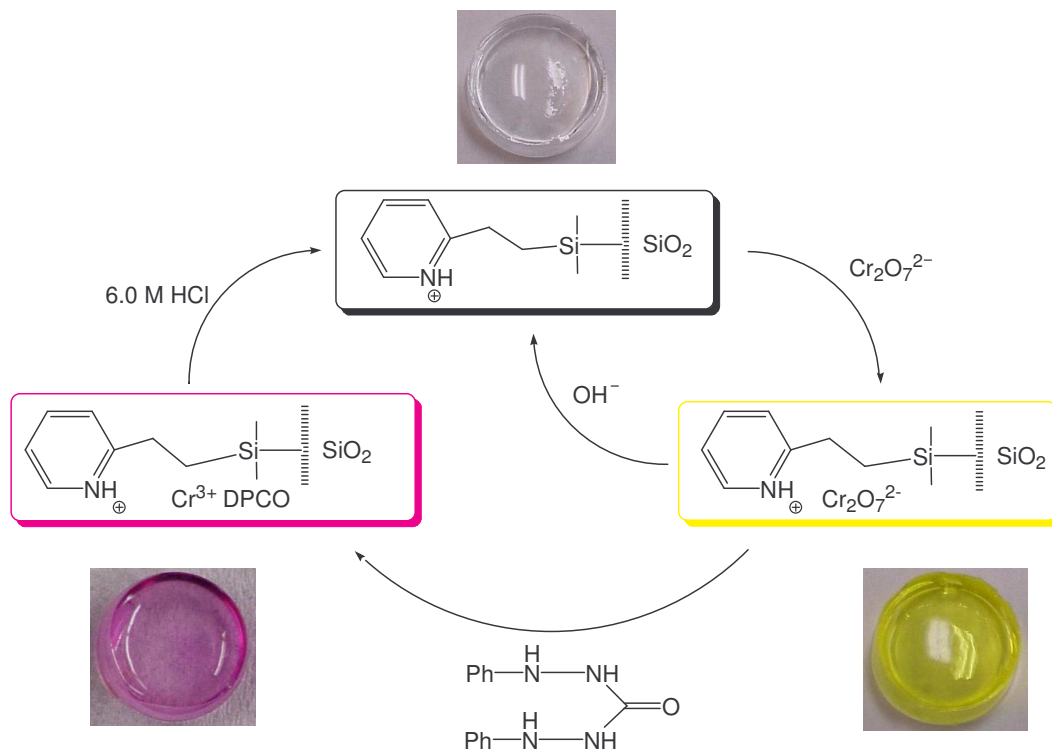
Figure 3.1. Schematic of the sensing cycle in the current system. Photographic images are not to scale.

3.2. Experimental

3.2.1. Chemical Reagents

Tetramethyl orthosilicate (TMOS, $Si(OMe)_4$, 98%, Sigma-Aldrich), 2-[2-(trimethoxysilyl)ethyl]-pyridine (Gelest), methanol (MeOH, HPLC grade, Fisher), ethylene glycol (certified A.C.S., Fisher), 1,5-diphenylcarbazide (DPC, A.C.S. reagent, Sigma-Aldrich), sodium hydroxide (NaOH, certified A.C.S., Fisher), sulfuric acid (H_2SO_4, certified A.C.S., Fisher), disodium ethylenediamine tetraacetate (EDTA, certified A.C.S., Fisher), and hydrochloric acid (HCl, certified A.C.S., Fisher) were all used as received. Standard solutions of Cr(VI) were prepared by serial dilution of a 1017 µg/mL AA standard (Sigma-Aldrich). Solutions and standards were prepared using deionized (DI) water (18 MΩ-cm) from a Barnstead International E-pure 4-holder deionization system. All solutions used in the studies were prepared fresh. In particular, the DPC solutions were always prepared immediately before use, as studies have shown that their sensitivity can decrease with time.[3]

3.2.2. Monolith Preparation

Detailed procedures of the preparation of functionalized sol-gel monoliths have been reported previously.[32] An analogous procedure was used for the sol-gel preparation in the current study. Batches of pyridine-grafted monoliths were prepared by mixing 4.5 mL of TMOS, 4.5 mL of MeOH, 2.3 mL of ethylene glycol, and, in studies in which the effect of ligand percentage was not studied, 1.2 mL

71

of 2-[2-(trimethoxysilyl)ethyl]-pyridine in a large vial. The sol solution was then

stirred to ensure a homogeneous mixture, and 625 µL of aliquots were pipetted

into each of 20 small (diameter = 13.4 mm) glass vials. NaOH (50 mM, 135 µL)

was then added to each of the vials, and gelation occurred within *ca.* 10 minutes.

The gels were covered with MeOH and allowed to stand for *ca.* 18 hours. The

MeOH was then removed, and the gels were allowed to shrink in air for *ca.* 6

hours before they were again covered in MeOH. After standing for a further 18

hours, the MeOH was removed and replaced stepwise with 75% MeOH, 50%

MeOH, 25% MeOH, and finally pure water to condition the gels and prevent them

from cracking. The resulting optically transparent monoliths, having *ca.* 12 mm

diameters and 5 mm thicknesses, were kept in water until use. Blank monoliths

were prepared in a similar manner with the exclusion of the 2-[2-

(trimethoxysilyl)ethyl]-pyridine. Figure 3.2 illustrates the sol-gel monolith

formation.

3.2.3. Instrumentation

UV-visible spectra were collected using a Hewlett-Packard 8452

photodiode array UV-vis spectrophotometer or a Thermo Spectronic BioMate 5

scanning UV-vis spectrophotometer. Atomic absorption (AA) analyses were

performed with a Perkin-Elmer 5100 atomic absorption spectrophotometer using

an air/acetylene flame under standard conditions.[44] Brunauer-Emmett-Teller

(BET) measurements were carried out using a Nova 1000 high-speed surface

area and pore size analyzer by Quantachrome Corp using N_2 gas absorption.
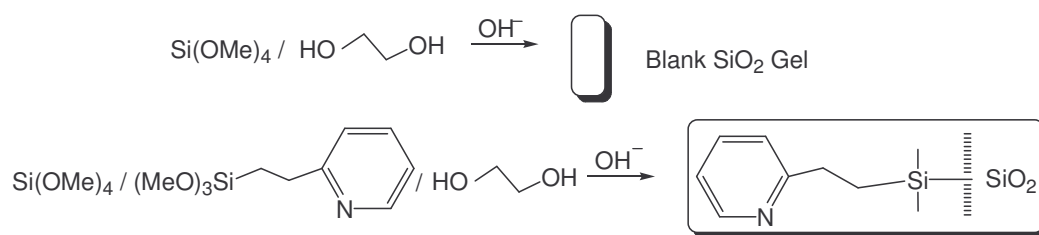
Figure 3.2. Reaction schemes for the formation of blank and functionalized sol-gel monoliths.

Scanning electron microscopy (SEM) images were obtained using a Hitachi

S4100 SEM with the field-emission gun operating at 10.0 kV. X-ray

photoelectron spectroscopy (XPS) was performed using a Phi 5100LS

spectrometer with an Al Kα source operating at 300 W and generating x-rays

with 1486.6 eV of energy. Specimens were analyzed at an electron take-off

angle of 70°, measured with respect to the surface plane. In addition, the

pressure of the chamber during analysis was 2 x 10^{-8} mtorr, and the pass energy

was 89.45 eV. When acquiring the XPS data, a neutralizer was used to cancel

the positive charging affects of the sample bombardment by x-ray photons. This

neutralizer floods the sample surface with electrons to compensate for the

electrons that are ejected by the photons. The neutralizer was set to an emission

control of 21 mA and an electron energy of 70%.

3.2.4. BET, SEM, and XPS Measurements

For the BET, SEM, and XPS studies, a pyridine-functionalized sol-gel

monolith was ground into a powder and dried at 100 °C for at least 24 hours prior

to measurement. For the BET studies, the powder was evacuated under vacuum

and then cooled to -196 °C using liquid nitrogen before analysis. The adsorption

portion of the N_2 isotherm was used to calculate the pore size distribution of the

sol-gel monoliths.[45]

3.2.5. Analysis Procedures

For the monitoring of Cr(VI) uptake, each monolith was placed in a

solution of varying concentration for a period of time. After the allotted exposure time had passed, each gel was removed from solution, thoroughly rinsed with DI water, and either analyzed by UV-vis spectroscopy or placed in another solution for further study. In many cases, the supernatant from these gels was filtered and then analyzed by AAS using standard instrumental parameters[44] and a five-point calibration plot to determine chromium content. Solutions containing DPC were prepared by mixing 0.020 g of 1,5-diphenylcarbazide and 5.0 mL of acetone in a 100 mL volumetric flask. 2.4 mL of a sulfuric acid solution, prepared by diluting 8.75 mL of concentrated sulfuric acid to 25 mL in a separate volumetric flask, were then added, and the flask was diluted appropriately. After chromium and diphenylcarbazide exposure, the gels were washed numerous times with 6.0 M HCl and then DI water before reuse in subsequent analyses.

3.3. Results and Discussion

3.3.1. Monolith Uptake of Cr(VI)

Figure 3.3 shows the ability of the pyridine-functionalized sol-gel monoliths to absorb Cr(VI). As can be seen in Figure 3.3A, when a solution of Cr(VI) with an absorption maximum at 350 nm is exposed to a pyridine-functionalized sol-gel monolith, the resulting colorless solution shows a much lower absorption at the same wavelength. This is due to the fact that the Cr(VI) has been removed from solution and is electrostatically bound to the pyridine groups present within the monolith. Figure 3.3B demonstrates that, when the functionalized monolith is
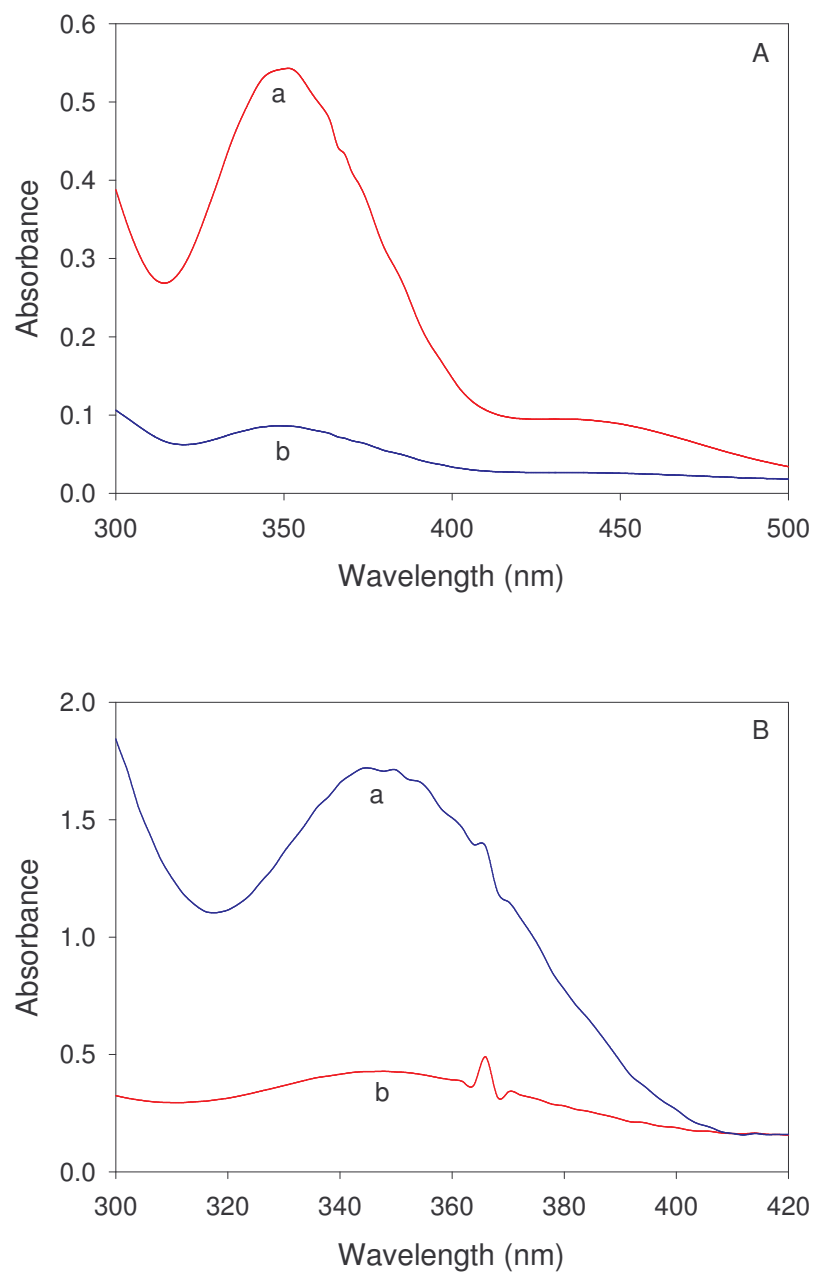
Figure 3.3. (A) 20 ppm Cr(VI) solution before (a) and after (b) exposure to a pyridine-functionalized monolith. (B) Spectra of pyridine-functionalized (a) and blank (b) monoliths after exposure to the same 20 ppm Cr(VI) solution. The Cr(VI) solutions also contained 0.1 M HCl.

76

removed from solution, it shows a very strong absorbance at about 350 nm, corresponding to Cr(VI) uptake.[8] This absorbance is even stronger than that of the original solution, due to the fact that the majority of the Cr(VI) has been concentrated within the gel. A blank monolith containing no pyridine functional groups and immersed in the same Cr(VI) solution shows a much smaller absorption.

The Cr(VI) uptake of the monoliths was further assessed by analyzing through AAS the Cr content of solutions that had been exposed to gels prepared by the methods discussed in the Experimental Section. Table 3.1 summarizes the results from one such study. Compared to the blank monoliths, the pyridine-functionalized sol-gel monoliths show a strong uptake of Cr(VI) from solution, absorbing *ca.* 75% more Cr(VI) than the blanks. In addition, the functionalized gels showed a high degree of reproducibility regarding Cr(VI) removal, indicating the consistency of the gels within the same batch as well as from batch to batch.

3.3.1.1. Effect of Mol% Ligand on Cr(VI) Uptake

In order to evaluate the affect of the monolith ligand mol percentage on Cr(VI) uptake, K_d terms were used. The K_d term is defined as

$$K_d = \frac{\mu g \text{ of } Cr(VI) \text{ absorbed / g of gel}}{\mu g \text{ / mL of equilibrium } Cr(VI) \text{ concentration}}$$

and is often used to describe the efficiency of an extraction system.[36,46]

Table 3.1. Study of the Cr(VI) removal from solution by various monoliths.[a] Concentrations are given in ppm.

Gel Used	Initial Conc.	Final Conc.	% Removed
Blank Gels	19.6	18.7 ± 0.9	$4.5 \pm 0.5\%$
Pyridine-Functionalized Batch 1	20.7	4.7 ± 0.3	$77.3 \pm 1.4\%$
Pyridine-Functionalized Batch 2	20.6	3.8 ± 0.1	$81.7 \pm 0.5\%$
Pyridine-Functionalized Batch 3	20.7	4.3 ± 0.2	$79.1 \pm 1.1\%$

[a] Each monolith was immersed in 5 mL of Cr(VI) / 0.1 M HCl solution for 5 hours. The values given are based on measurements of three gels from each batch.

Monoliths were prepared containing various mol percentages of 2-[2-(trimethoxysilyl)ethyl]-pyridine. Each was exposed to 5 mL of a solution containing 20 ppm Cr(VI) and 0.1 M HCl for 5 hours. The supernatant of each gel was then analyzed by AAS, and the K_d terms were calculated. Figure 3.4 shows a plot of K_d versus mol % ligand. As can be seen, the K_d values steadily increase and begin to level off at a mol percentage of 2.8%. At mol percentages greater than 2.8%, the K_d terms increase slightly, but it was found that gels with this increased amount of ligand were more brittle and structurally unstable. For this reason, monoliths that were used in further studies consisted of 2.8 mol% of 2-[2-(trimethoxysilyl)ethyl]-pyridine, as this amount of ligand provides optimum Cr(VI) extraction while maintaining a high degree of gel durability.

3.3.1.2. Effect of Solution pH on Cr(VI) Uptake

Based on Figure 3.1, it is logical to assume that the solution pH should have an impact on the Cr(VI) absorption since the uptake seems to be a result of electrostatic interactions between the negatively-charged Cr(VI) ions and the positively-charged pyridine groups. A study was done in which monoliths were immersed in 20 ppm Cr(VI) solutions of varying pH. After two hours of exposure, the gels were removed and analyzed by UV-vis spectroscopy. The results are shown in Figure 3.5. At solutions of high pH, there is relatively little absorption of the Cr(VI) species. This is likely due to the fact that the pyridine groups present within the monoliths are deprotonated and unable to maintain strong electrostatic
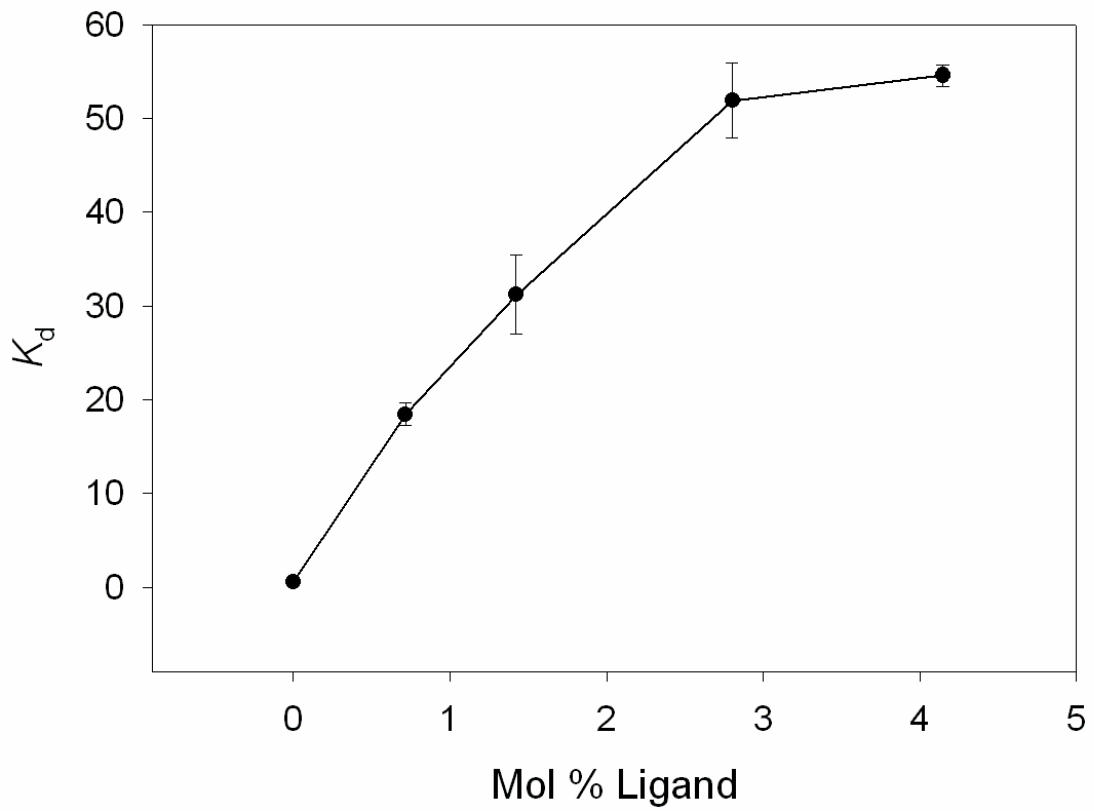
Figure 3.4. Plot of K_d vs. mol % ligand. Each data point represents an average

of measurements from three different monoliths.
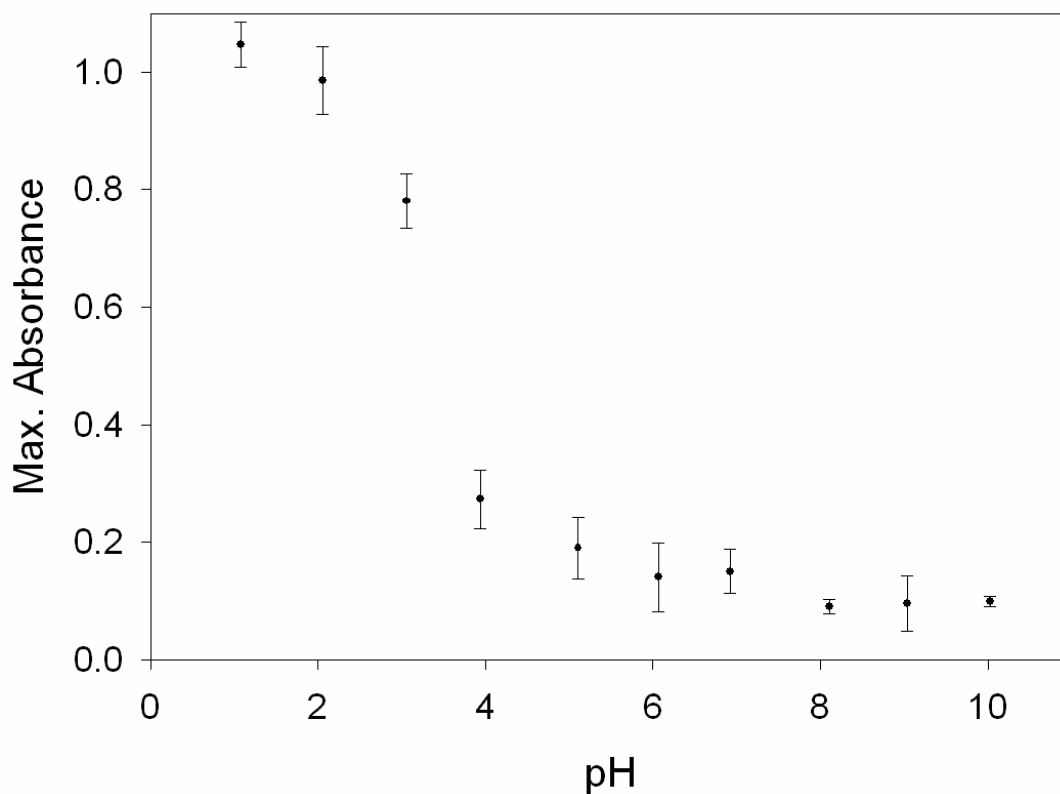
Figure 3.5. The dependence of monolith Cr(VI) removal on pH. Each monolith

was immersed in 20 mL of a 20 ppm Cr(VI) solution for 2 hours and then

analyzed by UV-vis spectroscopy. The solutions were pH adjusted using HCl

and NaOH. Data points represent an average of measurements from three gels.

interactions with the Cr(VI) species. Furthermore, the spectra collected of the gels that had soaked in Cr(VI) solutions of basic pH showed a maximum absorbance at about 370 nm.[47] This absorbance shift to higher wavelengths occurs because CrO_4^{2-} is the dominant species present in basic solutions of Cr(VI).[38] It is interesting to note that, even at high pH values, there is Cr(VI) removal from solution. This seems to suggest that the interaction between Cr(VI) and pyridine is more than a simple ion-exchange process, as has been reported previously.[23,25] Cr(VI) solutions having pH values greater than 10 were not analyzed in this study because the large concentration of OH^- ions in such solutions undergoes nucleophilic attack on the Si-(O-Si) bonds present within the gel, forming Si-OH and destroying the monolith network.

Based on the results shown in Figure 3.5, the monoliths absorb much larger amounts of Cr(VI) at lower pH values. This is likely due to the fact that pyridinium and silanol groups present within the gel are more sufficiently protonated at lower pH. The isoelectric point of silica sol-gel is close to pH = 2,[26] and the pK_a value of 2-methylpyridine has been reported as 5.96.[48] Thus, solutions of pH = 2 or lower should be sufficient for maximum gel protonation and, as a consequence, maximum Cr(VI) uptake. Taking this into account, as well as the critical role pH plays on analyte absorption (Figure 3.5), all Cr(VI) solutions were prepared containing 0.1 M HCl.

3.3.1.3. Effect of Gel Immersion Time

The uptake of Cr(VI) anions by pyridine-functionalized monoliths was

measured by monitoring the absorbance increases over time of gels exposed to

20 ppm Cr(VI) solutions.[47] The results are shown in Figure 3.6. Initially, the

absorbance increases rather linearly and quickly as the Cr(VI) species are taken

in by the gel. After *ca.* 100 minutes, however, the slope of the plot begins to

flatten out as more pyridinium sites are occupied by the Cr(VI) anions. After

about 300 minutes, the absorption changes very little. At this point, the

absorbance has reached *ca.* 95% of its maximum value, indicating that the

monolith has become saturated with Cr(VI). Figure 4.6 demonstrates the fact

that functionalized monoliths immersed in ppm level Cr(VI) solutions exhibit a

distinct color change after only a few minutes of exposure time. However, in

order for maximum Cr(VI) absorption to take place, the gels must be exposed to

the solution for an extended period.

3.3.2. Monolith Characterization

3.3.2.1. BET Analysis

BET gas adsorption experiments indicate that the pyridine-functionalized

sol-gel monolith is quite porous, with an average pore radius of *ca.* 29 Å and a

specific surface area of 502 m^2/gram. A plot of pore volume as a function of pore

radius (Figure 3.7A) indicates that the monolith has a pore size distribution that is

consistent throughout the bulk of the material. The peak of this plot near 29 Å

represents the size of the pores that contribute most to the pore volume. This

high degree of monolith porosity should aid in the transport of analyte species
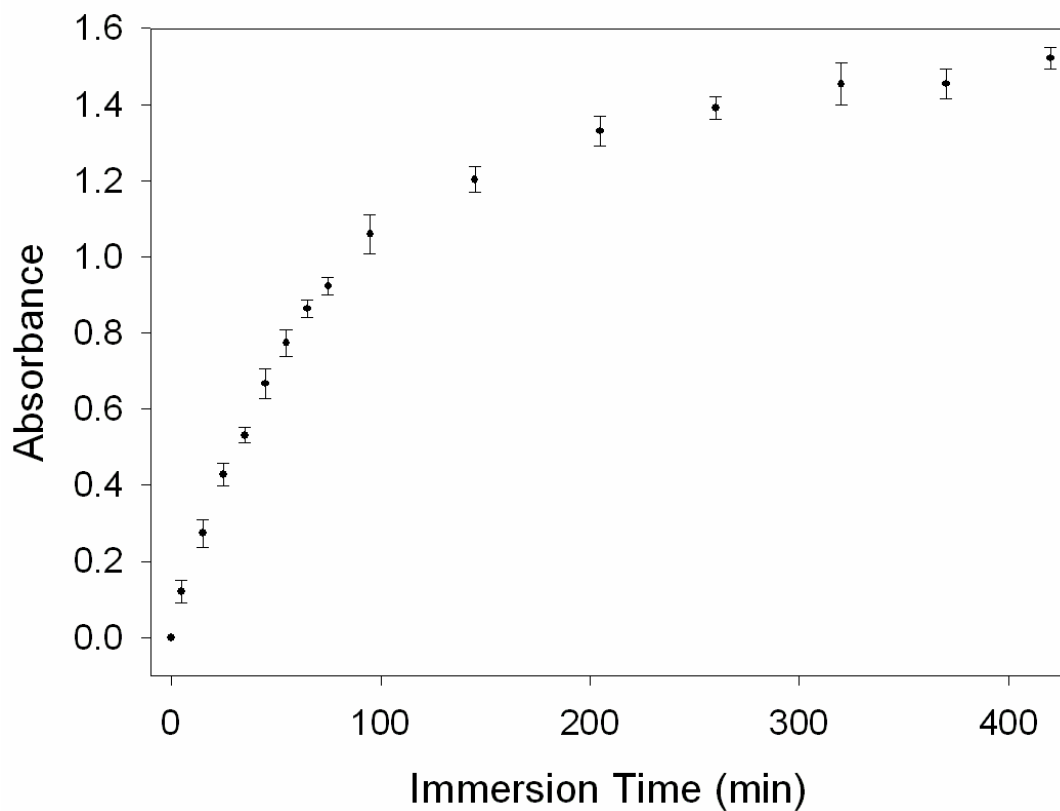
Figure 3.6. Cr(VI) uptake as a function of immersion time for a pyridine-functionalized sol-gel monolith. Four monoliths were each exposed to 20 mL of 20 ppm Cr(VI) / 0.1 M HCl, and their absorbance was periodically measured using UV-vis spectroscopy.
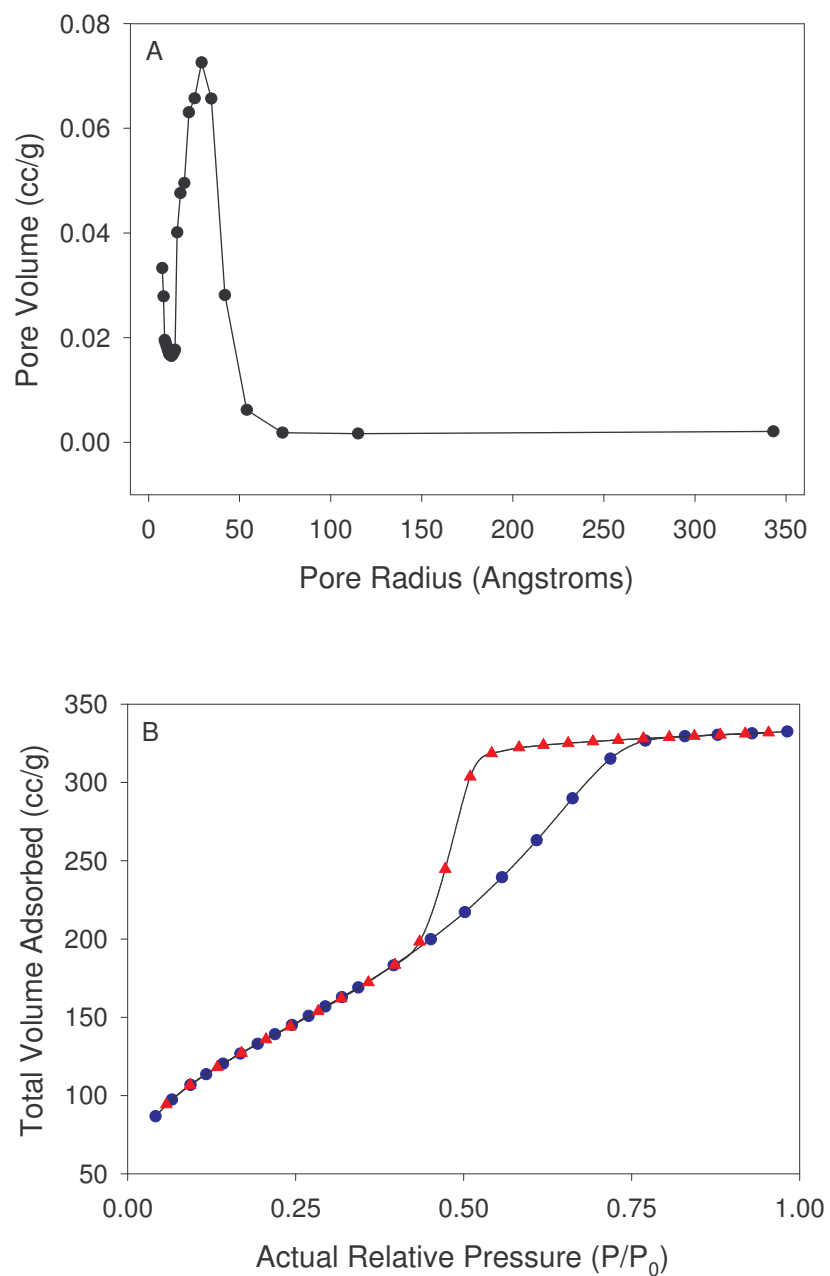
Figure 3.7. (A) BET pore size distribution for a pyridine-functionalized monolith.

(B) N$_2$ gas adsorption-desorption isotherm for the monolith; adsorption ($\bullet$),

desorption ($\blacktriangle$).

throughout the gel. Figure 3.7B shows the N_2 adsorption isotherm plot with a Z-shaped hysteresis loop. This hysteresis loop is common in porous materials including inorganic oxides and glasses.[49,50] In addition, these results are consistent with BET data obtained from similarly-prepared monoliths.[32a]

3.3.2.2. SEM and XPS Analyses

SEM images of a pyridine-functionalized monolith, obtained at 20,000× and 30,000× magnification,[47] show that the surface is not smooth. The network of particles packed together is indicative of a base-catalyzed process in which colloidal silica clusters are initially formed and then linked through gelation.[51]

XPS spectra were also obtained of pyridine-functionalized monoliths. Peaks of Si, C, O, and N were observed.[47] These peaks are consistent with the formation of a sol-gel monolith functionalized with pyridine.

3.3.3. Monoliths and the Optical Determination of Cr(VI)

The pyridine-functionalized monoliths discussed thus far are ideal for use as optical sensors as a result of their transparent, porous nature. When monoliths were exposed to Cr(VI) solutions of varying concentrations, a linear relationship (R^2 = 0.9997) was found between their absorbance at 350 nm and the Cr(VI) concentration in solution (Figure 3.8). This indicates the potential usefulness of these monoliths as sensors for Cr(VI) at the ppm level.

When the monoliths are exposed to ppb level Cr(VI) solutions, no visible color change due to Cr(VI) absorption is evident at 350 nm; concentrations at this
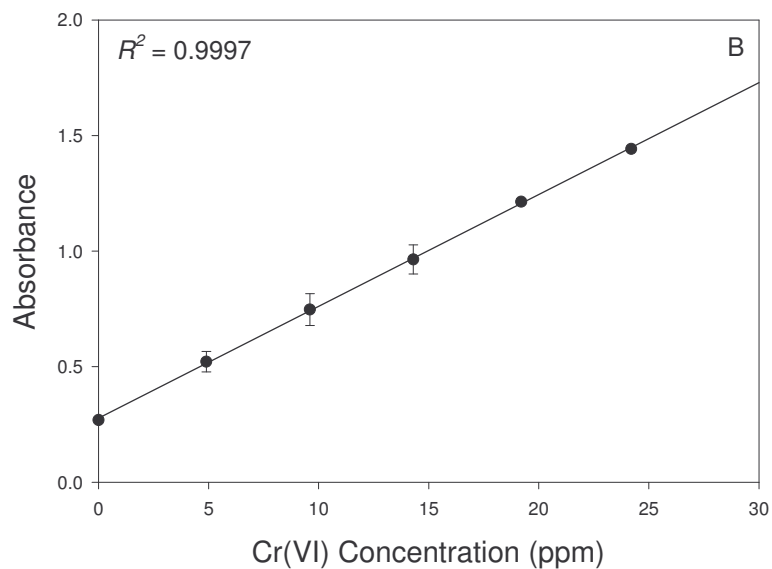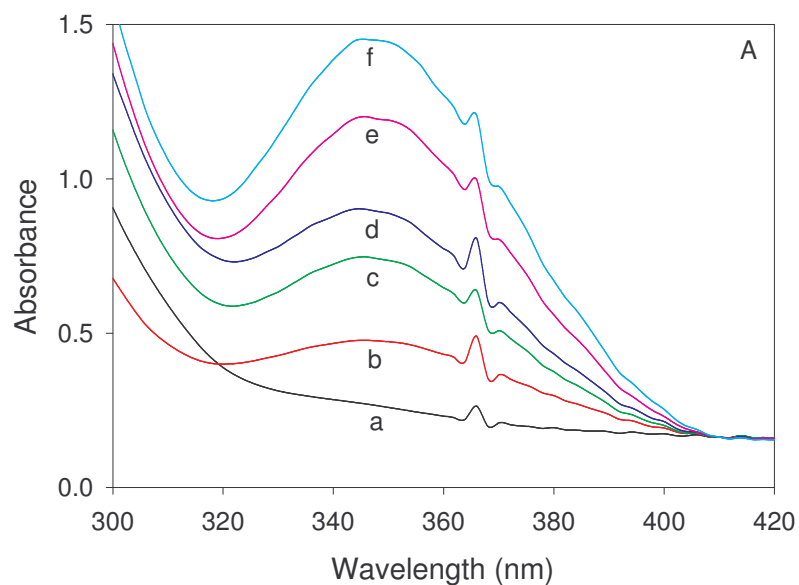
Figure 3.8. (A) Spectra acquired of functionalized monoliths immersed for 2.5 hours in 20 mL solutions consisting of 0.1 M HCl and a variable amount of Cr(VI): (a) 0 ppm; (b) 4.9 ppm; (c) 9.6 ppm; (d) 14.3 ppm; (e) 19.2 ppm; (f) 24.2 ppm. (B) The corresponding calibration plot. Data points represent an average of measurements from three gels.

level are below the limit of detection using this wavelength for measurement. However, when gels that have been previously exposed to ppb level Cr(VI) solutions are immersed in a diphenylcarbazide solution, a magenta color forms within the gel. This occurs because, after the Cr(VI) has been preconcentrated within the gel at the pyridinium sites, the diphenylcarbazide is able to diffuse through the porous gel structure and react with the bound Cr(VI). This reaction results in the formation within the gel of a magenta-colored complex between Cr(III) and diphenylcarbazone that can be monitored using UV-vis spectroscopy.

Figure 3.9 shows the obtained spectra and corresponding calibration plot of monoliths that have been exposed to ppb levels of Cr(VI) followed by subsequent immersion in diphenylcarbazide solution. As can be seen in the spectra, absorption maxima occur at about 540 nm, consistent with reported absorption spectra of the Cr(III)-diphenylcarbazone complex.[1-7] Each monolith was immersed in a minimal amount (~2 mL) of diphenylcarbazide solution to prevent the colored product from leaving the gel after complex formation. The colored complex is usually formed immediately as the porous nature of the monoliths allows the diphenylcarbazide to diffuse through the gels and react with the bound Cr(VI) quickly. However, the gels were typically allowed to soak in diphenylcarbazide solution for 60 minutes, as this length of time seemed to yield optimal color development.[47] Using this technique, Cr(VI) concentrations as low as 10 ppb could be determined.

In a separate study, monoliths were exposed to ppb level Cr(VI) solutions for a period of time, and their supernatants were then exposed to a
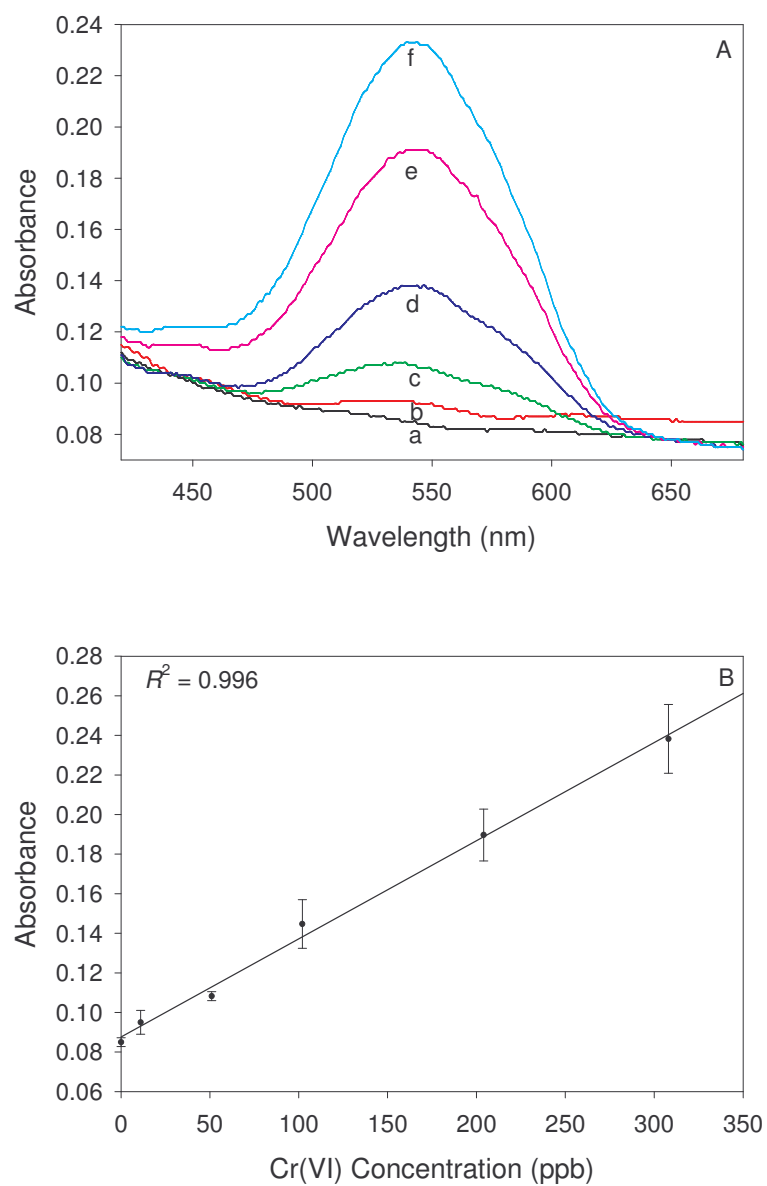
Figure 3.9. (A) Spectra of Cr(VI)-containing functionalized monoliths after exposure to diphenylcarbazide. Each gel had been previously exposed for 5 hours to a 20 mL solution consisting of 0.1 M HCl and: (a) 0 ppb; (b) 11 ppb; (c) 51 ppb; (d) 102 ppb; (e) 204 ppb; (f) 308 ppb Cr(VI). (B) The corresponding calibration plot. Data points represent an average of measurements from three gels.

diphenylcarbazide solution to determine the amount of Cr(VI) remaining.[47] The

results showed that, for monoliths exposed to solutions consisting of 156 ppb

Cr(VI), the average amount of Cr(VI) remaining in solution was 16.8 ppb. For

monoliths exposed to 59 ppb Cr(VI), the average amount of Cr(VI) remaining

in solution was below the limit of detection for the employed spectroscopic

method. This further indicates that, even at the ppb level, Cr(VI) is indeed

preconcentrated within the sol-gel monoliths.

3.3.4. Monolith Regeneration

Once the monoliths have absorbed Cr(VI) anions from solution, their

subsequent removal for monolith regeneration can be very difficult.   Various

studies were carried out to determine what medium best removed Cr(VI) from the

monoliths. The results are summarized in Table 3.2.

It is perhaps not surprising that, once a functionalized monolith has been

exposed to Cr(VI), soaking the gel in basic NaOH solution does not completely

remove all of the Cr(VI) anions present. As was seen in Figure 3.5, the pyridine-

functionalized sol-gel monoliths absorb Cr(VI) even from basic solutions. This

suggests that repeated washing of the gels with the base should not be sufficient

to remove all of the Cr(VI) bound in the monoliths. The data presented in Table

3.2 seem to confirm this fact. The percentage of Cr(VI) absorbed in the second

and third cycles drops well below the initial amount absorbed, even after several

days of washing the monoliths with basic OH^- solution. Thus, washing the gels

with base is insufficient for their complete regeneration.

Table 3.2. Cr(VI) uptake by monoliths undergoing different regeneration procedures.[a]

Gel Regeneration Method	1st Cycle	2nd Cycle	3rd Cycle
	% Absorbed	% Absorbed	% Absorbed
NaOH	$78.8 \pm 1.0\%$	$66.4 \pm 1.0\%$	$50.0 \pm 1.0\%$
DPC, 0.1 M EDTA	$78.5 \pm 1.6\%$	$54.6 \pm 2.9\%$	$55.8 \pm 1.2\%$
DPC, 6.0 M HCl	$77.2 \pm 0.3\%$	$74.1 \pm 1.3\%$	$72.2 \pm 1.9\%$

[a] Each monolith was immersed in 5 mL of *ca.* 20 ppm Cr(VI) / 0.1 M HCl solution for 5 hours, and the supernatant from each gel was analyzed by AAS. The gels were then regenerated by the given procedure and used for subsequent Cr(VI) analysis. The values given are based on measurements from three gels.

In order to completely regenerate the gels for further use, the Cr(VI) must first be reduced to Cr(III). Exposing the monoliths to diphenylcarbazide accomplishes this task. However, once the Cr(III)-diphenylcarbazone complex has formed within the gel, it must be removed so that subsequent Cr(VI) sensing cycles can take place. It was found that exposing the monoliths to 0.1 M EDTA completely removed the magenta-colored complex from the gels. It is not clear what process occurs in the EDTA wash. It is reasonable to assume that EDTA replaces diphenylcarbazone in the Cr(III)-DPCO complex. It was determined, however, that when these gels are again exposed to Cr(VI) for subsequent sensing, the amount of Cr(VI) absorbed from solution was much less than that absorbed in the initial cycle (Table 3.2). This is possibly a result of the Cr(III)-EDTA complex forming an ionic pair with the pyridinium group in the monolith. The charge on the Cr(III)-EDTA complex $[Cr(EDTA)]^-$ is -1. As such, this species will likely interact with the positively charged pyridinium group in the gel and remain entrapped in the monolith. Thus, washing the monolith with EDTA after prior exposure to diphenylcarbazide forms a Cr(III)-EDTA complex which occupies the pyridinium sites and prevents regeneration of the molith from taking place.

In search of a reagent to regenerate the monoliths, it was found that a simple wash of monoliths containing the Cr(III)-diphenylcarbazone complex with 6.0 M HCl resulted in completely colorless gels. Subsequent Cr(VI) uptake studies showed that the monoliths had been almost completely regenerated for further sensing use (Table 3.2). The disappearance of the magenta-color

suggests that the acid has decomposed the Cr(III)-diphenylcarbazone species, helping their removal from the monoliths. In addition, the acid wash may reactivate the sol-gels. In a study of Cr(VI) extraction and reduction,[39] Dave and coworkers have reported the use of an acidic solution to refurbish protons in their sol-gel matrix. The addition of a 6.0 M HCl solution may aid in the removal of the Cr(III) and diphenylcarbazone from the gel by fully protonating the pyridinium sites. These positively-charged pyrdinium groups may help to repulse and expel the Cr(III). Gels that have been exposed to both ppm and ppb levels of Cr(VI) can be regenerated for subsequent sensing cycles using this technique.

3.3.5. Measurement of a Cr(VI)-containing Sample

The selectivity of pyridinium organic functional groups for Cr(VI) has been previously reported.[23,25] In order to demonstrate the feasibility of using these monoliths for Cr(VI) sensing in environmental applications, a sample of water was obtained from a nearby lake and spiked with 85 ppb Cr(VI) and pH adjusted to 1. A monolith was then exposed to 20 mL of this solution for 6 hours, rinsed thoroughly with DI water, and further exposed to a diphenylcarbazide solution for one hour. A UV-vis spectrum of the gel was taken, and this spectrum was compared to that of a control gel that was exposed to the same Cr(VI) concentration (prepared in DI water) for the same length of time and having the same acidity. The monolith exposed to the spiked lake water sample showed a maximum absorbance at 540 nm of 0.036 relative to a gel exposed to 0 ppb Cr(VI), while the control monolith showed a maximum absorbance at 540 nm of

0.034 relative to a gel exposed to 0 ppb Cr(VI).[47] The relatively small error,

5.9%, associated with these absorbance values suggests that any biological

and/or chemical interferents present in the lake water sample do not have a

significant impact on the acquired measurements. This demonstrates the

potential of these pyridine-functionalized monoliths for use in environmental

Cr(VI) monitoring applications.

3.4. Conclusions

Pyridine-functionalized sol-gel monoliths have been prepared for the

determination of Cr(VI) in solution. These optically transparent, porous gels were

found to preconcentrate Cr(VI) through the electrostatic interaction between the

positively-charged pyridinium groups present within the monolith and the

negatively-charged Cr(VI) anions in solution. At the ppm level, the Cr(VI)

concentration was determined by monitoring the absorption of the

preconcentrated colored analyte at 350 nm. At the ppb level, the

preconcentrated Cr(VI) could be analyzed by exposing the gel to

diphenylcarbazide and monitoring the absorbance at 540 nm of the colored

product present within the monolith. The use of the gels for the analysis of Cr(VI)

at both the ppm and ppb levels suggests that they have a wide dynamic range

and can be used for monitoring Cr(VI) at a variety of concentrations.[47] In

addition, these monoliths can be regenerated through exposure to 6.0 M HCl,

making their repeated use for Cr(VI) analysis possible. As a result, these

monoliths are unique in that they make use of diphenylcarbazide for ppb level

determination of Cr(VI) while maintaining the ability to be regenerated for

subsequent sensing use. Their incorporation into a flow cell for the online

monitoring of Cr(VI), for e.g. environmental applications, is entirely possible.

References

1.   Zevin, M.; Reisfeld, R.; Oehme, I.; Wolfbeis, O.S. *Sens. Actuators* **1997**, *B38-39*, 235.

2.   Scindia, Y.M.; Pandey, A.K.; Reddy, A.V.R.; Manohar, S.B. *Anal. Chim. Acta* **2004**, *515*, 311.

3.   Urone, P.F. *Anal. Chem.* **1955**, *27*, 1354.

4.   Pflaum, R.T.; Howick, L.C. *J. Am. Chem. Soc.* **1956**, *78*, 4862.

5.   Allen, T.L. *Anal. Chem.* **1958**, *30*, 447.

6.   Willems, G.J.; Blaton, N.M.; Peeters, O.M.; De Ranter, C.J. *Anal. Chim. Acta* **1977**, *88*, 345.

7.   Dedkova, V.P.; Shvoeva, O.P.; Sawin, S.B. *J. Anal.Chem.* **2001**, *56*, 758.

8.   Mignani, A.G.; Romolini, A. *Spectrosc. Lett.* **2002**, *35*, 467.

9.   Tao, S.; Winstead, C.B.; Xian, H.; Soni, K. *J. Environ. Monit.* **2002**, *4*, 815.

10.   Balasubramanian, S.; Pugalenthi, V. *Talanta* **1999**, *50*, 457.

11.   Posta, J.; Berndt, H.; Luo, S.K.; Schaldach, G. *Anal. Chem.* **1993**, *65*, 2590.

12.   Bazzi, A.; Kreuz, B.; Wuokila, J.; Maqboul, A. *J. Chem. Ed.* **2005**, *82*, 435.

13.   Ji, H.-F.; Thundat, T.; Dabestani, R.; Brown, G.M.; Britt, P.F.; Bonnesen, P.V. *Anal. Chem.* **2001**, *73*, 1572.

14.   Zhang, Y.; Ji, H.-F.; Brown, G.M.; Thundat, T. *Anal. Chem.* **2003**, *75*, 4773.

15.   Pinnaduwage, L.A.; Boiadjiev, V.I.; Brown, G.M.; Thundat, T.; Petersen, S.W. *Sens. Lett.* **2004**, *2*, 25.

16.   Tian, F.; Boiadjiev, V.I.; Pinnaduwage, L.A.; Brown, G.M.; Thundat, T. *J.*

Vac. Sci. Technol. A **2005**, *23*, 1022.

17.   Cox, J.A.; Kulesza, P.J. *Anal. Chim. Acta.* **1983**, *154*, 71.

18.   Paniagua, A.R.; Vazquez, M.D.; Tascon, M.L.; Sanchez Batanero, P. *Electroanal.* **1993**, *5*, 155.

19.   Svancara, I.; Foret, P.; Vytras, K. *Talanta* **2004**, *64*, 844.

20.   Welch, M.W.; Nekrassova, O.; Compton, R.G. *Talanta* **2005**, *65*, 74.

21.   Yang, Y.-J.; Huang, H.-J. *Anal. Chem.* **2001**, *73*, 1377.

22.   Lin, L.; Lawrence, N.S.; Thongngamdee, S.; Wang, J.; Lin, Y. *Talanta* **2005**, *65*, 144.

23.   Turyan, I.; Mandler, D. *Anal. Chem.* **1997**, *69*, 894.

24.   Ge, H.; Zhang, J.; Wallace, G.G. *Anal. Lett.* **1992**, *25*, 429.

25.   Carrington, N.A.; Yong, L.; Xue, Z.-L. *Anal. Chim. Acta* **2006**, *572*, 17.

26.   Brinker, C. J.; Scherer, G. W. *Sol-Gel Science*, Academic Press: San Diego, 1990.

27.   Hench, L.L.; West, J.K. *Chem. Rev.* **1990**, *90*, 33.

28.   Avnir, D. *Acc. Chem. Res.* **1995**, *28*, 328.

29.   Dave, B.C.; Dunn, B.; Valentine, J.S.; Zink, J.I. *Anal. Chem.* **1994**, *66*, 1120A.

30.   (a) Allain, L.R.; Sorasaenee, K.; Xue, Z.-L. *Anal. Chem.* **1997**, *69*, 3076. (b) Allain, L.R.; Xue, Z.-L. *Anal. Chim. Acta* **2001**, *433*, 97. (c) Allain, L.R.; Canada, T.A.; Xue, Z.-L. *Anal. Chem.* **2001**, *73*, 4592. (d) Canada, T.A.; Allain, L.R.; Beach, D.B.; Xue, Z.-L. *Anal. Chem.* **2002**, *74*, 2535. (e) Allain, L.R.; Xue, Z.-L. *Anal. Chem.* **2000**, *72*, 1078. (f) Canada, T.A.;

Xue, Z.-L. *Anal. Chem.* **2002**, *74*, 6073. (g) Canada, T.A.; Beach, D.B.;
Xue, Z.-L. *Anal. Chem.* **2005**, *77*, 2842. (h) Im, H.-J. ; Yang, Y.-H. ;
Allain, L.R. ; Barnes, C.E. ; Dai, S. ; Xue, Z.-L. *Environ. Sci. Technol.*
2000, *34*, 2209.

31.   (a) Rickus, J.L.; Dunn, B.; Zink, J.I. in *Optical Biosensors* (Eds: Ligler,
        F.S.; Rowe Taitt, C.A.) 2002, pp. 427-456. (b) Lan, E.H.; Dave, B.C.;
        Fukuto, J.M.; Dunn, B.; Zink, J.I.; Valentine, J.S. *J. Mater. Chem.* **1999**, *9*,
        45.

32.   (a) Clavier, C.W.; Rodman, D.L.; Sinski, J.F.; Allain, L.R.; Im, H.-J.; Yang,
        Y.; Clark, J.C.; Xue, Z.-L. *J. Mater. Chem.* **2005**, *15*, 2356. (b) Clavier,
        C.W. MS Thesis, The University of Tennessee, **2001**, Chapter 3.

22.   Rodman, D.L.; Pan, H.; Clavier, C.W.; Feng, X.; Xue, Z.-L. *Anal. Chem.*
        2005, *77*, 3231.

34.   See, e.g., (a) Ross, S.E.; Shi, Y.; Seliskar, C.J.; Heineman, W.R.
        Electrochim. Acta **2003**, *48*, 3313. (b) Hu, Z.; Slaterbeck, A.F.; Seliskar,
        C.J.; Ridgway, T.H.; Heineman, W.R. *Langmuir* **1999**, *15*, 767.

35.   Schubert, U.; Husing, N.; Lorentz, A. *Chem. Mater.* **1995**, *11*, 2010.

36.   Feng, X.; Fryxell, G.E.; Wang, L.-Q.; Kim, A.Y.; Liu, J.; Kemner, K.M.
        Science **1997**, *276*, 923.

37.   Bichromate ($HCrO_4^-$) is believed to be the predominant Cr(VI) species in
        dilute, acidic solution at pH < 6.5. However, there have been
        controversies recently about whether bichromate ($HCrO_4^-$) exists. See,
        e.g. (a) House, D.A. *Adv. Inorg. Chem.* **1997**, *44*, 341. (b) Poulopoulou,

V.G.; Vrachnou, E.; Koinis, S.; Katakis, D. *Polyhedron* **1997**, *16*, 521. (c) Ramsey, J.D.; Xia, L.; Kendig, M.W.; McCreery, R.L. *Corrosion Sci.* **2001**, *43*, 1557.

38.   Greenwood, N.N.; Earnshaw, A. Chemistry of the Elements, 2nd ed., Elsevier Science, London, 1997, pp. 1002-1040.

39.   Deshpande, K. ; Cheung, S. ; Rao, M.S. ; Dave, B.C. *J. Mater. Chem.* **2005**, *15*, 2997.

40.   Camelot, M. *Rev. Chim. Miner.* **1969**, *6*, 853.

41.   Corey, E.J.; Schmidt, G. *Tetrahderon Lett.* **1979**, *5*, 399.

42.   Martin-Zarza, P.; Gili, P.; Rodriguez-Romero, F.V.; Ruiz-Perez, C.; Solans, X. *Polyhedron* **1995**, *14*, 2907.

43.   Sisler, H.; Ming, W.Ch.L.; Metter, E.; Hurley, F.R. *J. Am. Chem. Soc.* **1953**, *75*, 446.

44.   Perkin-Elmer Corp., *Analytical Methods for Atomic Absorption Spectroscopy*, 1996.

45.   Studies have shown that the application of desorption branches of isotherms to calculate pore size distributions may lead to artificial narrowing of peaks. See ref. 49 for more details.

46.   Chen, X.; Feng, X.; Liu, J.; Fryxell, G.E.; Gong, M. *Sep. Sci. Technol.* **1999**, *34*, 1121.

47.   See Appendix B.

48.   Gero, A.; Markham, J.J. *J. Org. Chem.* **1951**, *16*, 1835.

49.   Kruk, M.; Jaroniec, M. *Chem. Mater.* **2000**, *12*, 222.

50. Kruk, M.; Jaroniec, M. *Chem. Mater.* **2001**, *13*, 3169.

51. Buckley, A.M.; Greenblatt, M. *J. Chem. Educ.* **1994**, *71*, 599.

Part 4

Palladium and the Electrochemical Quartz Crystal Microbalance:

A New Method for the In-situ Analysis of the Precious Metal in

Aqueous Solutions

4.1. Introduction

Ever since the ability of palladium to absorb hydrogen gas was reported in 1866, the precious metal and its derivatives have been extensively used with a considerable impact in many industries.[1-4] About 10% of the palladium produced in the world is used for catalytic reactions in chemical, pharmaceutical and petroleum industries,[1-4] while 46% is used in the manufacture of electronic components, and 25% is used in dentistry.[4]

Atomic absorption (AA) and emission (AE) spectroscopy and inductively-coupled plasma mass spectrometry (ICP-MS) are the conventional techniques commonly employed for the detection and quantification of palladium.[5-7] Although these methods provide good sensitivity, they require expensive instrumentation. In addition, they are not used in in-situ analyses. Colorimetric techniques are also commonly employed for the determination of palladium. One such method relies on Pd(II) complexation with N,N-dimethyl-4-nitrosoaniline.[8] The resulting yellow-orange complex can be analyzed using UV-Vis spectroscopy with low detection limits. This technique suffers, however, from a relatively lengthy sample preparation step and, again, its inability to analyze samples in-situ.

Electrochemical techniques are also commonly used in palladium quantification. Adsorptive stripping voltammetry and differential-pulse polarography are two reported electrochemical methods for Pd analysis.[9-12] Such techniques involve the preconcentration of palladium for analysis and provide very low detection limits. However, dropping mercury electrodes are

commonly used to carry out such analyses, and their use has been somewhat reduced due to the hazards associated with handling mercury. More recently, carbon paste electrodes have been used.[13-14] Despite the low sensitivity provided by such electrodes, the carbon surface must be renewed before each measurement. Recently, Aghamohammadi and Alizadeh reported polymeric membrane and coated wire palladium(II)-selective electrodes for palladium analysis.[15] Such an analysis is based on the ion pair formation between $PdBr_4^{2-}$ anions and hexadecylpyridinium cations that are doped in a poly(vinyl chloride) matrix plasticized with *o*-nitrophenyloctylether. The authors indicated fast response times by the portable probe and interferences from several ions commonly present in aqueous solutions.

The quartz crystal microbalance (QCM) and electrochemical quartz crystal microbalance (EQCM) techniques have been used for the determination of several metals.[16] Copper,[17,18] nickel,[19] zinc,[19] lead,[20] cadmium,[20] mercury,[21] and other metals have been quantified using QCM. However, to our knowledge, little has been reported of the quantitative analysis of palladium or other precious metals by EQCM.[16,22-24] In addition, most EQCM processes use conventional gold-coated quartz crystals in their analyses. The proposed technique utilizes less common carbon-coated quartz crystals to carry out the desired palladium determination.

The present work describes a new method by which Pd(II) ions can be *directly* detected and quantified using EQCM. In our study, Pd(II) ions are deposited onto an unmodified carbon-coated quartz crystal using a negative

potential, and the corresponding change in frequency is measured. *No complexing agent is used in the current process.* Palladium on the carbon-coated quartz crystal is then easily stripped, regenerating the crystal for further use in the next cycle of palladium analysis. Unlike carbon paste electrodes that require repeated polishing for renewal of the electrode surface, repeated scans can be carried out without removing the crystal from solution. In addition, unlike conventional techniques of Pd determination such as AAS and ICP-MS, the proposed technique can be used for the in-situ analysis of this precious metal. The use of this simple, direct and reproducible technique is discussed.

4.2. Experimental

4.2.1. Reagents

Stock solutions of $PdCl_2$ (Strem Chemicals, 99.9%) and $PdSO_4$ (Alfa Aesar, 99%) were prepared in volumetric flasks and diluted appropriately using deionized water. Electrolyte solutions were prepared from KCl (Mallinckrodt Chemicals), H_2SO_4 (Fisher Scientific), and/or NaF (Sigma-Aldrich, 99.99%), respectively. $FeCl_2 \cdot 2H_2O$, KH_2PO_4, and $NaNO_3$ (all Fisher Scientific) were used as received for the interference studies. AA standards (Acros Organics) were purchased to verify the concentrations of the palladium solutions.

4.2.2. Carbon-coated Quartz Crystals

The polished, mounted, and bonded crystals were used as received from

the International Crystal Manufacturing Company, Inc. (Oklahoma City, OK). Each crystal had a fundamental frequency of approximately 7.995 MHz and an electrode diameter of 0.546 cm, consisting of a 1000 Å film of carbon deposited on a 100 Å layer of chromium.

4.2.3. Instrumentation

A model 400 Electrochemcial Quartz Crystal Microbalance and corresponding software from CH Instruments, Inc. (Austin, TX), were used for the electrochemical studies. Platinum wire and silver/silver chloride were used as the auxiliary and reference electrodes, respectively. A Teflon crystal cell, similar to that reported by Gomes,[16] was used for the batch analysis of the Pd(II)-containing solutions. A model 5100 Atomic Absorption (AA) Spectrophotometer from Perkin-Elmer was used to verify Pd(II) concentrations, and a Hewlett-Packard 8452 photodiode array UV-vis spectrophotometer was used for the method validation study.

4.2.4. Experimental Procedure

Before each experimental run, the crystal cell was purged of O_2 with N_2 gas for 15 min, and the N_2 flow over the solution continued throughout each experiment. Several scans were then run, using only the electrolyte solution, to establish a constant frequency baseline (±5 Hz). All Pd(II) depositions took place in the presence of an electrolyte solution, typically consisting of H_2SO_4 (50.4 mM) and KCl (3.22 mM). Based on the cyclic voltammogram, Figure 4.1, Pd

106
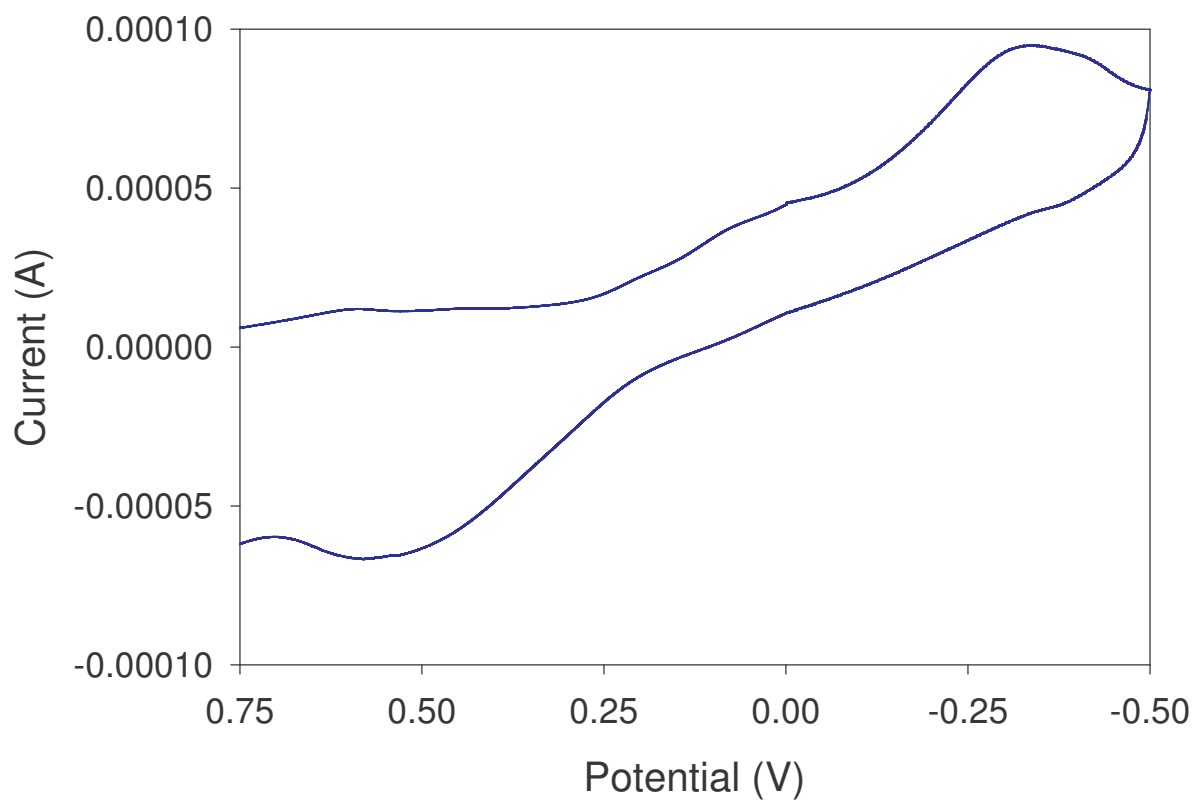
Figure 4.1. Cyclic voltammogram of a PdCl$_2$ solution.

deposition was carried out at –0.4 V, and subsequent stripping took place at 0.6 V. Between experimental runs, the crystal cell was rinsed with several aliquots of deionized water and electrolyte solution.

4.3. Results and Discussion

4.3.1. Initial Studies Using Conventional Gold QCM Crystals

Prior to the use of the carbon-coated quartz crystals for Pd(II) analysis, we conducted Pd(II) studies using gold-coated quartz crystals to quantitatively analyze aqueous $PdCl_2$ solutions. However, the applied anodic potentials necessary to strip Pd from the quartz crystals after deposition were found to strip the gold film as well, leading to the degradation of the quartz crystals. This was likely due to the formation of an alloy between Au and Pd.[26-28] Figure 4.2 demonstrates the frequency change that results when a stripping potential of 0.6 V is applied to a gold-coated quartz crystal that has palladium deposited onto its surface. During the stripping process, the gold film is removed in addition to the palladium, resulting in a frequency change several orders of magnitude greater than expected. As a result, conventional gold quartz crystals were unsuitable for Pd analysis after the gold film had been removed.

4.3.2. Palladium Deposition

Figure 4.3 shows frequency curves for palladium deposited from a $PdCl_2$ solution at a potential of –0.4 V over a time period of 60 s. Each concentration
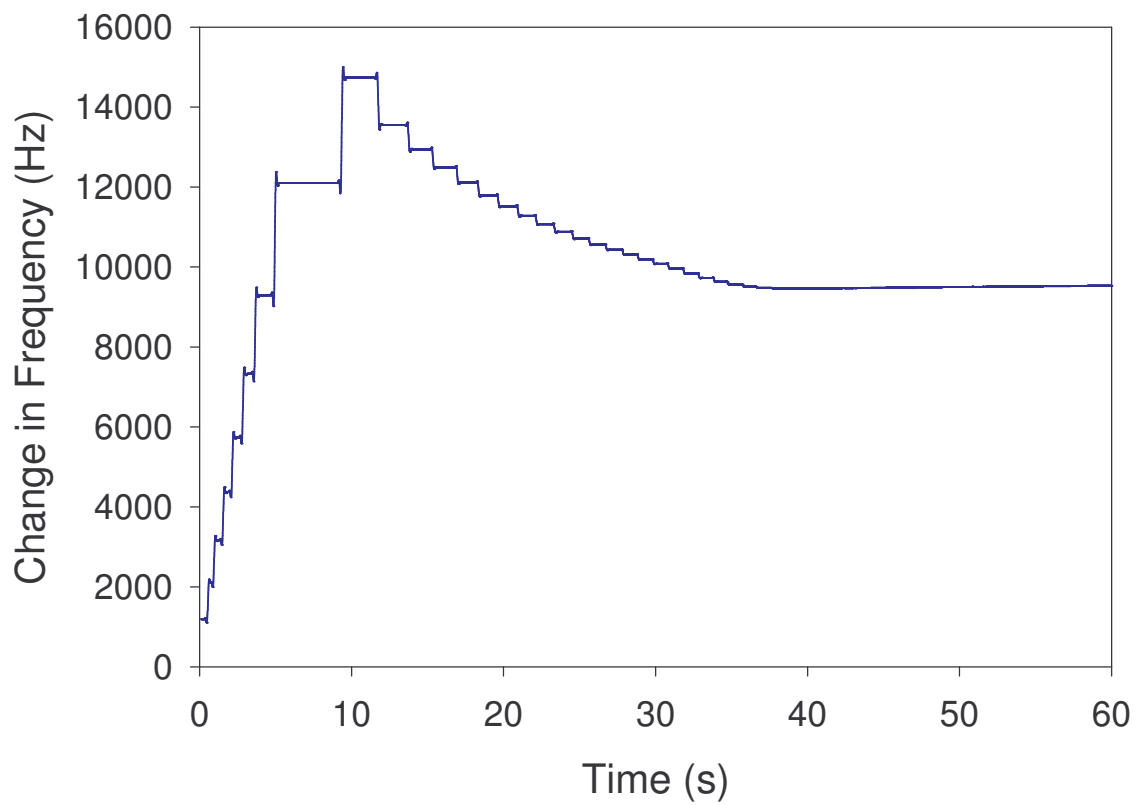
Figure 4.2. Frequency change that occurs when deposited Pd is stripped from gold QCM crystal.
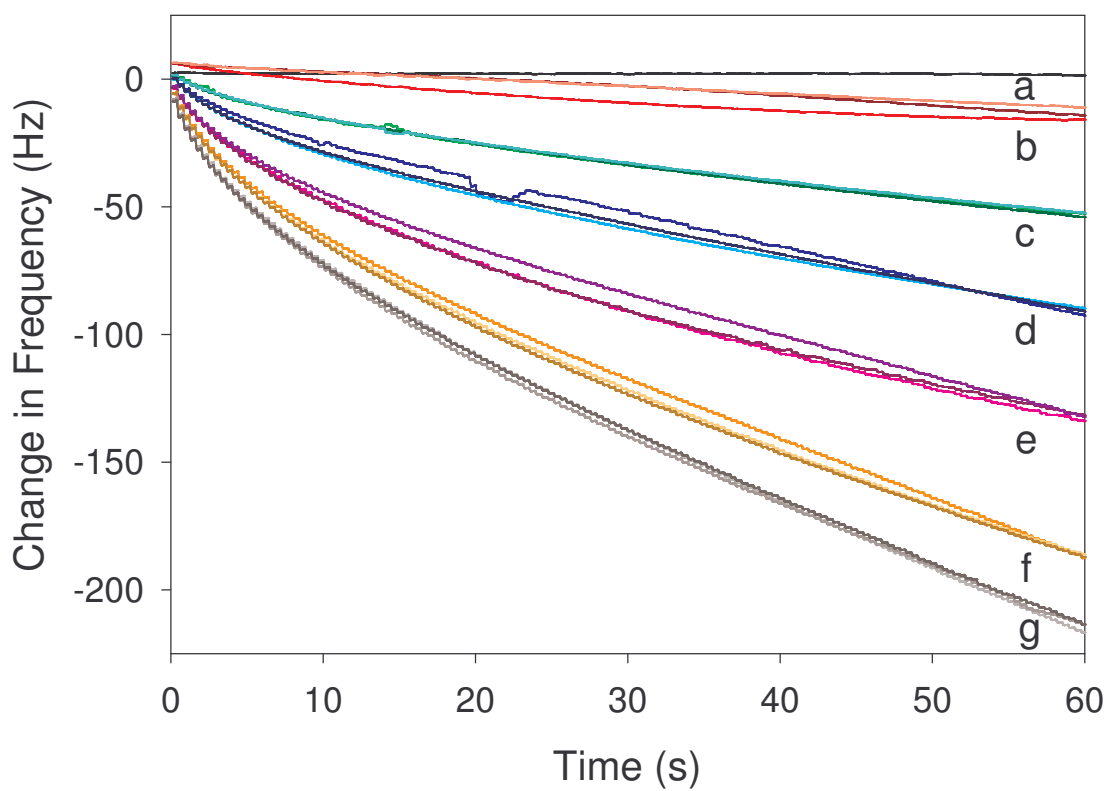
Figure 4.3. Frequency changes for the deposition of Pd from various $PdCl_2$ concentrations: (a) baseline; (b) 0.0156 mM; (c) 0.0780 mM; (d) 0.156 mM; (e) 0.234 mM; (f) 0.312 mM; (g) 0.390 mM. Three separate deposition measurements were run for each concentration.

was analyzed three times. As is expected from the Sauerbrey equation (Eq. 1.2),[23,24,29-31] the overall frequency change increases as the adsorbed mass of palladium increases. The shape of the curves seems to indicate that the deposition process is controlled by diffusion. Initially, the Pd(II) ions in close proximity to the electrode surface are reduced to Pd metal and plated out onto the crystal, decreasing its vibrational frequency. As time proceeds, however, an overpotential is necessary to deliver Pd(II) ions from the bulk solution to the electrode surface. Thus, each curve begins to slightly flatten out as time proceeds.

From these six concentrations, a calibration plot was established (Figure 4.4) based on the overall frequency change for each concentration over a time period of sixty seconds. Each point consists of an average of three deposition measurements, with each data point having an average standard deviation of <2 Hz. The lowest Pd(II) concentration detected using this technique was 0.0156 mM Pd^{2+}, or 1.66 ppm. We found that this technique may achieve an even lower limit of detection if a longer deposition time is used. Buttry has shown, however, that EQCM measurements are easily affected by temperature changes,[23] and longer deposition times are more likely influenced by changes in temperature caused by the environment. Thus, longer deposition times may be more prone to error. It can be certain, however, that crystals of a higher fundamental frequency will give lower limits of detection.

In a separate study,[25] a 0.0780 mM Pd^{2+} solution was measured multiple times to further investigate the reproducibility of the proposed method. For seven
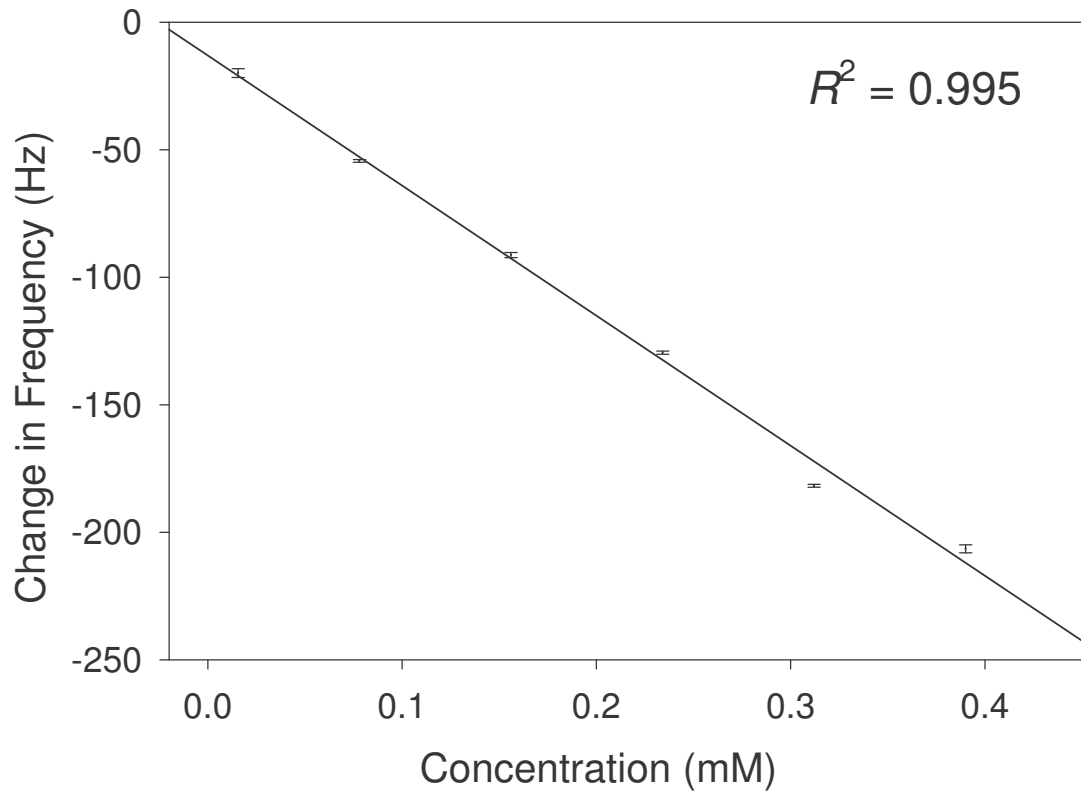
Figure 4.4. Calibration plot based on the deposition frequency changes shown

in Figure 4.3.

deposition measurements, the average change in frequency was 48.44 Hz with a relative standard deviation of 4.15%. Such a stable response over numerous deposition cycles indicates that this technique can be used for repeated Pd^{2+} analyses. However, the error associated with these measurements, as well as other measurements in this study, may be the result of hydrogen electrosorption in palladium during metal deposition. Czerwinski and coworkers[33-35] have shown that hydrogen electrosorption in palladium is accompanied by an additional frequency shift that can be attributed to the stresses generated inside the Pd metal. Thus, hydrogen sorption on palladium deposited during the reported analyses could result in an added frequency shift that adversely influences the collected measurements.

4.3.3. Stripping Palladium

Figure 4.5 shows the stripping curves measured after deposition of palladium from solutions containing varying concentrations of the metal. As expected, the frequency change is typically greater for solutions containing a higher Pd(II) concentration. The stripping curves, however, do not provide as accurate an assessment of the Pd(II) concentration as the deposition curves; the corresponding calibration plot has a much lower correlation coefficient (Figure 4.6). It is not clear what caused this inaccurate assessment of the Pd(II) concentration in the stripping measurements; it is possible that carbon particles were removed as well as palladium from the crystal surface, yielding increased frequency changes and a lower degree of reproducibility of the stripping signals.
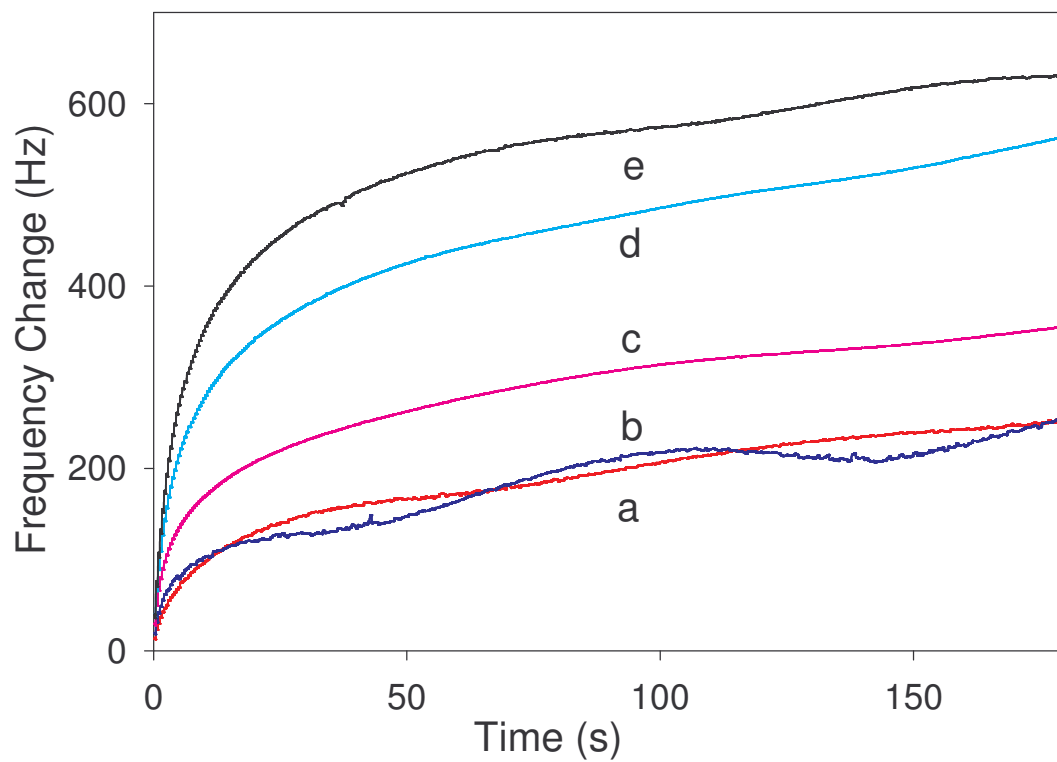
Figure 4.5. Frequency changes for Pd stripping after deposition from $PdCl_2$ solutions of varying concentrations: (a) 0.0780 mM; (b) 0.156 mM; (c) 0.234 mM; (d) 0.312 mM; (e) 0.390 mM.
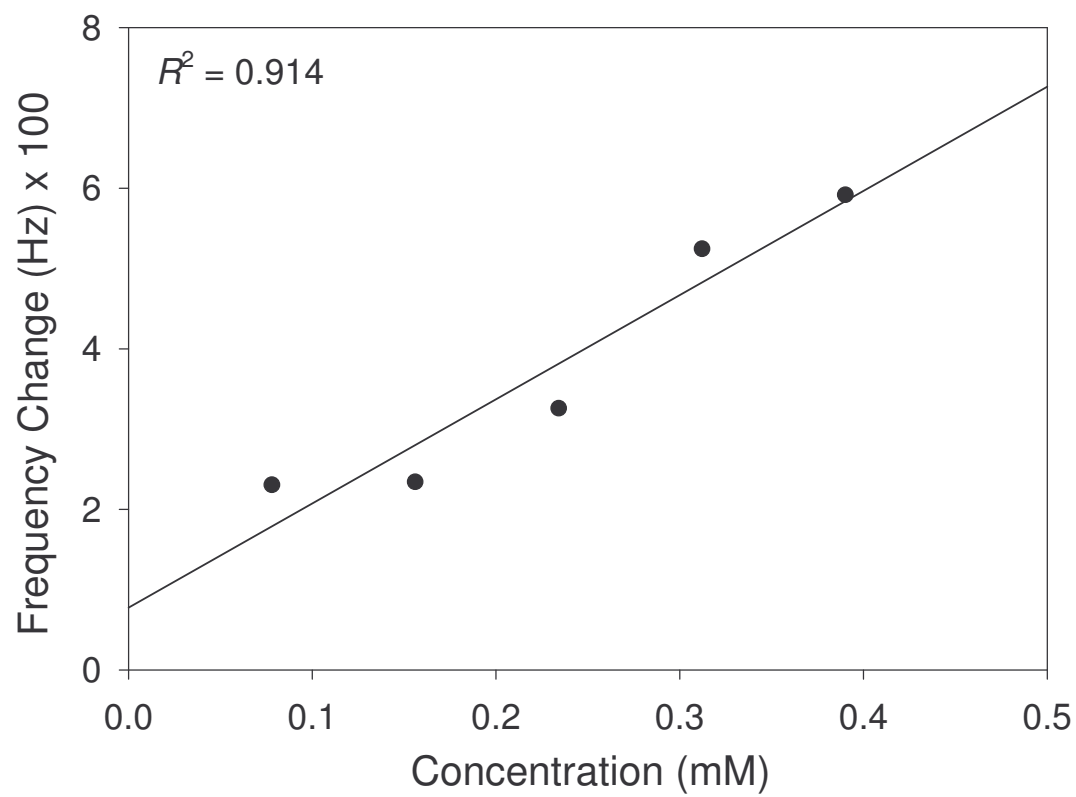
Figure 4.6. Calibration plot based on the stripping frequency changes shown in Figure 4.5.

However, the stripping step was found adequate in the removal of palladium from the quartz crystal, thus regenerating it for further usage.

4.3.4. Pd(II) Analysis in $PdCl_2$ and $PdSO_4$ Solutions

The reduction potential of Pd(II) is dependent on the ligands bonded to Pd(II) ions.[23,32] When no ligands (other than water) are present, palladium(II) in e.g., an aqueous $PdSO_4$ solution exists as the water complex $Pd(H_2O)_4^{2+}$ (or simply Pd^{2+}) with the corresponding reduction potential in Eq. 4.1. The presence of Cl^- ions yields the $PdCl_4^{2-}$ complex and a new reduction potential in Eq. 4.2. Thus, it is possible that frequency changes for equal concentrations of $PdSO_4$ and $PdCl_2$ could be different.

$$Pd^{2+} + 2e^- \rightleftharpoons Pd\ (s) \qquad\qquad E^o = 0.915\ V \qquad\qquad \text{(Eq. 4.1)}$$

$$PdCl_4^{2-} + 2e^- \rightleftharpoons Pd\ (s) + 4Cl^- \qquad E^o = 0.62\ V \qquad\qquad \text{(Eq. 4.2)}$$

A study was carried out using $PdSO_4$ and $PdCl_2$ solutions that had an AA signal ratio of ($[PdSO_4]/[PdCl_2]$ =) 0.891. Using an electrolyte solution consisting of H_2SO_4 and KCl, the EQCM measurements gave a frequency change ratio of 0.852 for these two solutions, yielding a difference of 4.38%. The similarity between these two ratios suggests that, when KCl was present as an electrolyte, the equilibrium in Eq. 4.1 operated. For the Pd(II) solutions without Cl^- ions, the addition of KCl converted Pd^{2+} ions into $PdCl_4^{2-}$ so that the calibration plot

discussed earlier may be used for the analysis of Pd(II) in $PdSO_4$. This is important from a chemical analysis standpoint; for certain Pd(II) solutions, the addition of KCl might be sufficient to yield $PdCl_4^{2-}$ for the quantitative Pd(II) determination.

4.3.5. NaF as an Electrolyte

Based on the previous results and Eqs. 4.1 and 4.2, it is logical to assume that the use of a particular electrolyte will affect the amount of palladium deposited onto the quartz crystal. When NaF is used in place of KCl as an electrolyte in a $PdSO_4$ solution, the overall change in frequency associated with the deposition of palladium is decreased by ca. 8%. Since Pd^{2+} ions have a higher reduction potential than that of $PdCl_4^{2-}$ ions (Eqs. 4.1 and 4.2), the reduction of Pd^{2+} ions in the absence of Cl^- ions is expected to be more thermodynamically favored, perhaps resulting in a greater frequency change. The fact that this did not occur may be attributed to the kinetics of our EQCM process. When Cl^- ions are not present, the free Pd^{2+} ions are solvated with water molecules. The slow diffusion of the bulkier, solvated $Pd(H_2O)_4^{2+}$ ions to the electrode surface may have limited the rate of their reduction at the electrode surface.

The difference in using NaF and KCl as an electrolyte was also observed when stripping palladium from the quartz crystal (Figure 4.7). The overall frequency changes associated with palladium stripping in the presence of KCl as
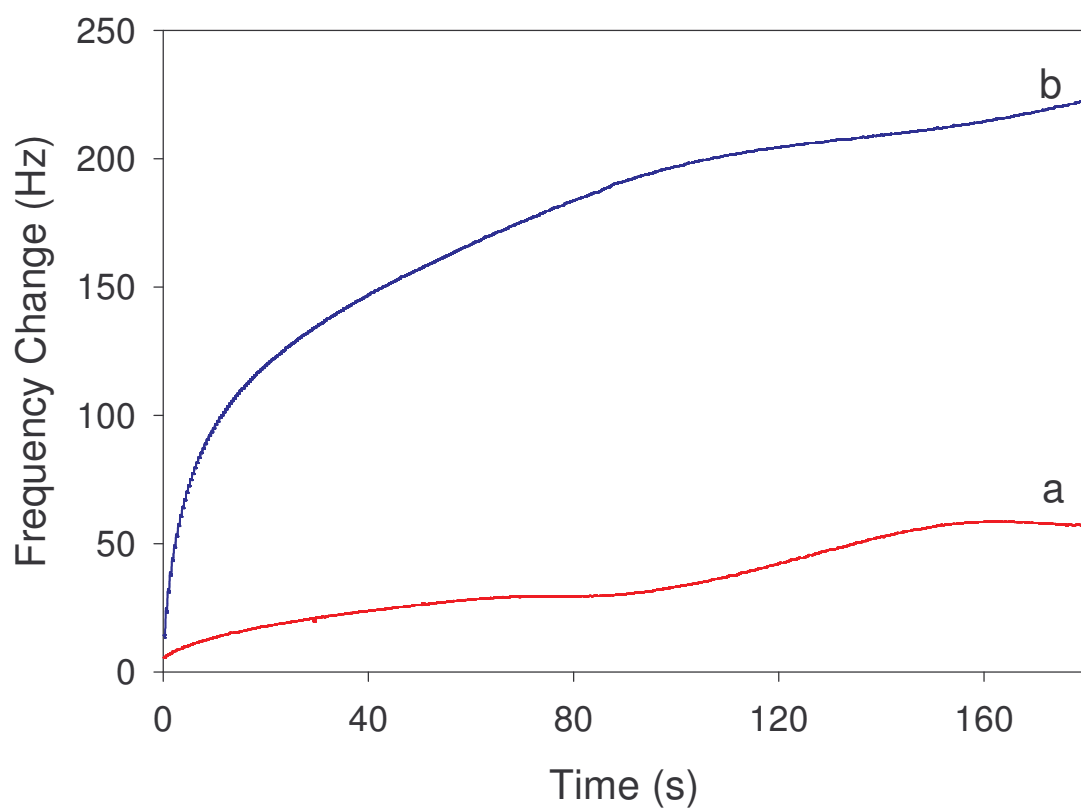
Figure 4.7. Frequency changes associated with the stripping of palladium in: (a) 5.93 mM NaF and (b) 5.01 mM KCl.

the electrolyte are much greater than those occurring when NaF is used. This large difference can most likely be attributed to the formation of the $PdCl_4^{2-}$ complex that may have assisted the Pd removal from the carbon electrode and increased the useful lifetime of the EQCM device.

4.3.6. pH and Other Interference Effects

Solutions of various pH values were tested to determine their role, if any, in the deposition process. The results (Table 4.1) suggest that the relative acidity of the solution has a small impact on the changes in frequency. The amount of palladium deposited is independent of the pH of the acidic samples.

An analysis of the total current used in the reduction of Pd^{2+} to Pd reveals that additional charge may be generated by a species other than the Pd^{2+} ions in the solution. From the experimental results and the Sauerbrey equation, the amount of palladium metal deposited onto the crystal is calculated. The amount of charge, Q, generated during the deposition can be calculated using Eq. 4.3.

$$Q = \text{n}FN \qquad (4.3)$$

where Q = the amount of charge, n = the number of electrons involved in the electrode reaction F = Faraday's constant, and N = the number of moles of electrolyzed species.

Table 4.1. pH and interference effects.

Solution	Average Frequency Change (Hz)[a]
pH 2.17 H_2SO_4	-152 ± 5
pH 1.60 H_2SO_4	-149 ± 2
50.4 mM H_2SO_4[b]	-147 ± 3
0.300 M H_2SO_4	-150 ± 3
0.600 M H_2SO_4	-146 ± 3
3.42 mM $FeCl_2 \bullet 2H_2O$[c]	-142 ± 2
9.16 mM $NaNO_3$[c]	-144 ± 2
4.41 mM KH_2PO_4[c]	-148 ± 4

All solutions contained 3.22 mM KCl and 0.234 mM $PdCl_2$.

[a] Values given are an average of three measurements.

[b] Standard solution.

[c] Solutions contain 50.4 mM H_2SO_4.

In most cases, the amount of charge recorded during deposition exceeded the amount predicted by Eq. 4.3. For example, in one experimental run, the frequency of the crystal decreased by 147 Hz, corresponding to a deposition of 2.23 nmol of Pd. The amount of charge associated with this deposition, calculated using Eq. 4.3, is 0.430 mC. The actual amount of charge recorded during this deposition was 1.19 mC, or approximately three times the predicted charge. It is therefore reasonable to assume that the excess charge was generated by a species other than Pd^{2+} ions in the solution. The H^+ ions are most likely responsible for this excess charge. Taking into account the relatively high acid concentrations in our studies and the corresponding H^+ reduction potential, the large overpotential (-0.4 V) used in the deposition of palladium may be sufficient to reduce H^+ to H_2, resulting in the passage of excess current.

A possible application of the proposed technique could involve the detection of palladium metal present in spent catalysts.[36] Table 4.1 lists some common interferents, such as Fe^{2+}, that may be present in such a spent Pd catalyst and their effects on the EQCM frequency change.

Despite the fact that there is over a ten-fold excess of Fe^{2+} over Pd^{2+} in solution, the frequency change difference between the $FeCl_2$-containing $PdCl_2$ solution and the control $PdCl_2$ solution is minimal, correlating to a 3% error. This is perhaps not surprising, given the fact that Fe^{2+} has a very low reduction potential.[23] It is therefore unlikely that a significant amount of Fe^{2+} ions were reduced to interfere with the Pd deposition. In addition, significant concentrations of $H_2PO_4^-$ and NO_3^- did not show a substantial interference in the Pd deposition

process (Table 4.1).

4.3.7. Validation Study of the New Method

In order to demonstrate that the proposed technique can be applied for actual Pd^{2+} determination, an unknown sample was prepared by spiking tap water with an aliquot of palladium AA standard. One portion of the sample was analyzed using the standard N,N-dimethyl-4-nitrosoaniline method.[8,25] In this technique, Pd^{2+} forms a yellow-orange complex with N,N-dimethyl-4-nitrosoaniline that is monitored by UV-vis spectroscopy. The analysis by the N,N-dimethyl-4-nitrosoaniline method showed that the concentration of Pd^{2+} in the sample was 0.0985 mM.[25]

Another portion of this sample was then modified with electrolyte and analyzed as discussed in the Experimental Section. Using this EQCM technique, it was determined that the concentration of the sample was 0.104 mM Pd^{2+}. Compared to the concentration obtained using the proposed EQCM technique, the percent error for the study is 5.6%. In comparison, the standard deviation of the EQCM data used to give the calibration plot is 4.15%. The studies here suggest that the use of carbon-coated quartz crystals for the quantitative determination of Pd^{2+} is a process with a small error.

4.4. Conclusions

Successful Pd(II) quantification in $PdCl_2$ and $PdSO_4$ has been achieved using carbon-coated quartz crystals. The method presented proved to be simple

and reliable, utilizing a bare carbon-coated crystal that is easily regenerated for multicycle use and requiring no complexing agent or preconcentration of analyte. In addition, it has an advantage over conventional techniques in that it is relatively inexpensive and can be applied to the in-situ analysis of palladium. Although the limit of detection that it provides is higher than other reported techniques, the proposed method has potential use in many flow analysis applications, e.g. as an in-situ sensor for Pd(II) present in a flowing stream of catalytic waste. Offline techniques, such as ICP-MS and AAS, and modified carbon paste electrodes requiring complexing agents for analyte preconcentration are not as suitable for such tasks.

References

1.   Neal, A.H. in: U.V. Rao (Ed.), Precious Metals, Proceedings of the 10th International Precious Metals Institute Conference, International Precious Metals Institute, Pensacola, FL, 1986, pp. 455-466.

2.   Garrett, C.E.; Prasad, K. *Adv. Synth. Catal.* **2004**, *346*, 889.

3.   Armor, J.N. *J. Membr. Sci.* **1998**, *147*, 217.

4.   Greenwood, N.N.; Earnshaw, A. Chemistry of the Elements, second ed., Elsevier Science, London, 1997, pp 1144-1151.

5.   Godlewska-Żylkiewicz, B. *Microchim. Acta* **2004**, *147*, 189.

6.   Kallmann, S. *Talanta* **1987**, *34*, 677.

7.   Qu, Y. *Analyst* **1996**, *121*, 139.

8.   Sarkar, P.; Paria, P.K.; Majumdar, *Indian Chem. Soc.* **1988**, *65*,117.

9.   Kalvoda, R. *Electroanal.* **2000**, *12*, 1207.

10.   Zuhri, A.; Wolfgang, V. *Fresen. J. Anal. Chem.* **1998**, *360*, 1.

11.   Basu, B.; Rajagopalan, S. *Analyst* **1992**, *117*, 1623.

12.   Wang, J.; Varughese, K. *Anal. Chim. Acta* **1987**, *199*, 185.

13.   Raber, G.; Kalcher, K.; Neuhold, C.; Talaber, C.; Kolbl, G. *Electroanal.* **1995**, *7*,138.

14.   Sun, Q.; Wang, C.; Li, L.; Li, H. *Fresen. J. Anal. Chem.* **1999**, *363*, 114.

15.   Aghamohammadi, M.; Alizadeh, N. *Anal. Chim. Acta* **2003**, *480*, 299.

16.   Gomes, M.T.S.R. *IEEE Sensors J.* **2001**, *1*, 109.

17.   Nomura, T.; Kumagai, M.; Sato, A. *Anal. Chim. Acta* **1997**, *343*, 209.

18.   Schmidt, H.-J.; Pittermann, U.; Schneider, H.; Weil, K.G. *Anal. Chim. Acta.* **1993**, *273*, 561.

19.	Jones, J.L.; Miure, J.P. *Anal. Chem.* **1969**, *41*, 484.

20.	Andersen, N. *Anal. Chim. Acta* **1998**, *368*, 191.

21.	Andersen, N.; Holst-Hansen, P.; Britz, D. *Anal. Chim. Acta* **1996**, *329*, 253.

22.	Deposition of precious metals by the EQCM technique has been reported to study the deposition process or to make new electrodes. See, e.g., (a) Ariizumi, N.; Shibata, M.; Furuya, N. *Hyomen Gijutsu* **1997**, *48*, 1134. (b) Naohara, H.; Ye, S.; Uosaki, K. *J. Phys. Chem. B* **1998**, *102*, 4366. (c) Uosaki, K.; Ye, S.; Kondo, T.; Naohara, H. in: Soriaga, M.P.; Stickney, J.; Bottomley, L.A.; Kim Y.-G. (Eds), Thin Films: Preparation, Characterization, Applications, Kluwer, Dordrecht, Netherlands, 2002, pp. 17-35. (d) Oliveira, R.T.S.; Santos, M.C.; Bulhoes, L.O.S.; Pereira, E.C. *J. Electroanal. Chem.* **2004**, *569*, 233. (e) Yanez, C.; Gutierrez, C.; Ureta-Zanartu, M.S. *J. Electroanal. Chem.* **2003**, *541*, 39. (f) Vigier, F.; Gloaguen, F.; Leger,J.-M.; Lamy, C. *Electrochim. Acta* **2001**, *46*, 4331. (g) Myllynen, S.; Wasberg, M.; Eskelinen, E.; Haukka, M.; Pakkanen, T.A. *J. Electroanal. Chem.* **2001**, *506*, 115-126. (h) Frelink, T.; Visscher, W.; van Veen, J.A.R. *Langmuir* **1996**, *12*, 3702.

23.	Buttry, D.A. in: Bard, A.J. (Ed.), Electroanalytical Chemistry, vol. 17, Marcel Dekker, New York, 1990, pp 1-85.

24.	Buttry, D.A.; Ward, M.D. *Chem. Rev.* **1992**, *92*, 1355.

25.	See Appendix C.

26.	Varga, P.; Hetzendorf, G. *Surf. Sci.* **1985**, *162*, 544.

27. Chung, Y.S.; Evans, K.; Glaunsinger, W. *Mater. Res. Soc. Symp. Proc.* **1997**, *472*, 185.

28. MacDonald, J.J.; Conway, B.E. *Proc. Roy. Soc. (London) Ser. A* **1962**, *269*, 419.

29. Sauerbrey, G.Z. *Phys.* **1959**, *155*, 206.

30. Ullevlg, D.M.; Evans, J.F.; Albrecht, M.G. *Anal. Chem.* **1982**, *54*, 2341.

31. Bard, A.J.; Faulkner, L.R. Electrochemical Methods, second ed., Wiley, New York, 2001.

32. Llopis, J.F.; Colom, F. in: Bard, A.J. (Ed.), Encyclopedia of Electrochemistry of the Elements, vol. 6, Marcel Dekker, New York, 1976, p. 258.

33. Czerwinski, A.; Kiersztyn, I.; Grden, M.; Czalpa, J. *J. Electroanal. Chem.* **1999**, *471*, 190.

34. Grden, M.; Kotowski, J.; Czerwinski, A. *J. Solid State Electr.* **1999**, *3*, 348.

35. Grden, M.; Kotowski, J.; Czerwinski, A. *J. Solid State Electr.* **2000**, *4*, 273.

36. Spent Pd catalysts may contain ligands that require a pre-treatment to convert Pd into aqueous Pd^{2+} ions before the EQCM analysis. This is a subject that requires separate studies.

Part 5

Spectroscopic and Electrochemical Approaches to Iron(III) Sensing

5.1. Introduction

Iron is essential for cellular metabolism and aerobic respiration.[1,2] Its deficiency and overload are both hematological diseases.[2] An average adult has a total body iron content of ca. 3.5 g, and two-thirds of this iron is present as hemoglobin iron, and ca. one-third is present as tissue iron.[2e] Iron deficiency is a major health problem worldwide,[2a-f] and it is the most common nutritional deficiency. It is the most prevalent among women, young children and the elderly and occurs in, e.g., ca. 19% among women ages 16-19 and increases in minority populations. Iron deficiency anemia in children results in decreased motor activity and social interaction, and slowed child development.[3] In adults, iron deficiency anemia leads to decreased work productivity and increased susceptibility to infectious disease. In the elderly, anemia is associated with an increased mortality and morbidity risk.[2c,f] Iron overload occurs when the body's rate of iron acquisition exceeds the rate of loss, a result of inherited or acquired conditions.[2g-j] The acquired, secondary iron overload includes iron loading anemias, transfusional and African iron overloads, and iron overload in chronic liver disease.[2g-j]

Clinically, iron status is usually measured by hematological and biochemical methods.[2b,4] Iron in both ferritin and transferrin (a protein for iron ion delivery) in serum (clear, non-cellular fluid component of blood after it has clotted) is determined. Iron in serum ferritin is determined by, e.g., immunoradiometric assay methods,[4a] and it is known to be affected by

129

inflammation and liver disease.[2b] Iron in transferrin (also called serum iron[4a,b])

and total iron binding capacity (TIBC) in transferrin are important determinants in

assessing iron status. In the analysis of the former, Fe(III) is released from

transferrin by acid, reduced to Fe(II), and then analyzed by visible spectroscopy

(after forming a colored complex)[4a,b] or coulometry.[5,6] This spectroscopic method

is routinely used, but there are concerns about accuracy and the wide variation in

the results.[4a,7] TIBC is determined by adding sufficient Fe(III) to saturate iron

binding sites on transferrin and then measuring iron content in the saturated

transferrin.[4a,b] These two measurements are subject to interferences by certain

drugs.[6b,d,e] The TIBC measurement provides a diagnostic test for both iron

deficiency and iron overload,[4d,e] but it has been reported to be less precise.[6c]

Iron concentration in plasma (non-cellular liquid component of un-clotted blood)

has also been analyzed,[4c,f-h] and it is less affected than that in serum by

hemolysis (destruction/dissolution of red blood cells with release of hemoglobin)

from the clotting process in the serum preparation.[4f] Other methods of the

measurement of iron in biological fluids, such as inductively coupled plasma

mass spectroscopy, proton induced X-ray emission and neutron activation

analysis, often require sophisticated and expensive instrumentation.[4c,j] Atomic

absorption spectroscopy (AAS) is unreliable for serum due to sensitivity

limitations and interferences by the matrix and hemoglobin.[4b]

There is a need to develop new measurement techniques for the analysis

of iron to supplement the hematological and biochemical methods. Our research

group has recently reported a new sample pretreatment method for the decomposition of organic compounds in complex sample matrices, including blood.[8-10] In this pretreatment method, known as the Advanced Oxidation Process (AOP), hydrogen peroxide is added to the sample, and it is irradiated with UV light. This irradiation causes hemolytic splitting of the oxygen-oxygen bonds in the hydrogen peroxide molecules, yielding hydroxyl radicals. These radicals react with organic species present, decomposing them to carbon dioxide and water. This frees up any metal species that are present so that they may be subsequently analyzed using traditional spectroscopic or electrochemical techniques.

Methods of iron analysis were investigated for use after sample pretreatment by AOP. These methods involved the use of calcein-doped sol-gel films for the determination of iron by fluorescence quenching, modified carbon paste electrodes for enhanced iron determination using preconcentration followed by square-wave voltammetry, and bismuth film electrodes for enhanced iron determination by catalytic voltammetry. Ideally, one or a multiple of these techniques could be coupled with the previously developed AOP process for use in the analysis of iron in biological samples. These proposed methods would possibly offer alternative techniques for iron determination in biological samples, providing the total body iron concentration and perhaps serving as complimentary procedures to the currently used methods.

5.2. Experimental

5.2.1. Chemical Reagents and Materials

Tetramethyl orthosilicate (TMOS, $Si(OMe)_4$, 98%, Sigma-Aldrich), methanol (MeOH, HPLC grade, Fisher), cetyl trimethyl ammonium bromide (CTAB, 99+%, Acros Organics), calcein (The G. Frederick Smith Chemical Co.), 1,10-phenanthroline (certified A.C.S., Acros Organics), graphite powder (<20 µm, synthetic, Sigma-Aldrich), Nafion (Sigma-Aldrich), mineral oil (Sigma-Aldrich), sodium acetate (CH_3COONa, certified A.C.S., Fisher), potassium chloride (KCl, Mallinckrodt Chemicals), potassium bromide (KBr, Mallinckrodt Chemicals), potassium bromate ($KBrO_3$, Mallinckrodt Chemicals), sodium hydroxide (NaOH, certified A.C.S., Fisher), triethanolamine (TEA, 97%, Acros Organics), and hydrochloric acid (HCl, certified A.C.S., Fisher) were all used as received. Standard solutions of Fe(III) were prepared by serial dilution of a 1000 µg/mL AA standard (Sigma-Aldrich). Solutions and standards were prepared using deionized (DI) water (18 MΩ-cm) from a Barnstead International E-pure 4-holder deionization system. All solutions used in the studies were prepared fresh.

For the calcein-doped sol-gel thin films studies, glass microscope slides (Fisher) were cut into 1.0 x 1.5 cm pieces. Each piece was then roughened on carborundum, washed thoroughly with soap and water, and then allowed to soak in a base bath for one day. After this, the glass slides were washed sequentially with deionized water, acetone, isopropanol, and methanol. They were then air dried under nitrogen gas.

The working electrodes used during the bismuth film experiments were glass-encased glassy carbon electrodes (3 mm diameter, Cypress Systems, Inc.). Before each coating process, these electrodes were polished using 0.05 micron alumina powder. Each electrode was then rinsed with water and sonnicated for 20 minutes. The bismuth plating solutions used during these studies were prepared by dissolving Bi needles (99.998%, Alfa Aesar) in nitric acid (HNO_3, trace metal grade, Fisher) and diluting appropriately. Platinum wire and silver/silver chloride were used as the auxiliary and reference electrodes, respectively, for all of the electrochemical studies.

5.2.2. Instrumentation

A homemade spin-coater was used to deposit doped sol-gel films onto the microscope slides. Fluorescence studies were carried out using an AMINCO-Bowman Series 2 (AB2) Spectrofluorometer. A CH Instruments model 400A potentiostat with electrochemcial quartz crystal microbalance (EQCM) capability and corresponding software were used for the electrochemical studies.

5.2.3. Preparation of Sensing Materials

5.2.3.1. Preparation of Calcein-Doped Sol-Gel Films

A sol solution consisting of 200 μL TMOS, 60 μL H_2O, 130 μL MeOH, 17 μL 0.012 M HCl, 0.07 g calcein, and 0.004 g CTAB was prepared and stirred for 50 minutes. A 1.0 x 1.5 cm glass slide was then affixed to the spin coater, and

this sol solution was pipetted onto the glass surface. The spin coater was then

spun at 3000 rpm for 45 s, producing a thin, yellow coating on the glass slide

surface. The doped thin film was then allowed to dry in the hood for 5 days,

followed by 5 days of drying in the oven at 40 °C. Additional calcein-doped sol-

gel films were prepared in a similar fashion. The procedure for preparing these

films was adapted from a similar procedure previously used to prepare acid and

base sol-gel sensors doped with indicator dyes.[11]

5.2.3.2. Preparation of Modified Carbon Paste Electrodes

A calcein-modified carbon paste electrode was prepared by combining 1.2

g of graphite powder, 0.38 g of calcein, and 0.90 g of mineral oil in a mortar and

mixing them together with a pestle. The paste mixture was then packed into a

glass tube (0.5 cm i.d., 6.5 cm length) using a spatula and Teflon plunger. A

copper wire was then inserted into one end of the carbon paste to provide the

electrical connection to the potentiostat. Preparation of a 1,10-phenanthroline-

modified carbon paste electrode occurred using a similar procedure, and this

method has been reported previously.[12]

5.2.3.3. Preparation of Bismuth Film Electrodes

The method for the preparation of the bismuth film electrode for Fe(III)

sensing has been reported previously.[13] Briefly, a bismuth plating solution

consisting of 0.5 M KBr, 1.0 M HCl, and 0.02 M Bi was prepared. A glassy

carbon electrode was then exposed to this solution, and a potential of -0.25 V

was then applied for 60 s. The electrode was then rinsed with DI water, and the bismuth film formed at the electrode surface could then be used for subsequent iron(III) sensing cycles.

5.3. Results and Discussion

5.3.1. Studies Involving Calcein-Doped Sol-Gel Films

Calcein (Figure 5.1A) is a well known fluorophore, having an excitation wavelength of 488 nm and an emission wavelength of 517 nm, and has been used for the determination of iron.[14-17] When calcein binds to iron in a stoichiometric manner, fluorescence quenching takes place. Thus, a higher level of iron present in a calcein solution results in a lower fluorescent intensity. Figure 5.1B demonstrates this fact.

Figure 5.2 shows a picture of a calcein-doped sol-gel film deposited onto a glass substrate using the procedure discussed in the experimental section. As can be seen, the film has a yellow color, characteristic of calcein that is doped into the film. A study was carried out in which the calcein-doped sol-gel film was placed in a fluorometer after exposure to DI water, and the emission spectrum was collected. The coated slide was then exposed to a 109 ppb Fe(III) solution for 10 min. It was subsequently rinsed with DI water, and its emission spectrum was then collected again using the fluorometer. The emission spectra collected before and after exposure to Fe(III) are shown in Figure 5.3. The fluorescence
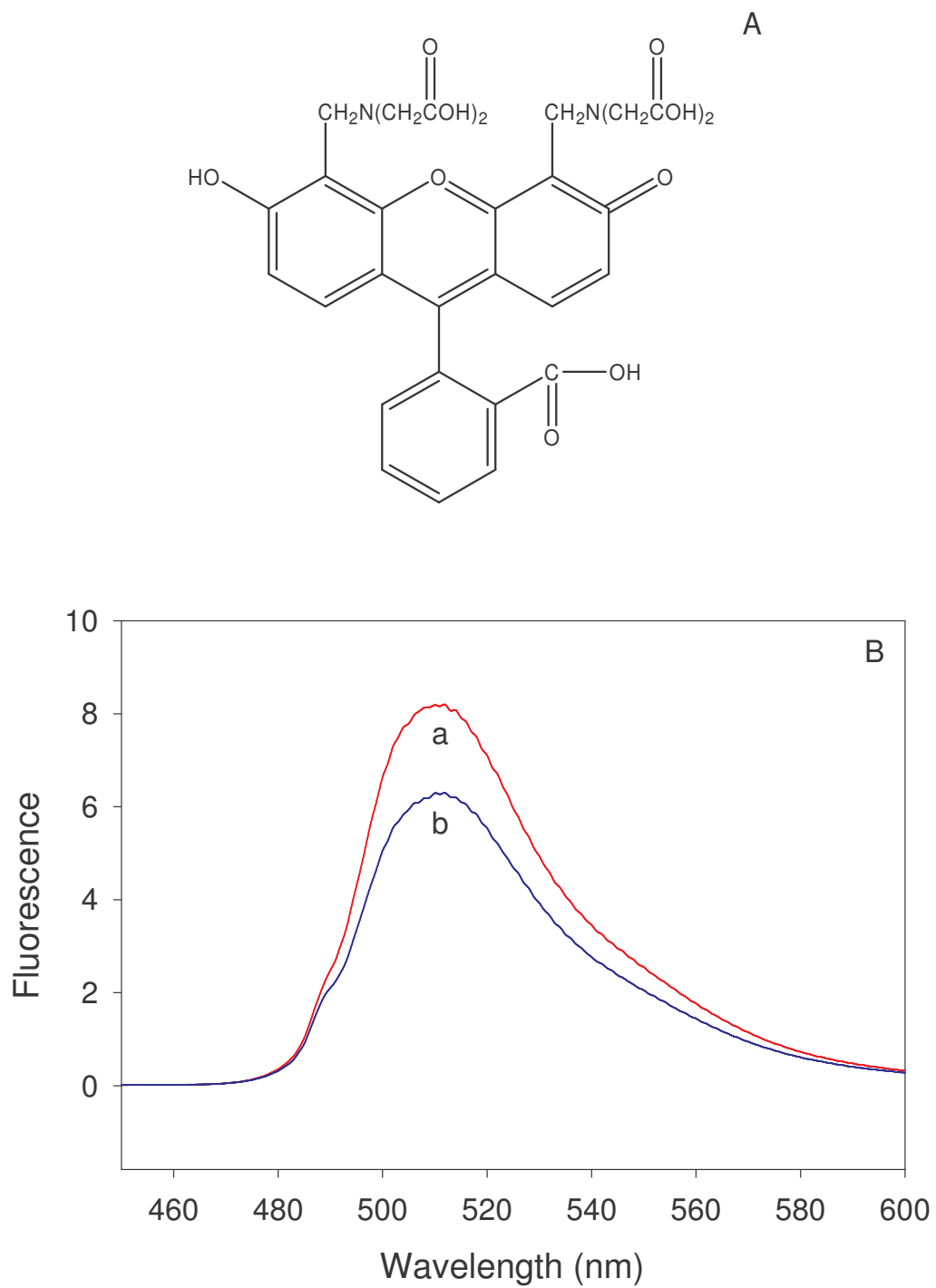
Figure 5.1. (A) Calcein structure. (B) Emission spectra of a 0.714 μM calcein solution before (a) and after (b) addition of 32.75 ppb Fe(III).
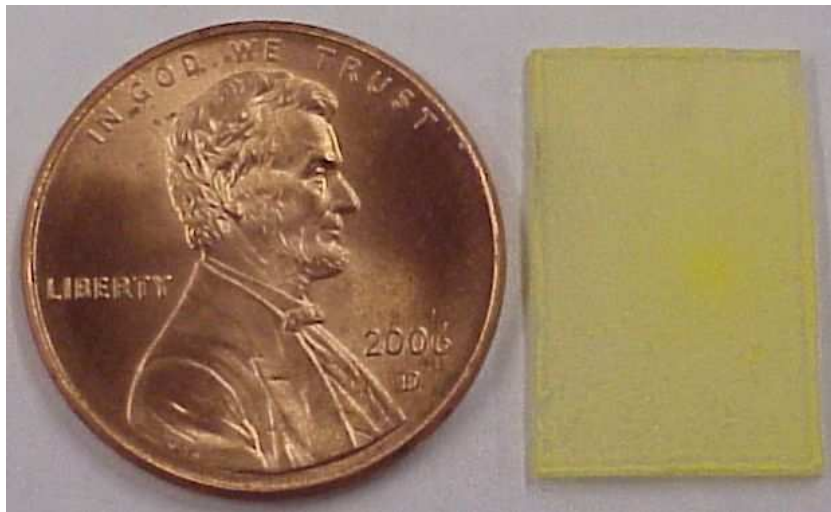
Figure 5.2. A calcein-doped sol-gel thin film deposited onto the surface of a glass slide.
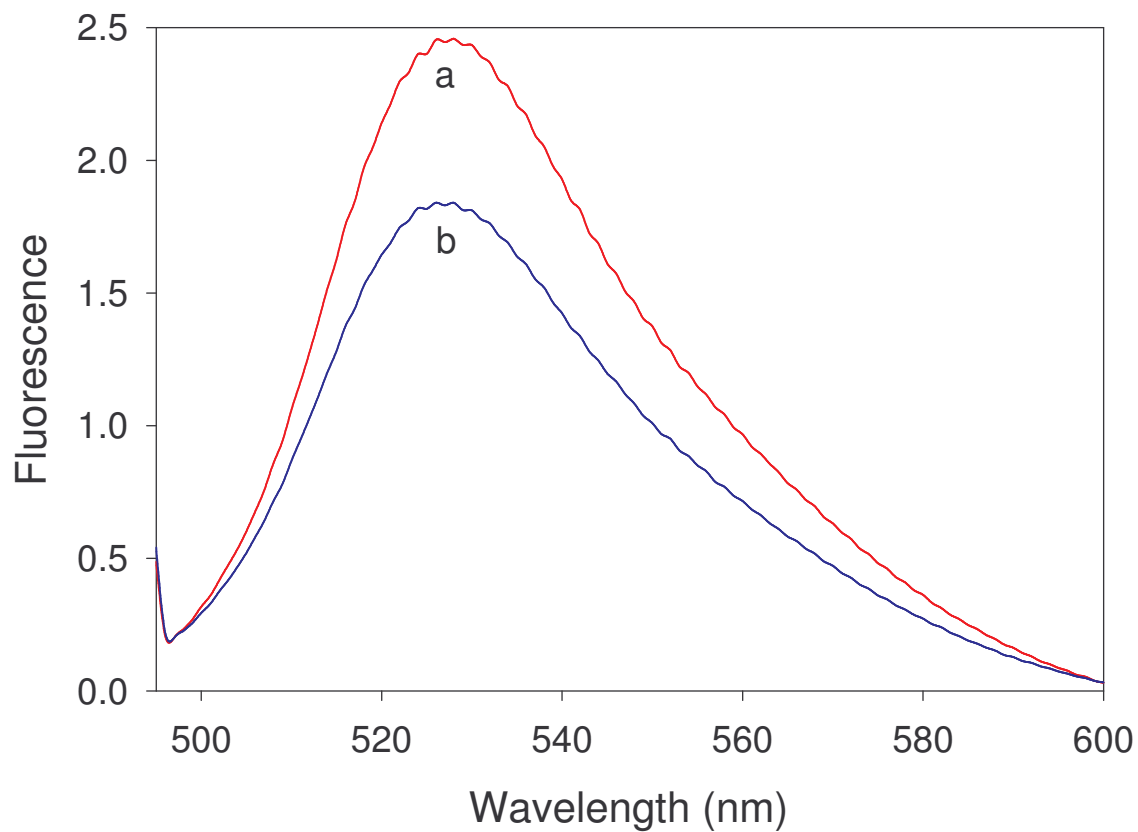
Figure 5.3. Fluorescence spectra of a calcein-doped sol-gel film after exposure

to DI water (a) and after exposure to 109 ppb Fe(III) (b).

intensity emitted by the doped calcein molecules decreases after the film has been exposed to the Fe(III) solution. This is a result of the Fe(III) ions diffusing into the sol-gel film and binding with calcein molecules, causing fluorescence quenching to take place. It should be possible to use such calcein-doped thin films for the detection of Fe(III), and their incorporation into a sensing cell using ATR fluorescence should make it possible to detect Fe(III) down to low ppb and possibly even ppt levels.

5.3.2. Studies Involving Modified Carbon Paste Electrodes

In addition to spectroscopic sensing, electrochemical methods for Fe(III) determination were also investigated. Since calcein is a well-known fluorophore and has been shown to complex with Fe(III),[14-17] efforts were made to incorporate calcein into carbon paste electrodes using the procedure discussed in the experimental section. Once a calcein-modified carbon paste electrode was prepared, it was exposed to Fe(III) solutions for 10 min. to preconcentrate the analyte species at the electrode surface. Square-wave voltammetry was then carried out to reduce the Fe(III) to Fe(II), and a peak corresponding to this reduction emerged around 0.12 V. Figure 5.4 shows voltammograms obtained when the electrode was exposed to various Fe(III) concentrations. The peak current increases with increasing Fe(III) concentration. After each analysis, the electrode was exposed for 10 min. to 1 mM deferoxamine mesylate, as this compound is capable of regenerating calcein after its exposure to Fe(III) for multiple analyses.[14]
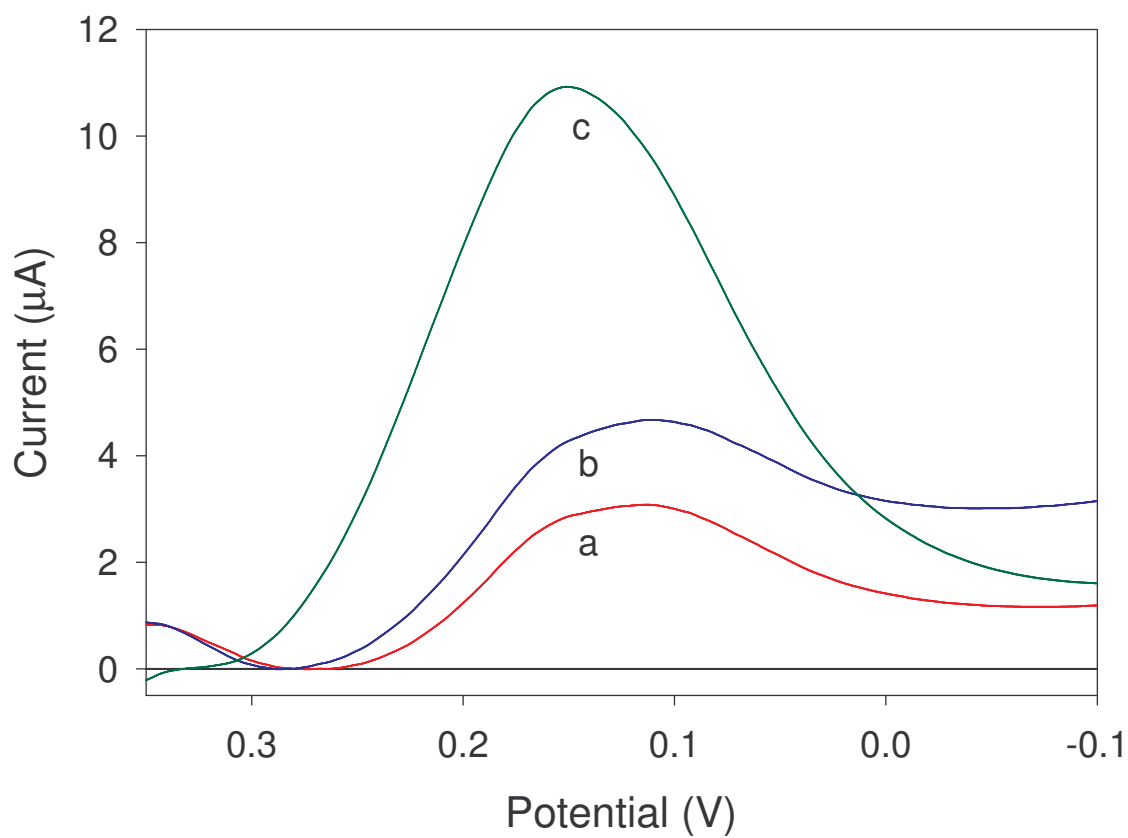
Figure 5.4. Square-wave voltammograms (background subtracted) collected at a calcein-modified carbon paste electrode of solutions containing 0.1 M KCl, 0.1 M HCl, and: (a) 0 ppm Fe(III); (b) 0.0212 ppm Fe(III); (b) 0.547 ppm Fe(III); (c) 7.65 ppm Fe(III).

In addition to calcein, 1,10-phenanthroline was investigated as a complexing agent for use in modified carbon paste electrodes. 1,10-phenanthroline will complex with Fe(III) and has demonstrated selectivity in previous work.[12,17] As a result, a carbon paste electrode modified with this complexing agent was prepared and then exposed to solutions of varying Fe(III) concentration for 10 min. After this preconcentration at the electrode surface, square-wave voltammograms were carried out. Figure 5.5 shows voltammograms obtained from solutions of varying Fe(III) concentration. The peak current increases with increasing Fe(III) concentration. It should be noted that the peak current corresponding to Fe(III) reduction to Fe(II) occurs at a different potential than that which was observed using the calcein modified electrode. This is most likely due to electrochemical differences of the iron complexes. It should also be noted that the carbon paste electrodes used in these reported studies provided varying results that were very difficult to reproduce. In addition, the carbon paste was rather unstable and often degraded in solution during analyses. For these reasons, bismuth film electrodes were pursued as a possible alternative method for the electrochemical sensing of Fe(III).

5.3.3. Studies Involving Bismuth Film Electrodes

Bismuth film electrodes have been used for the determination of a wide variety of metal species, including Cr,[18] V,[19] and Fe.[13] For the determination of Fe, a catalytic voltammetric cycle is used. In this process (shown in Figure 5.6),
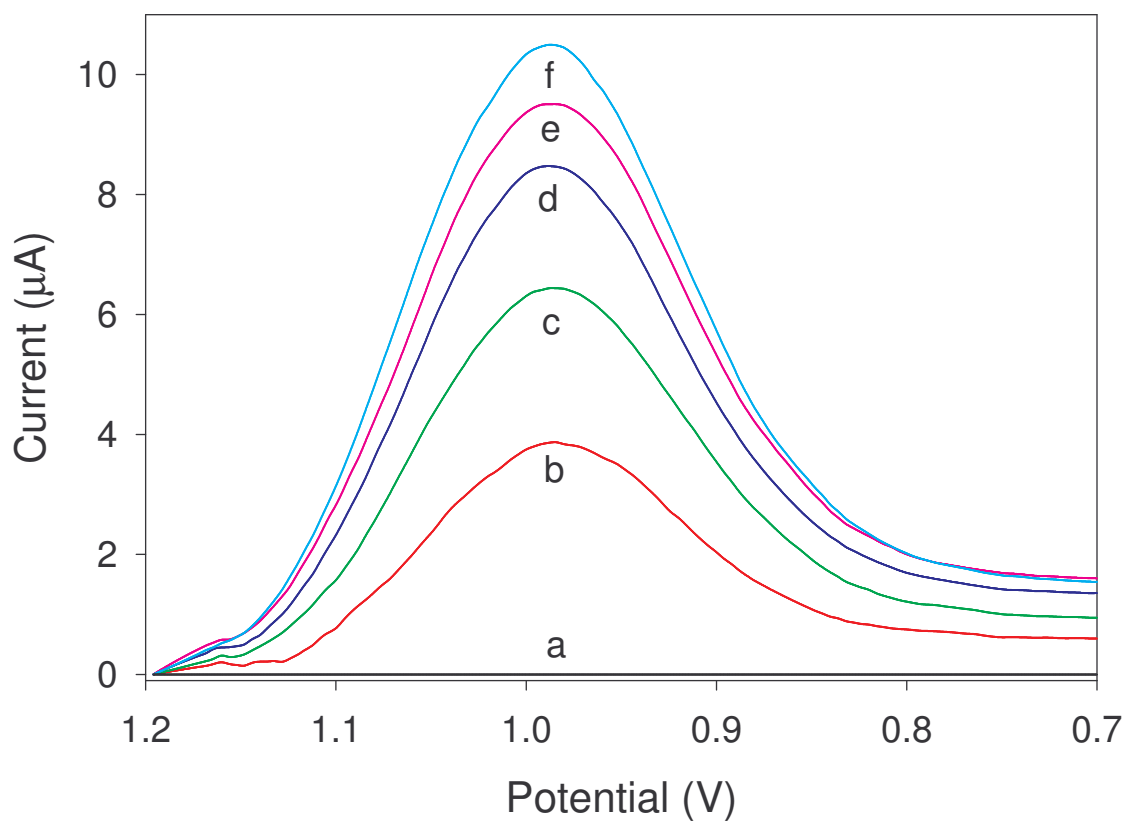
Figure 5.5. Square-wave voltammograms (background subtracted) collected at a 1,10-phenanthroline modified electrode. The solutions consisted of 0.1 M CH_3COONa (pH = 5.37) and: (a) 0 ppb Fe(III); (b) 106 ppb Fe(III); (c) 203 ppb Fe(III); (d) 301 ppb Fe(III); (e) 406 ppb Fe(III); (f) 504 ppb Fe(III).

$$Fe(III) + TEA \longleftrightarrow Fe(III)\text{-}TEA$$

$$Fe(III)\text{-}TEA + e \longrightarrow Fe(II)\text{-}TEA$$

$$Fe(II)\text{-}TEA + BrO_3^- + H_2O \longrightarrow Fe(III)\text{-}TEA + X + OH^-$$

Figure 5.6. Formation, reduction, and possible catalytic regeneration of the Fe-TEA complex. X is used to represent the product of the reduction of BrO_3^- (Br^- and/or $BrO\cdot$ radicals). (Adapted from Reference 13).

Fe(III) complexes with triethanolamine (TEA). When voltammetry is carried out

and the Fe(III) is reduced to Fe(II), the bromate ions in solution oxidize the Fe(II)
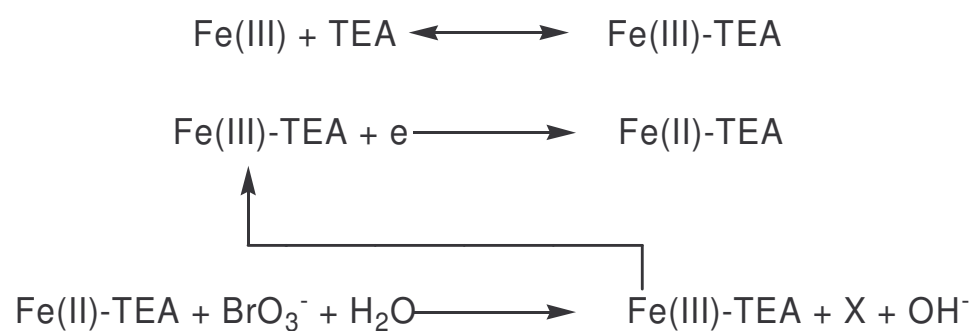
back to Fe(III), creating a catalytic effect. Although the presence of bromate

makes it impossible to distinguish Fe(II) from Fe(III), it enhances the overall

signal intensity and enables the determination of Fe(III) to sub ppb levels. In

addition, since this is a purely catalytic mechanism, no adsorption of the analyte

species at the electrode surface is necessary for preconcentration and

subsequent enhanced determination.[20] Fe(III) solutions can be analyzed quickly

and reproducibly in little time.

   A standard addition method was used to analyze Fe(III) solutions of

varying concentration. In this work, a glassy carbon electrode was coated with a

bismuth film as described in the experimental section. The Bi film electrode was

then exposed to pure electrolyte solution, consisting of 5 mM $KBrO_3$, 0.1 M

NaOH, and 0.01 M TEA. A square wave voltammogram was then collected.

Aliquots of Fe(III) were then added, and successive square wave

voltammograms were collected. These are shown in Figure 5.7A. As can be

seen, a peak occurs around -0.96 V, corresponding to the reduction of Fe(III)-

TEA to Fe(II)-TEA. The peak current is a function of Fe(III) concentration, with

higher concentrations giving larger peak currents. This relationship is linear (R^2

= 0.992), as is demonstrated in Figure 5.7B. In addition, the measurements were

highly reproducible, with three potential sweeps of the lowest concentration

having a standard deviation of 9.4×10^{-3} µA. Based on this standard deviation

and the calibration plot shown in Figure 5.7B, the limit of detection for the system
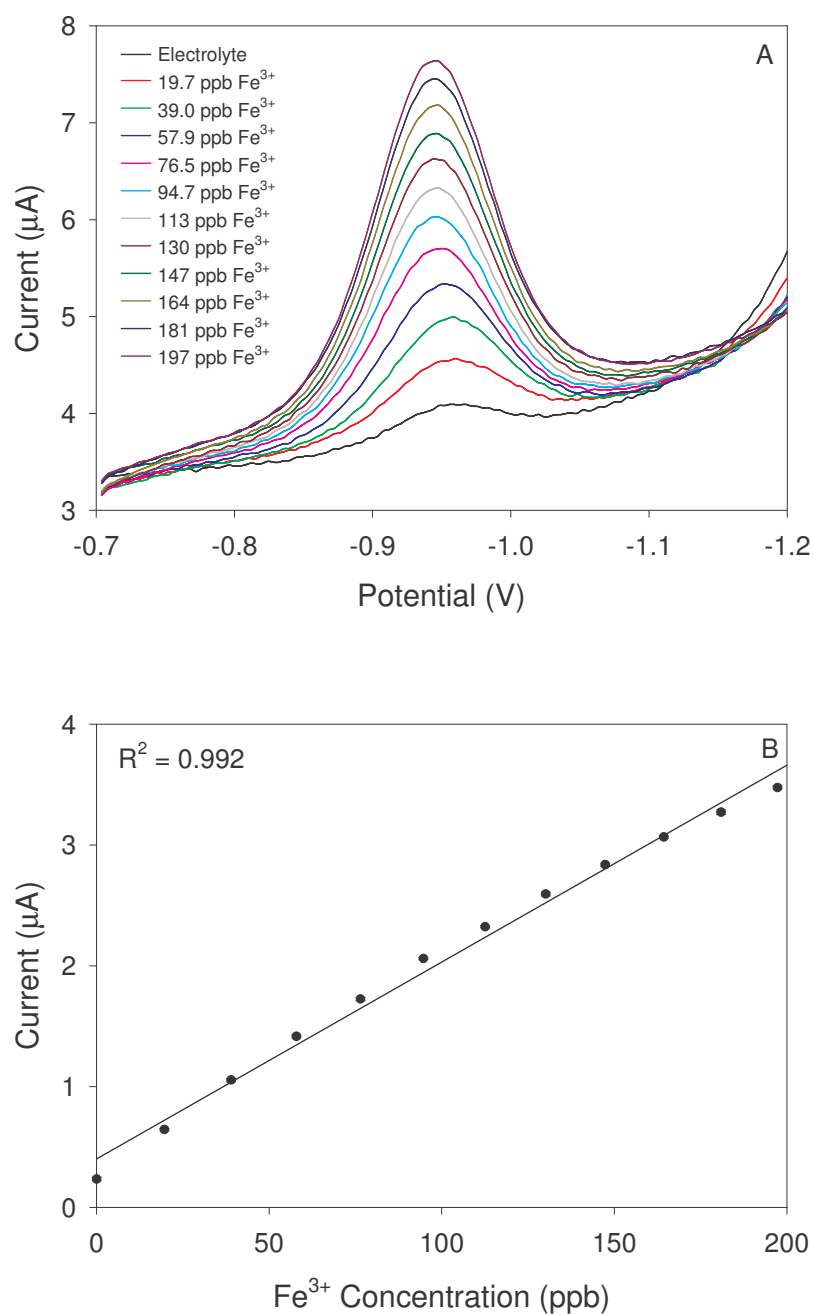
Figure 5.7. (A) Square-wave voltammograms of Fe(III) solutions of varying concentration in 5 mM $KBrO_3$, 0.1 M NaOH, and 0.01 M TEA. (B) The corresponding calibration plot. Data points represent an average of three different measurements.

was calculated to be 1.73 ppb Fe(III).

5.3.4. Preliminary Studies of Iron in Biological Samples

The original goal of this work was to develop a method for the determination of iron in biological fluids, specifically in porcine blood that was acquired from a local sausage factory. Given the ease of use, limit of detection, and reproducibility offered by the Bi film electrode, it was pursued as a means for analyzing iron in blood. Blood and other biological samples are very complex matrices, and they contain several organic components that interfere with the measurement of metal species that are present. To remove these organic components and free iron for analysis, the Advanced Oxidation Process (AOP), the pretreatment method that has been reported previously by our research group,[8-10] was used. In this method, 0.5 mL of porcine blood were diluted to 12 mL with DI water in a photoreactor, and 3 drops of concentrated HNO_3 were added to inhibit the enzyme catalase in the blood. 1 mL of 3% H_2O_2 was then added, and the sample was irradiated with UV light for 40 min. The pH of the solution was then adjusted to 9.5, and the sample was then irradiated again with UV light for 20 more min.

Once the AOP pretreatment process was finished, components were added to the sample to make it suitable for electrochemical analysis using a Bi film electrode. Specifically, the solution was made to contain 5 mM $KBrO_3$, 0.1 M NaOH, and 0.01 M TEA. The sample was then stirred and a square-wave voltammogram was carried out using the previous procedure for Fe(III) analysis.

146

Unfortunately, no peak corresponding to the reduction of Fe(III)-TEA to Fe(II)-TEA could be seen in the voltammogram. This is likely due to interference by the species remaining in the sample after the AOP treatment.

A study was carried out to analyze H_2O_2 and its effect on the electrochemical signal. A standard consisting of 20 mL of 48.5 ppb Fe(III) was analyzed, and it was then measured again after the addition of a 500 μL aliquot of 3% H_2O_2. The results can be seen in Figure 5.8. In the initial analysis, the characteristic peak corresponding to Fe(III)-TEA reduction to Fe(II)-TEA occurs at 0.96 V. After the addition of H_2O_2, however, this peak completely disappears, indicating that the hydrogen peroxide is in some way interfering with the measurement. From the voltammogram, it appears that the H_2O_2 is completely blocking the electrode surface, preventing the measurement of the complex from taking place. A report by Gun and co-workers has also shown that H_2O_2 interferes with and prevents catalytic voltammetry from taking place at a Bi film electrode.[21] In addition, work within our research group on vanadium determination at a Bi film electrode has shown similar results when hydrogen peroxide is present.[22]

To avoid the use of hydrogen peroxide, another sample was prepared in which 2 mL of blood were diluted to 25 mL with DI water. Components were then added so that the sample contained 5 mM $KBrO_3$, 0.1 M NaOH, and 0.01 M TEA. The sample was then exposed to a Bi film electrode, and square-wave voltammetry was carried out. Figure 5.9 shows one of the SWVs that was obtained using this sample. As can be seen, a peak occurs around -0.96 V,
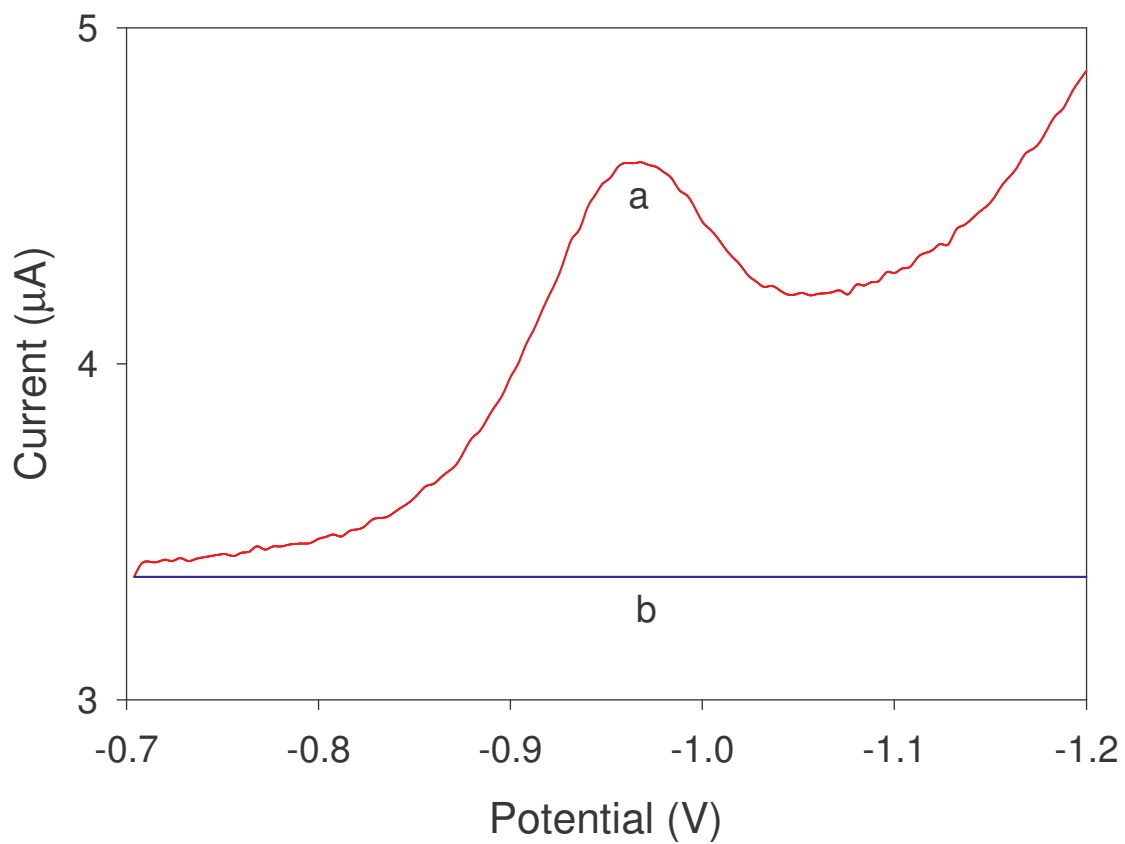
Figure 5.8. Square-wave voltammograms of a 48.5 ppb Fe(III) solution before (a) and after (b) exposure to 500 μL 3% H_2O_2.
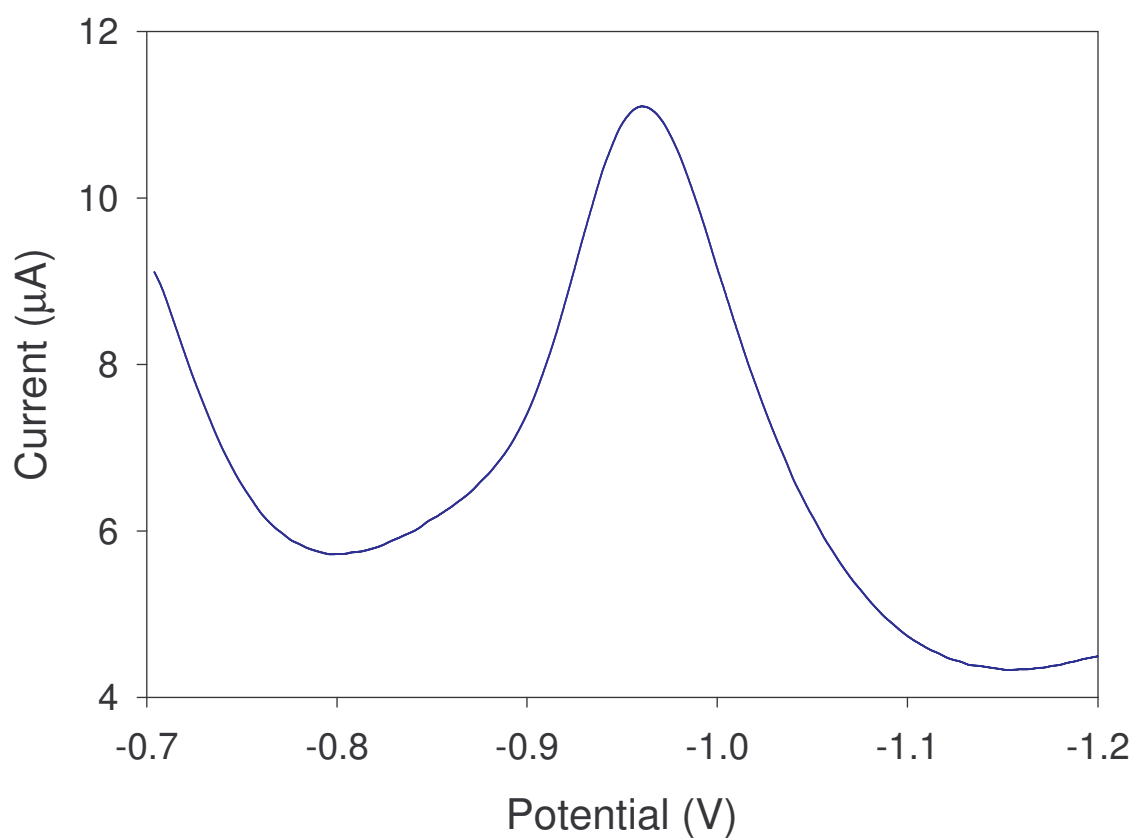
Figure 5.9. Square-wave voltammogram obtained from a sample consisting of 2 mL blood, 23 mL DI H_2O, 5 mM $KBrO_3$, 0.1 M NaOH, and 0.01 M TEA.

indicating that the reduction of Fe(III)-TEA to Fe(II)-TEA is taking place. Unfortunately, successive measurements collected in this sample were highly irreproducible, due to the high concentration of organic interferents present, and it was impossible to quantify the exact amount of iron present in the sample. However, this study demonstrates the feasibility of this bismuth film technique for the determination of iron in biological samples.

5.4. Conclusions

A variety of techniques have been presented for the determination of iron with possible applications in the analysis of biological samples. With further development of the instrumental set-up and thin film morphology, the calcein-doped sol-gels may show great promise as in-situ sensors for iron. In addition, the catalytic voltammetry technique for the analysis of Fe(III) using Bi film electrodes showed great promise, displaying a high sensitivity and reproducibility. Perhaps if coupled with a pretreatment technique other than AOP, such as microwave digestion, this method of analysis could provide a new approach to the determination of iron in biological samples.

References

1.   (a) Lippard, S. J.; Berg, J. M. *Principles of Bioinorganic Chemistry*, University Science Press, CA, 1994. (b) Fraústo da Silva, J. J. R.; Williams, R. J. P. *The Biological Chemistry of the Elements. The Inorganic Chemistry of Life*, 2nd Ed.: Oxford University Press, New York, 2001. (c) *Biological Inorganic Chemistry: Structure and Reactivity*, Bertini, I.; Gray, H. B.; Stiefel, E. I.; Valentine, J. S., Eds., University Science Books, Sausalito, CA, 2006.

2.   (a) Umbreit, J. *Am. J. Hematol.* **2005**, *78*, 225–231. (b) Cook, J. D. *Best Pract. Res. Clin. Haematol.* **2005**, *18*, 319-332. (c) Eisenstaedt, R.; Penninx, B.W.J.H.; Woodman, R. C. *Blood Rev.* **2006**, *20*, 213–226. (d) Brugnara, C. *Clin. Chem.* **2003**, *49*, 1573–1578. (e) Hussong, J. W. *Iron metabolism and hypochromic anemas* in *Clinical Hematology and Fundamentals of Hemostasis*, Harmening, D. M., 4th Ed., F. A. Davis Co.: Philadelphia, 2002, pp. 99-111. (f) Joosten, E. *Gerontology* **2004**, *50*, 49-56. (g) Doig, K. in *Hematology. Clinical Principles and Applications*, Rodak, B. F. 2nd Ed., W. B. Saunders Co.: Philadelphia, 2002, pp. 211-226. (h) Siah, C. W.; Trinder, D.; Olynyk, J. K. *Clin. Chim. Acta* **2005**, *358*, 24-36. (g) Porter, J. B. *Brit. J. Haemat.* **2001**, *115*, 239-252. (i) Porter, J. B. *Semin. Hemat.* **2005**, *42*, S14-S18. (j) Coyne, D. *Kidney Int., Suppl.* **2006**, *101*, S4-S8. (k) Adams, P. C.; Reboussin, D. M.; Barton, J. C.; McLaren, C. E.; Eckfeldt, J. H.; McLaren, G. D.; Dawkins, F. W.; Acton, R. T.; Harris, E. L.; Gordeuk, V. R.; Leiendecker-Foster, C.; Speechley, M.;

Snively, B. M.; Holup, J. L.; Thomson, E.; Sholinsky, P. *New Engl. J. Med.* **2005**, *352*, 1769-1778.

3. Pollitt, E. *Annu. Rev. Nutr.* **1993**, *13*, 521–537.

4. See, e.g., (a) Fairbanks, V. F.; Klee, G. G. *Biochemical Aspects of Hematology*, in *Tietz Textbook of Clinical Chemistry*, 3rd, Ed., Burtus C. A.; Ashwood, E. R. Eds.: W. B. Saunders Co., Philadelphia, 1999, pp. 1700-1704. (b) Alexander, N. M. in *Handbook on Metals in Clinical and Analytical Chemistry*, Seiler, H. G.; Sigel, A.; Sigel, H. Eds.: Marcel Dekker, New York, 1994, pp. 411-421. (c) Ramsay, W. N. M. *Clin. Chim. Acta* **1957**, *2*, 214-220. (d) Ramsay, W. N. M. *Clin. Chim. Acta* **1957**, *2*, 221-226. (e) Worwood, M. *Clin. Chim. Acta* **1997**, *259*, 3-23. (f) Kasperek, K.; Kiem, J.; Iyengar, G. V.; Feinendegen, L. E. *Sci. Total Environ.* **1981**, *17*, 133-143. (g) Flowers, C. H.; Cook, J. D. *Clin. Chem.* **1999**, *45*, 1826-1832. (h) Pootrakul, P.; Josephson, B.; Huebers, H. A.; Finch, C. A. *Blood*, **1988**, *71*, 1120-1123. (i) Leflon, P.; Plaquet, R. *Clin. Chem.* **1986**, *32*, 521-522.

5. McClean, S. W.; Purdy, W. C. *Anal. Chim. Acta* **1974**, *69*, 425-430.

6. (a) Matson, W. R.; Vitukevich, R. U.S. Patent No. 4233031, **1980**. (b) Palmer, J. H.; Sapienza, T. J.; Zink, E. W. *Clin. Chem.* **1988**, *34*, 1510-1511. (c) Skikne, B. S*. Clin. Chem.* **1987**, *33*, 1645-1647. (d) San Jose, M. E.; Sarandeses, A.; Alvarez, D.; Valdes, L.; Chomon, B.; Del Rio, M. J. *Scand. J. Clin. Lab. Invest.* **1993**, *53*, 653-658. (e) Yamaguchi, Y.; Iyama,

S.; Yamanishi, H.; Kimura, S.; Hata, N.; Amino, N. *Seibutsu Shiryo Bunseki* **1994**, *16*, 121-124. *Chemical Abstracts*: 122:285837.

7. (a) Tietz, N. W.; Rinker, A. D.; Morrison, S. R. *Clin. Chem.* **1994**, *40*, 546-551. (b) Tietz, N. W.; Rinker, A. D.; Morrison, S. R. *Clin. Chem.* **1996**, *42*, 109-111. (c) College of American Pathologists (CAP). *Comprehensive Chemistry Survey*, CAP, Northfield, IL, 1992.

8. Yong, L.; Armstrong, K.C.; Dansby-Sparks, R.N.; Carrington, N.A.; Chambers, J.Q.; Xue, Z.-L. *Anal. Chem.* **2006**, *78*, 7582.

9. Rodman, D.L.; Carrington, N.A.; Xue, Z.-L. *Talanta* **2006**, *70*, 426.

10. Rodman, D.L.; Carrington, N.A.; Xue, Z.-L. *Talanta* **2006**, *70*, 668.

11. (a) Allain, L. R.; Sorasaenee, K.; Xue, Z. *Anal. Chem.* **1997**, *69*, 3076. (b) Allain, L. R.; Xue, Z. *Anal. Chem.* **2000**, *72*, 1078.

12. Gao, Z.; Li, P.; Wang, G.; Zhao, Z. *Anal. Chim. Acta* **1990**, *241*, 137.

13. Bobrowski, A.; Nowak, K.; Zarebski, J. *Anal. Bioanal. Chem.* **2005**, *382*, 1691.

14. Ali, A.; Zhang, Q.; Dai, J.; Huang, X. *BioMetals* **2003**, *16*, 285.

15. Breuer, W.; Epsztejn, S.; Cabantchik, Z.I. *J. Biol. Chem.* **1995**, *270*, 24209.

16. Nivens, D.A.; Zhang, Y.; Angel, S.M. *J. Photoch. Photobio. A* **2002**, *152*, 167.

17. Stozhko, N.Yu.; Morosanova, E.I.; Kolyadina, L.I.; Azarova, Zh.M. *J. Anal. Chem.* **2004**, *59*, 960.

18. Lin, L.; Lawrence, N.S.; Thongngamdee, S.; Wang, J.; Lin, Y. *Talanta* **2005**, *65*, 144.

19. Wang, J.; Lu, D.; Thongngamdee, S.; Lin, Y.; Sadik, O.A. *Talanta* **2006**, *69*, 914.

20. Golimowski, J. *Anal. Lett.* **1989**, *22*, 481.

21. Gun, J.; Salaün, P.; van den Berg, C.M.G. *Anal. Chim. Acta* **2006**, *571*, 86.

22. Dansby-Sparks, R. unpublished results.

Part 6

Electrochemical Quartz Crystal Microbalance Studies of

the Cr(III)-DTPA Complex

6.1. Introduction

Electrochemical determination of ultratrace (ppt level) concentrations of Cr(VI) has often been conducted using catalytic adsorptive stripping voltammetry (CAdSV).[1,2] Wang and coworkers recently pioneered the use of bismuth film electrodes to replace toxic Hg electrodes.[1] CAdSV is based on the accumulation of analyte metal complexes on a suitable working electrode by potential-controlled adsorption and subsequent electrochemical oxidation or reduction of the preconcentrated species. Coupling the adsorptive accumulation with a catalytic reaction leads to a significant increase of the analytical signal and the sensitivity of detection. In the procedure reported by Wang and coworkers, Cr(VI) is reduced to Cr(III) electrochemically on the Bi film electrode, and Cr(III) then binds to diethylenetriaminepentaacetic acid (DTPA) to yield an electroactive species $[Cr^{III}(H_2O)HY]^{-}$ [3,4] which is adsorbed onto the Bi electrode surface. $[Cr^{III}(H_2O)HY]^{-}$ is further reduced to $[Cr^{II}H_2Y]^{-}$ electrochemically at -1.1 V. Nitrate in the electrolyte solution oxidizes the Cr(II) species back to Cr(III) $[Cr^{III}(H_2O)HY]^{-}$ in a catalytic cycle, which significantly increases the square-wave voltammetry signal. This electrochemical process is summarized in Figure 6.1. Our research group has recently reported the use of this CAdSV technique for the determination of Cr in hog blood samples after they have been pretreated using the Advanced Oxidation Process (AOP).[5]

Although the Cr-DTPA complex has been used widely for Cr(VI) electrochemical detection, this complex has never been characterized and the nature of the interaction between the Cr complex and an electrode surface is not
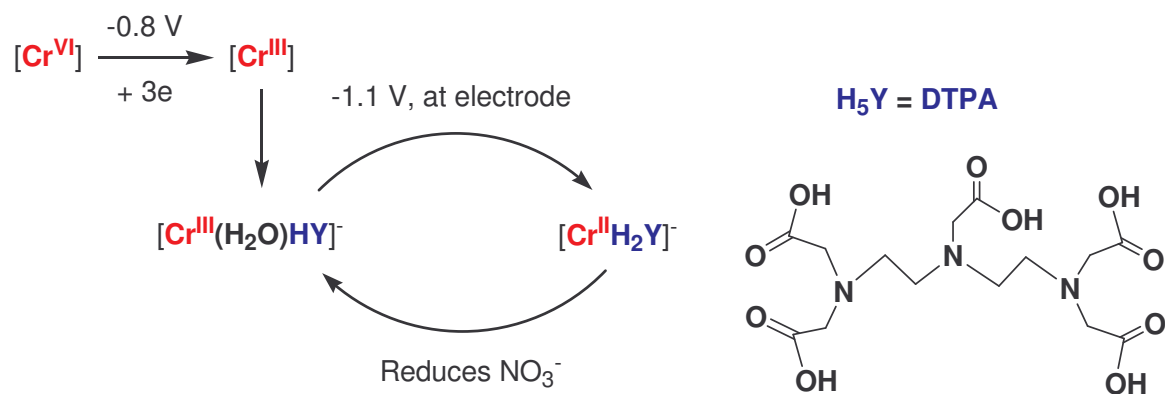
Figure 6.1. CAdSV process for the analysis of Cr(VI) at a bismuth film electrode.[3,4]

clear. In order to better understand this process for potential applications in improving the overall measurement cycle, fundamental studies involving the Cr-DTPA complex have been carried out using the electrochemical quartz crystal microbalance (EQCM).

6.2. Experimental

6.2.1. Chemical Reagents and Materials

Potassium bromide (KBr, Mallinckrodt Chemicals), hydrochloric acid (HCl, certified A.C.S., Fisher), potassium nitrate (KNO_3, certified A.C.S., Fisher), acetic acid (CH_3COOH, glacial, Fisher), sodium acetate (CH_3COONa, certified A.C.S., Fisher), and diethylenetriaminepentaacetic acid (DTPA; $\geq$99%, Fluka) were used as received. Standard solutions of Cr(VI) were prepared by serial dilution of a 1017 µg/mL AA standard (Sigma-Aldrich). Solutions and standards were prepared using deionized (DI) water (18 MΩ-cm) from a Barnstead International E-pure 4-holder deionization system. The bismuth plating solutions used during these studies were prepared by dissolving Bi needles (99.998%, Alfa Aesar) in nitric acid (HNO_3, trace metal grade, Fisher) and diluting appropriately to contain 0.5 M KBr and 1.0 M HCl. The electrolyte solution for the Cr(VI) analysis contained 0.1 M CH_3COONa and 0.25 M KNO_3, and it was pH adjusted to 6.0 with CH_3COONa. The DTPA solution was prepared by dissolving DTPA (0.1 M) in DI water while adjusting the pH to 6.0 with ammonium hydroxide (NH_4OH, Fisher).

For the electrochemical experiments, a Teflon cell was used to house the EQCM crystals. Polished, mounted, and bonded gold-coated quartz crystals (International Crystal Manufacturing Company, Inc.) were used as received. Each crystal had a fundamental frequency of approximately 7.995 MHz and an electrode diameter of 0.546 cm, consisting of a 1000 Å film of gold deposited on a 100 Å layer of chromium. Platinum wire and silver/silver chloride were used as the auxiliary and reference electrodes, respectively.

6.2.2. Instrumentation

A CH Instruments model 400A potentiostat with electrochemcial quartz crystal microbalance (EQCM) capability and corresponding software were used for the electrochemical studies.

6.3. Results and Discussion

In order to better understand the interaction between chromium, DTPA, and the Bi electrode surface, an electrochemical quartz crystal microbalance (EQCM) study was done. In this study, a gold QCM crystal was exposed to a solution consisting of 39.9 ppm Bi, 0.5 M KBr, and1.0 M HCl. A potential of -0.25 V was then applied for 120 s. As can be seen in Figure 6.2, the frequency of the gold QCM crystal drops as the potential is applied over time, due to the formation of a Bi film on the crystal surface. Based on the Sauerbrey equation (Eq. 1.2), the mass of bismuth deposited onto the crystal surface was calculated to be 4.15 x 10^{-7} g. The volume of this deposited mass was then determined to be 4.24 x
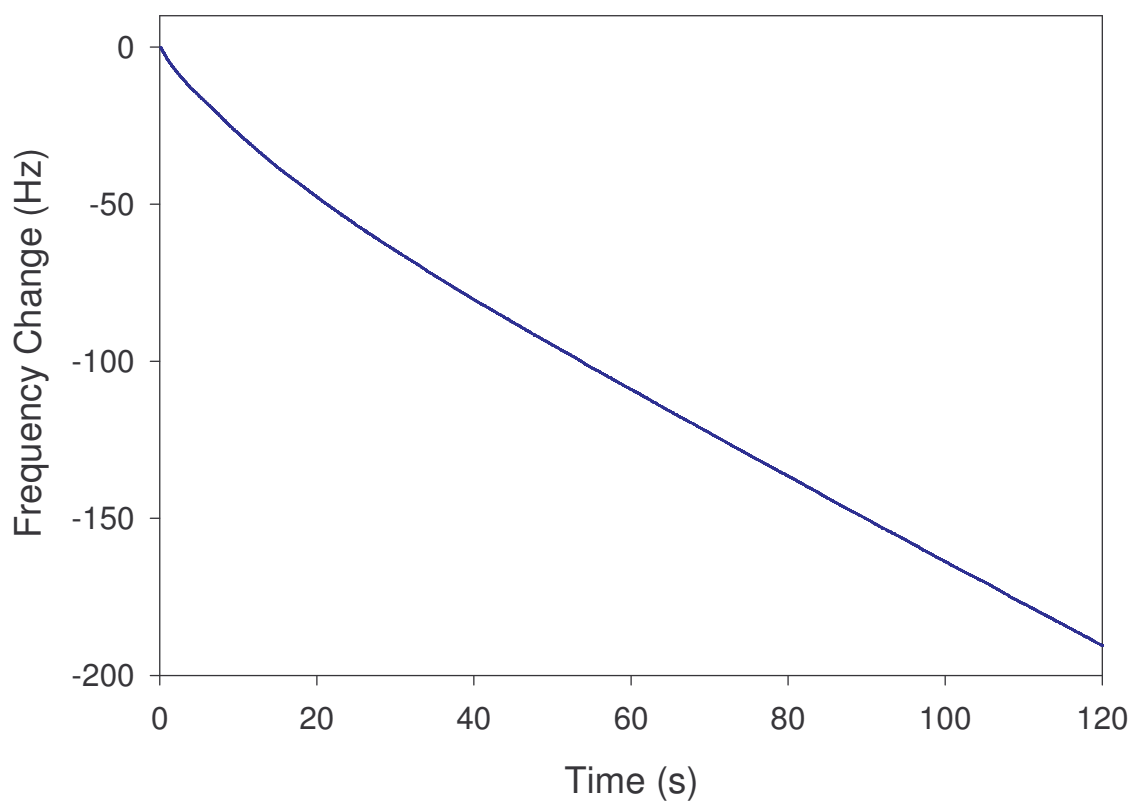
Figure 6.2. Change in frequency over time as a potential of -0.25 V is applied to a solution consisting of 39.9 ppm Bi, 0.5 M KBr, and1.0 M HCl.

10^{-8} cm^3, using the density of bismuth (9.808 g/cm^3). If uniform coverage of the bismuth film on the QCM crystal surface takes place, then the film should have a geometric area similar to that of the electrode, 0.234 cm^2. Taking into account the surface roughness factor of the electrode, estimated to be 2.50 based on earlier reports,[6,7] its true area can be determined to be 0.585 cm^2 using Eq. 6.1.[8] Using this value with the assumption that the deposited film forms a cylindrical shape, the thickness of the film can be calculated using Eq. 6.2. This thickness, determined to be 7.25 Å, is greater than the distance between Bi atoms in the metal, approximately 3.30 Å,[9] indicating that the film is layers thick and has a large enough area to cover the entire QCM electrode surface.

$$R = A_T / A_G$$
(Eq. 6.1)

where R is the surface roughness, A_T is the true area, and A_G is the geometrical area.

$$V = \pi \cdot r^2 h$$
(Eq. 6.2)

where V is the volume, r is the radius, and h is the height of the cylinder.

After rinsing the crystal cell with water and electrolyte solution, a solution (3 mL) consisting of 0.98 ppm Cr(VI), 0.1 M CH$_3$COONa, and 0.25 M KNO$_3$ (pH

adjusted to 6.0) was placed in the cell, along with 120 µL 0.1 M DTPA (pH

adjusted to 6.0). A potential of -0.8 V was then applied for 140 s, and the

frequency of the crystal was monitored. Figure 6.3 shows the drop in frequency

over time as the potential is applied. This is a result of the Cr(III)-DTPA complex

being adsorbed onto the crystal surface. Using the Sauerbrey equation (Eq. 1.2),

the amount of Cr(III)-DTPA complex adsorbed to the electrode surface was

determined to be 8.61 x 10^{-10} mol/cm^2. Through a simple conversion using

Avogadro's number, the surface coverage was determined to be 19.3

Å^2/molecule.

Crystal structure data of several reported M-DTPA complexes[10,11] were

used to obtan an approximate surface coverage of the deposited Cr-DTPA

complex. For example, a molecule of Bi(H$_2$DTPA)•2H$_2$O has a volume of 472

Å^3.[8] If it is assumed that this complex has a spherical shape, Eq. 6.2 can be

used to calculate the radius of one molecule.

$$V = \frac{4}{3} \pi \cdot r^3 \qquad \text{(Eq. 6.2)}$$

where V is the volume and r is the radius of the sphere.

The radius of one Bi(H$_2$DTPA)•2H$_2$O molecule was determined to be ca.

4.83 Å. Based on this value, it was determined that the area of the molecule is

73.3 Å^2 (πr^2). Comparing this with the calculated Cr(III)-DTPA surface coverage,
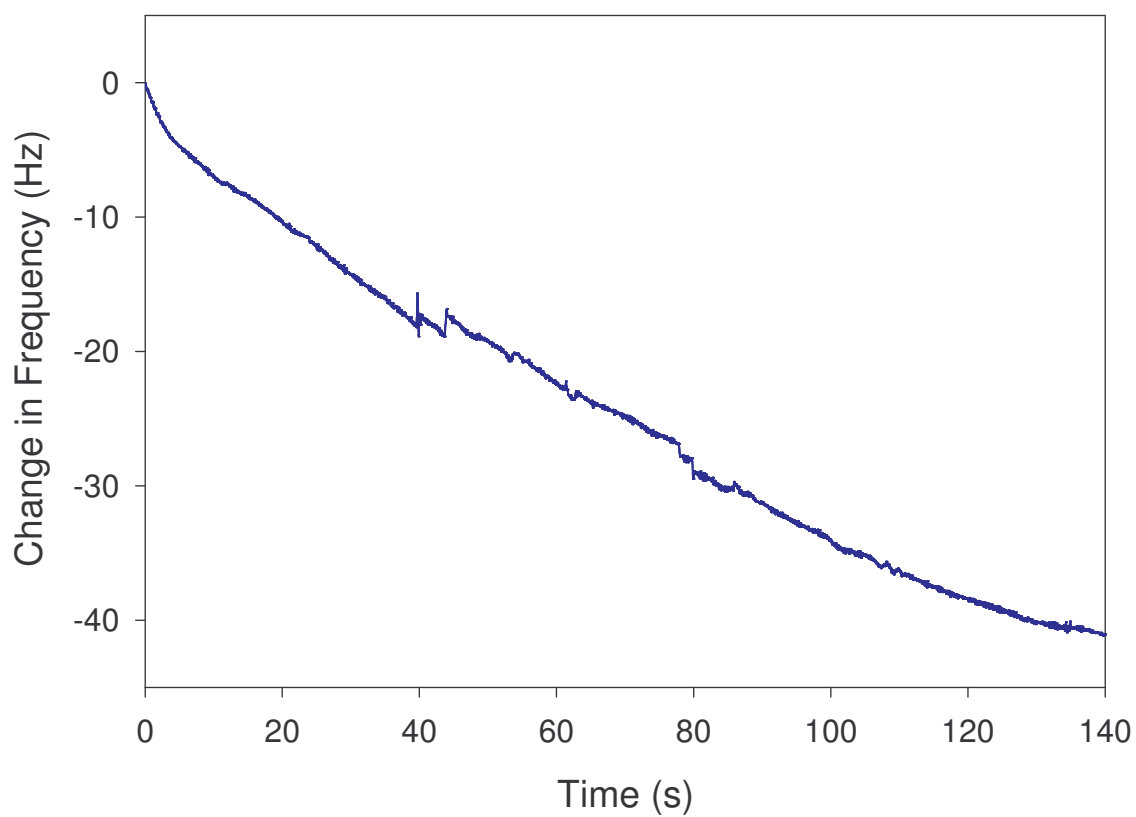
Figure 6.3. Change in frequency over time as the Cr(III)-DTPA complex is adsorbed onto the electrode surface.

9.3 Å^2/molecule, it can be estimated that there are 3.80 layers of Cr(III)-DTPA deposited on the crystal surface. Additional crystal structure data involving Hf^{IV}-DTPA and Sn^{IV}-DTPA resulted in very similar calculations, yielding 3.93 and 3.90 layers of deposited Cr(III)-DTPA, respectively. Thus, based on these calculations, it is reasonable to assume a multilayer formation of the Cr(III)-DTPA complex at the electrode surface.

Once the frequency drop over 140 s had taken place, a cyclic voltammogram was collected. The result is shown in Figure 6.4. The peak occurring around -1.1 V correlates well with previous reports describing [Cr^{III}(H$_2$O)HY]$^-$ reduction to [Cr^{II}H$_2$Y]$^-$ at a similar potential.[1-5] The frequency change of the crystal was also monitored while this cyclic voltammogram was collected (Figure 6.5). The frequency increases as the forward voltammetric sweep is carried out. This is a result of the adsorbed Cr(III)-DTPA complex at the Bi electrode surface being reduced and removed during the potential sweep, increasing the frequency of the crystal. During the reverse sweep, the crystal frequency stays fairly constant, as no mass changes due to electrochemical processes are taking place at the electrode surface.

It seems as if the Cr(III)-DTPA complex adsorbs very strongly to the Bi film surface. After the complex had been preconcentrated at the electrode surface by applying a potential of -0.8 V for 140 s, several successive CVs were collected (Figure 6.6). Over time, the peak currents associated with the reduction of [Cr^{III}(H$_2$O)HY]$^-$ to [Cr^{II}H$_2$Y]$^-$ decrease as more and more of the adsorbed complex
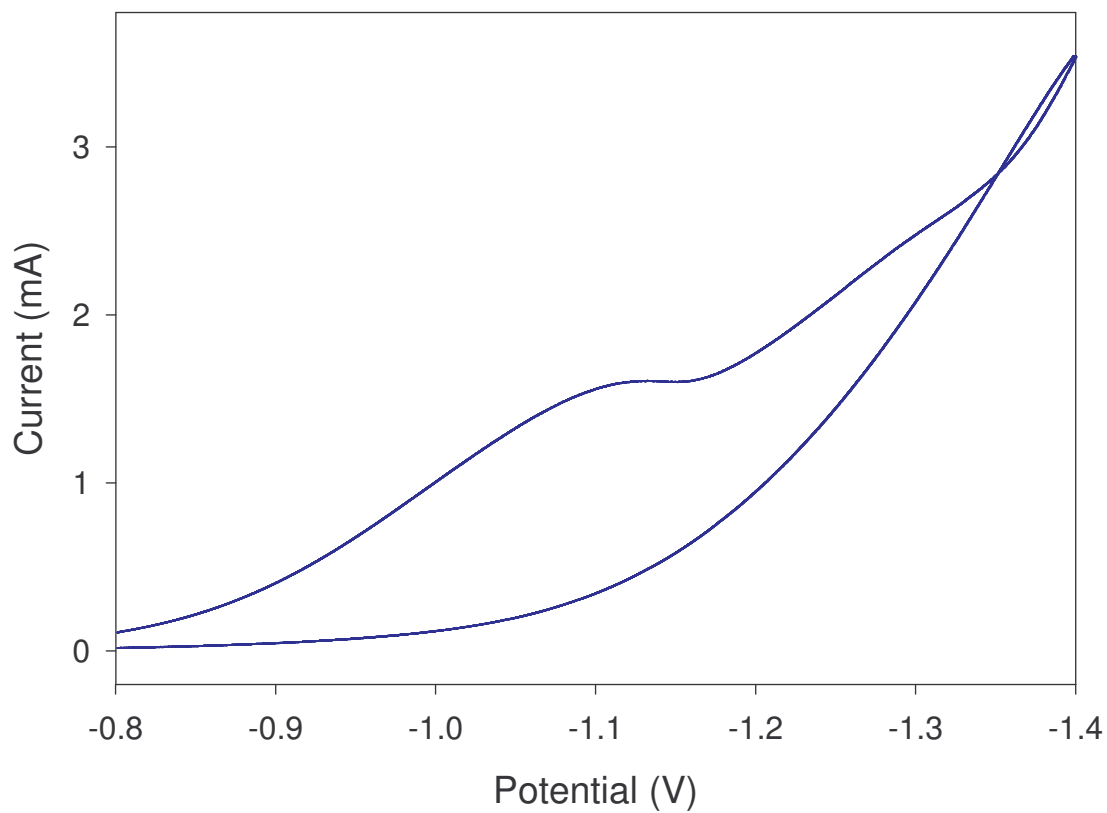
Figure 6.4. Cyclic voltammogram collected after adsorption of the Cr(III)-DTPA complex onto the EQCM crystal surface.
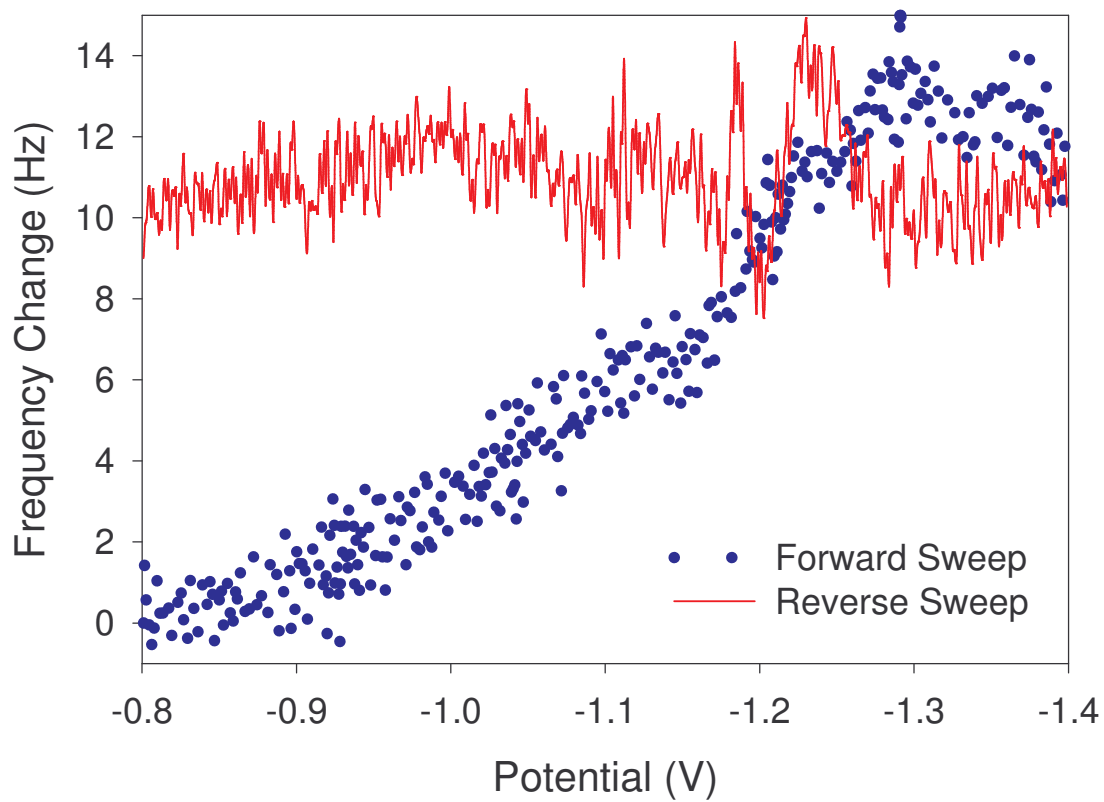
Figure 6.5. Frequency change during the forward (blue) and reverse (red) sweeps of the cyclic voltammogram shown in Figure 6.4.
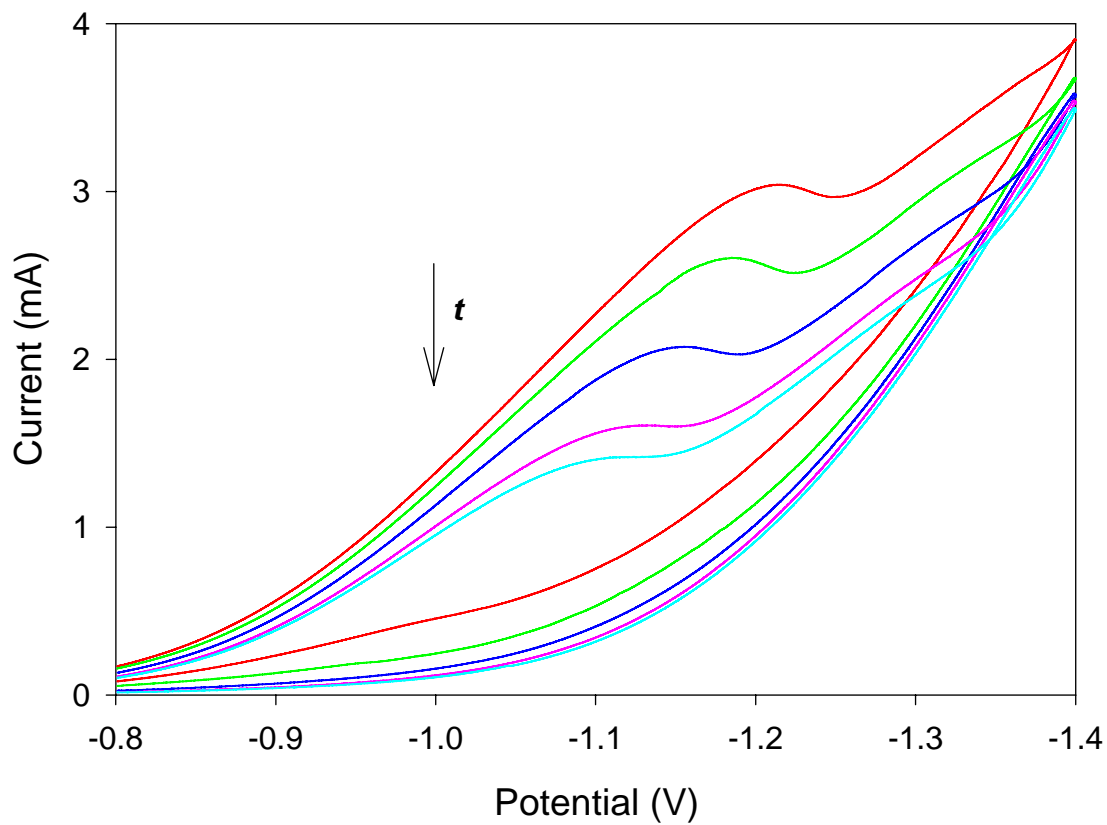
Figure 6.6. Successive cyclic voltammograms collected at a bismuth film QCM electrode after adsorption of the Cr(III)-DTPA complex.

is removed. However, even after 5 scans, the complex is still present, indicating that it is indeed strongly adsorbed to the Bi surface. It is likely for this reason that Wang and co-workers report a cleaning step during their Cr(VI) electrochemical analyses in which the electrode is held at -1.2 V for 30 s in pure electrolyte solution.[1] In carrying out this cleaning treatment, the majority of the Cr(III)-DTPA complex should be desorbed from the Bi film surface so that subsequent sensing cycles can be carried out.

6.4. Conclusion and Future Work

This brief, EQCM study seems to verify that the Cr(III)-DTPA complex is indeed adsorbed onto the bismuth film surface during the electroanalysis process. By monitoring the change in frequency of the quartz crystal as various potentials are applied, it was possible to diagnose the electrochemical processes taking place. Future EQCM studies could be used to determine the mechanism of DTPA binding in the system, i.e. whether it binds to the Bi film surface or the Cr(III) in solution first. In addition, should the crystal structure of the Cr(III)-DTPA complex be determined, it would provide useful insight into the binding between Cr, DTPA, and the Bi film surface.

References

1. Lin, L.; Lawrence, N.S.; Thongngamdee, S.; Wang, J.; Lin, Y. *Talanta* **2005**, *65*, 144.

2. Bas, B. *Anal. Chim. Acta* **2006**, *570*, 195.

3. Li, Y.; Xue, H. *Anal. Chim. Acta* **2001**, *448*, 121.

4. Sander, S.; Navratil, T.; Novotny, L. *Electroanal.* **2003**, *15*, 1513.

5. Yong, L.; Armstrong, K.C.; Dansby-Sparks, R.N.; Carrington, N.A.; Chambers, J.Q.; Xue, Z.-L. *Anal. Chem.* **2006**, *78*, 7582.

6. Lust, E.; Janes, A.; Sammelselg, V.; Miidla, P.; Lust, K. *Electrochim. Acta* **1998**, *44*, 373.

7. Lust, E.; Kallip, S.; Moller, P.; Janes, A.; Sammelselg, V.; Miidla, P.; Vaartnou, M.; Lust, K. *J. Electrochem. Soc.* **2003**, *150*, E175.

8. The surface roughness factor used for this calculation is based on the highest surface roughness factor given for Bi in references 6 and 7. The Bi investigated in those studies involved polished single crystal, electrochemically-etched, and chemically-etched electrodes. The Bi used in our studies is different in that it is a freshly deposited thin film.

9. Greenwood, N.N.; Earnshaw, A. *Chemistry of the Elements*, 2nd Ed.; Pergamon Press: New York, 1997, 551.

10. Brechbiel, M.W.; Gansow, O.A.; Pippin, C.G.; Rogers, R.D.; Planalp, R.P. *Inorg. Chem.* **1996**, *35*, 6343.

11. Ilyukhin, A.B.; Sergienko, V.S.; Davidovich, R.L.; Logvinova, V.B. *Russ. J. Inorg. Chem.* **1997**, *42*, 1341.

APPENDICES

Appendix A

A.1. Study of the Relationship Between Film Deposition Time and Cr(VI) Limit of Detection

Previous studies on the relationship between the applied negative potential and deposition time with film thickness and porosity have been carried out and reported.[1,2] Our own studies have shown that increased film thickness led to higher limits of detection for Cr(VI), presumably due to increased resistance to mass transfer of the analyte ions to the electrode surface. As can be seen in Figure A.1, reduced electrodeposition times lowered the limit of detection for the system. However, films resulting from deposition times shorter than 60 s showed no enhanced sensitivity for Cr(VI). This is presumably due to the fact that films formed at such shorter times were structurally unstable.

A.2. EQCM Study when Longer Deposition Times are Used

When a potential of -0.9 V was applied at a gold QCM crystal exposed to sol solution for an extended period of time, a much larger drop in frequency

---

[1] Deepa, P.N.; Kanungo, M.; Claycomb, G.; Sherwood, P.M.A.; Collinson, M.M. *Anal. Chem.* **2003**, *75*, 5399.

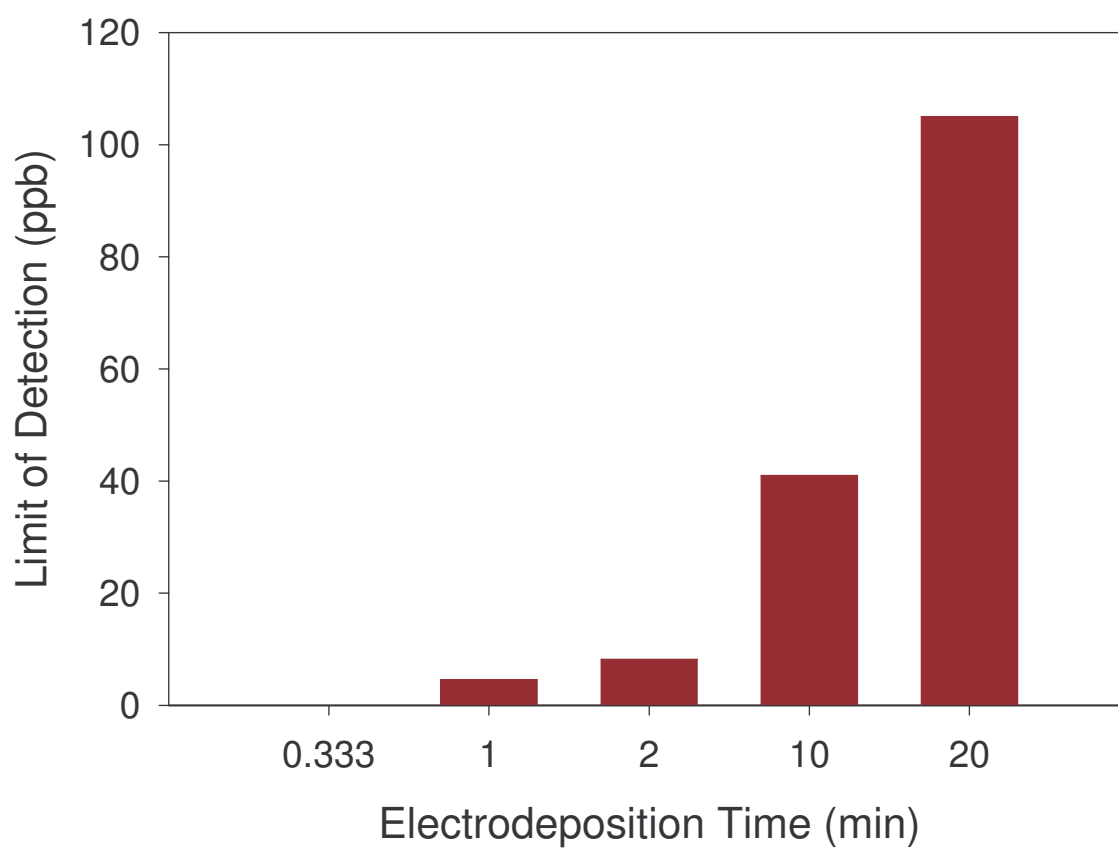[2] Walcarius, A.; Sibottier, E. *Electroanal.* **2005**, *17*, 1716.

Figure A.1. Variation of the limit of detection for Cr(VI) of the proposed system with the sol-gel electrodepostition time.

occurred (Figure A.2). Eventually, the sol-gel film becomes so thick that the
crystal stops oscillating.

A.3. XPS Study of Thicker Sol-gel Films

XPS spectra collected at very thick sol-gel coatings, such as that
deposited on the QCM crystal used to produce Figure A.3, showed even more
intense N, Si, and C peaks, even when the signal-to-noise ratio was smaller due
to less repetitive cycling and signal averaging.

A.4. Additional XPS Spectrum Indicating the Presence of Gold

XPS spectra collected at some of the electrodeposited sol-gel films
showed peaks corresponding to Au (Figure A.4). This is apparently due to
vacant areas amongst the sol-gel islands, caused by the evolution of hydrogen
gas during the electrodeposition process.

A.5. Study of the Effect of Ligand Percentage in the Sol Solution

Experiments were carried out to determine the optimal ratio of 4-[2-
(trimethoxysilyl)ethyl]-pyridine to TMOS in the starting sol solution. Figure A.5
shows a plot of the volume percentage of 4-[2-(trimethoxysilyl)ethyl]-pyridine
used in the ligand/TMOS mixture for the coating process versus the measured
peak current when each different coating is exposed to a solution consisting of
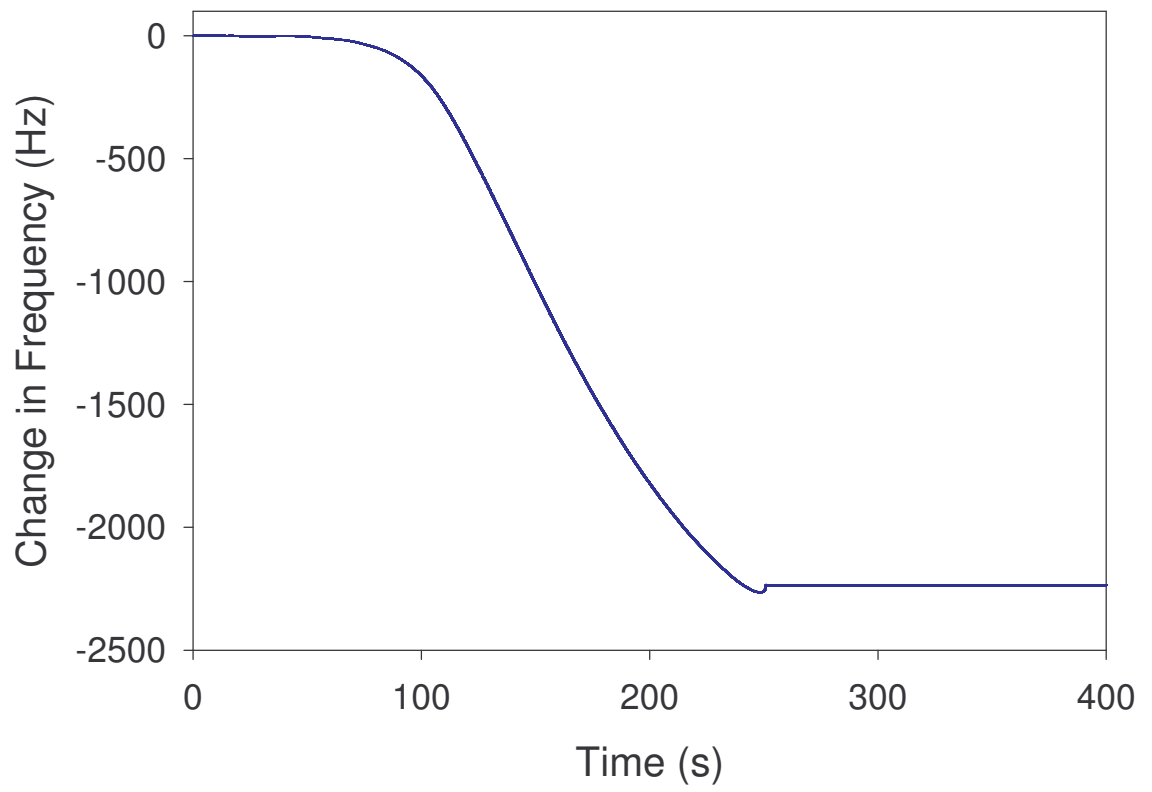48 ppb Cr(VI), 0.1 M HCl, and 0.1 M KCl for 10 minutes. As can be seen, the

Figure A.2. Frequency change for an extended electrodeposition at a QCM surface.
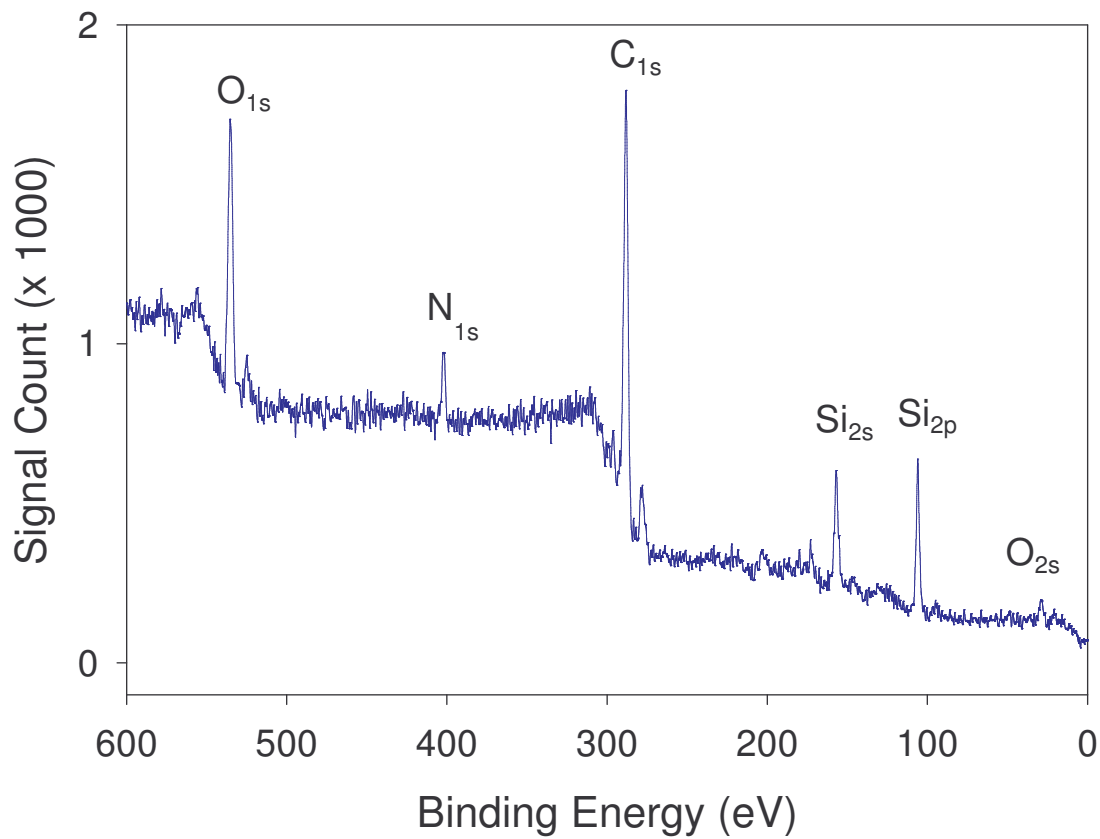
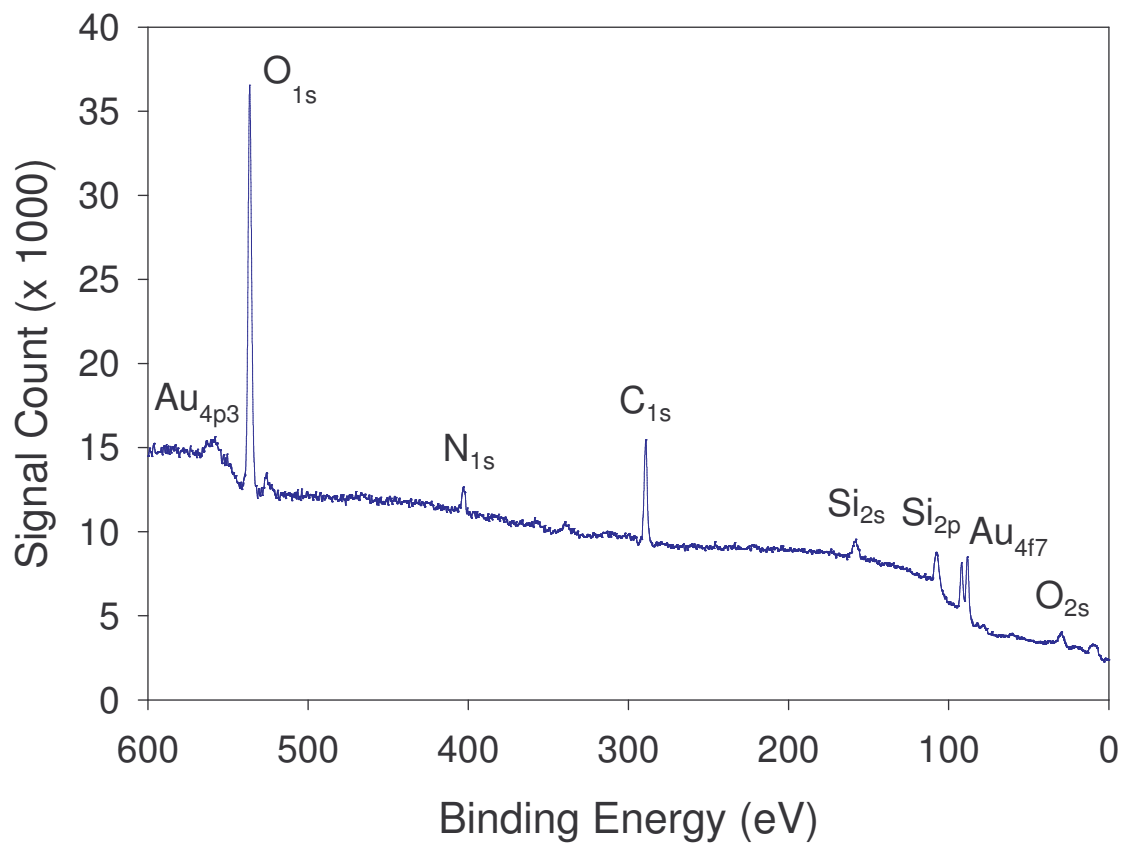**Figure A.3.** XPS spectrum collected at a thick functionalized sol-gel film deposited on a QCM crystal.

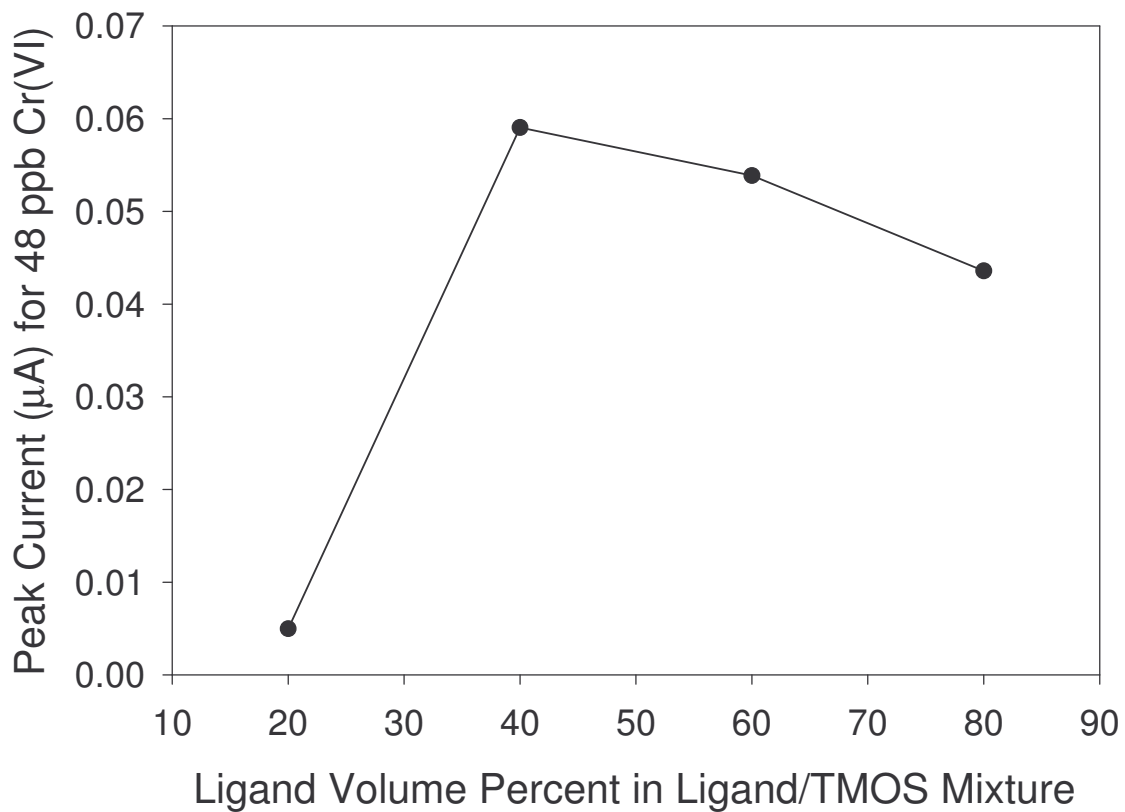**Figure A.4.** Additional XPS spectrum of a sol-gel electrodeposited on a gold QCM crystal.

Figure A.5. Plot of the optimal volume percentage of 4-[2-(trimethoxysilyl)ethyl]-pyridine in the sol solutions used for electrode coating versus the peak current obtained using each coated electrode for the analysis of a 48 ppb Cr(VI) solution.

optimal volume percentage of 4-[2-(trimethoxysilyl)ethyl]-pyridine in the

ligand/TMOS mixture occurs from 40-60%.

Appendix B

B.1. Spectra of Monoliths Exposed to Cr(VI) Solutions of Varying pH

Figure B.1 shows spectra of monoliths exposed to Cr(VI) solutions of varying pH. At higher pH values, the wavelength maxima occur around 370 nm due to the presence of CrO_4^-. At lower pH values, the maxima occur around 350 nm due to the presence of $HCrO_4^-$, $Cr_2O_7^{2-}$ and $HCr_2O_7^-$.

B.2. Spectra of the Increased Cr(VI) Absorbance Over Time by a Functionalized Monolith

Figure B.2 shows the increase of Cr(VI) absorbance over time for the functionalized monolith discussed in Section 3.3.1.3. For each measurement, the gel was removed from the Cr(VI) solution, rinsed with DI water, scanned using UV-vis spectroscopy, and then reinserted into solution.

B.3. SEM Images and XPS Spectrum Referred to in Section 3.3.2.2

Figures B.3 and B.4 show the SEM images and XPS spectrum referred to in Section 3.3.2.2 of the text.
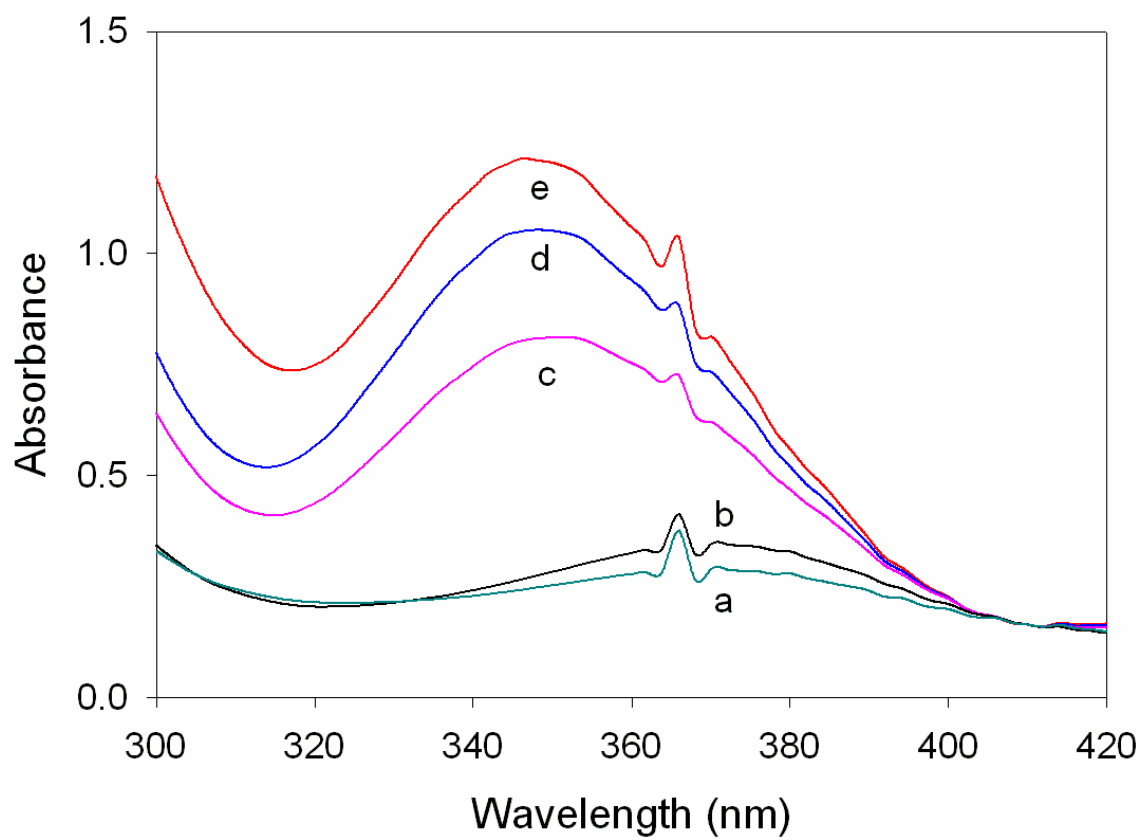
Figure B.1. Spectra obtained of functionalized monoliths after exposure to 20 ppm Cr(VI) of pH =: (a) 10.75; (b) 8.74; (c) 3.58; (d) 2.70; (e) 0.96.
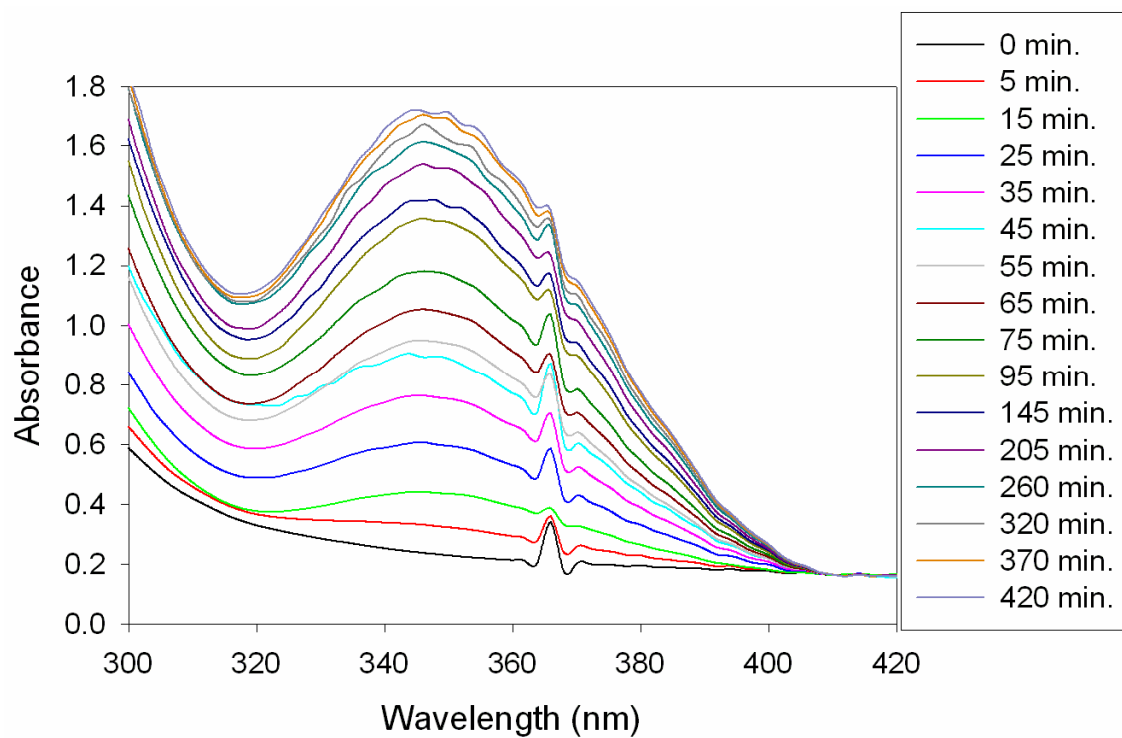
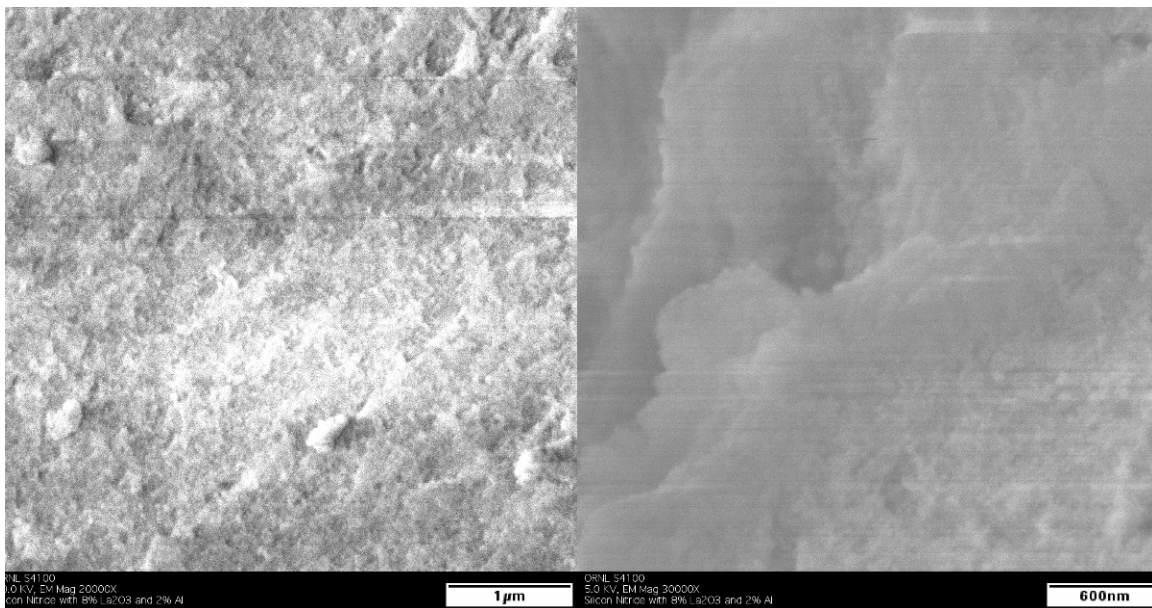**Figure B.2.** Cr(VI) uptake as a function of immersion time for a pyridine-functionalized monolith.

Figure B.3. SEM images of a pyridine-functionalized sol-gel monolith at 20 000

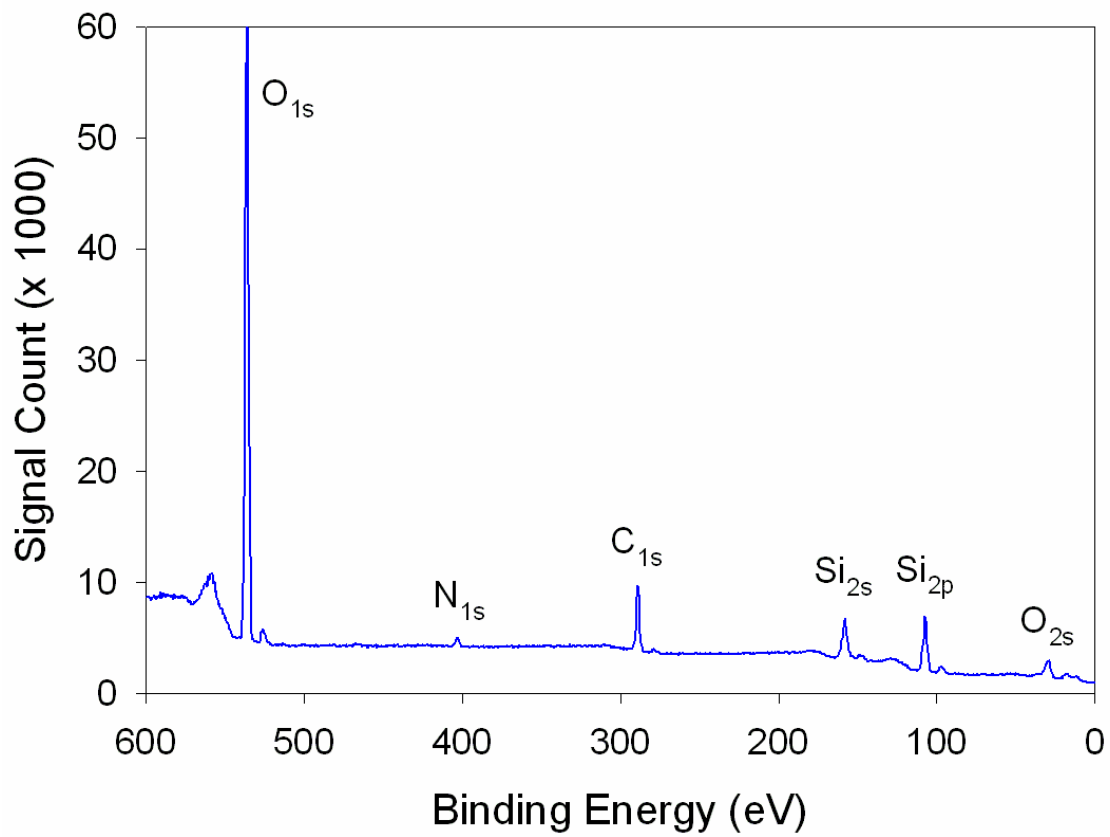x (right) and 30 000 x (left) magnification.

Figure B.4. XPS spectrum obtained of a functionalized sol-gel monolith.

B.4. Color Development of a Monolith in Diphenylcarbazide After Prior Exposure to a Cr(VI) Solution

Figure B.5 shows the color development at 540 nm of a gel that has been previously exposed to a 4.0 ppm Cr(VI) solution for three hours followed by immersion in a solution of diphenylcarbazide. The absorbance increases up until about 60 minutes. For this reason, gels were typically exposed to diphenylcarbazide solution for 60 minutes prior to analysis by UV-vis spectroscopy.

B.5. Analysis of Monolith Supernatant Solution with Diphenylcarbazide

Spectra were collected of ppb level Cr(VI) solutions exposed to diphenylcarbazide with no monoliths present. The spectra and corresponding calibration plot are shown in Figure B.6. As can be seen, there is a linear relationship between the Cr(VI) concentration and the absorbance. A study was carried out in which functionalized monoliths were exposed to ppb level Cr(VI) solutions and their supernatants analyzed using diphenylcarbazide (referred to in Section 4.3.3). Five monoliths were each exposed to 5 mL of a 156 ppm Cr(VI) / 0.096 M HCl solution, and five other monoliths were each exposed to 5 mL of a 59 ppb Cr(VI) / 0.096 M HCl solution. After soaking in the solutions for five hours, the gels were removed, and 2 mL of diphenylcarbazide solution was added to each of their supernatants. These solutions were then analyzed by UV-vis spectroscopy, and their spectra were compared to spectra of the original solutions before exposure to the monoliths. The results can be seen in Figure
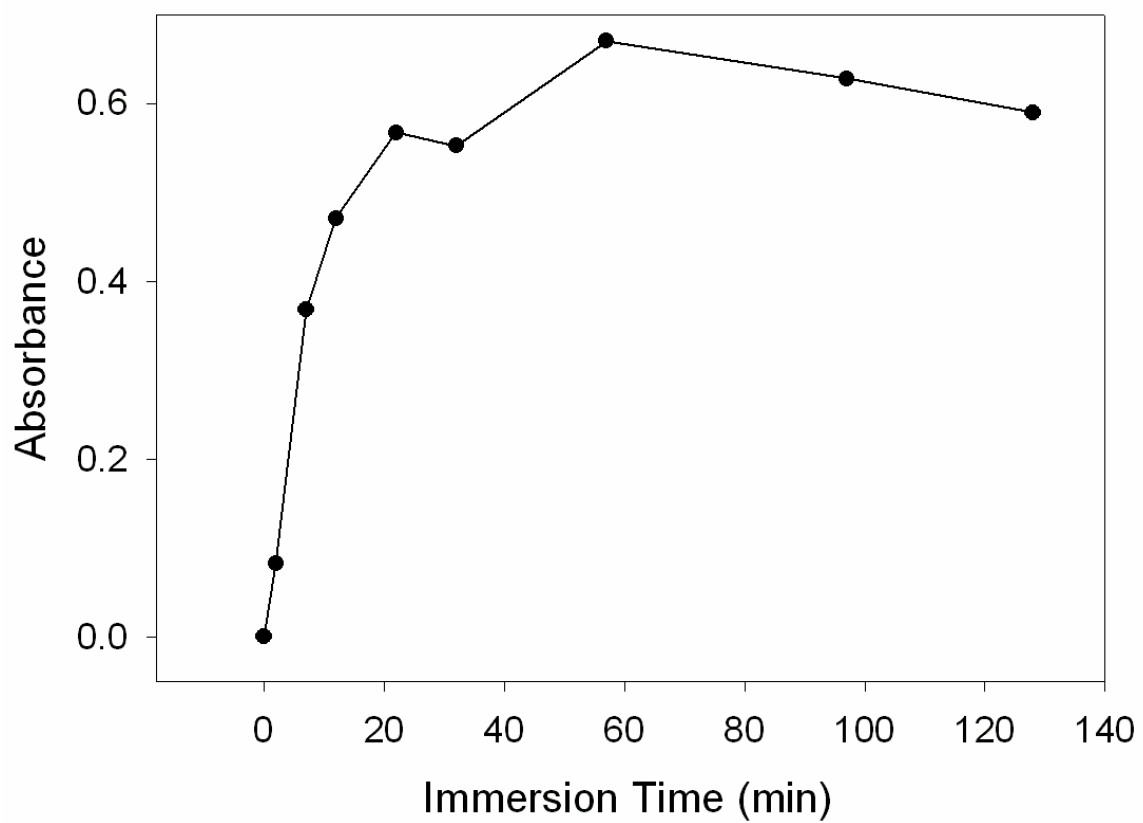
186

Figure B.5. Color development of a functionalized monolith (having prior exposure to 4.0 ppm Cr(VI)) after immersion in a diphenylcarbazide solution.
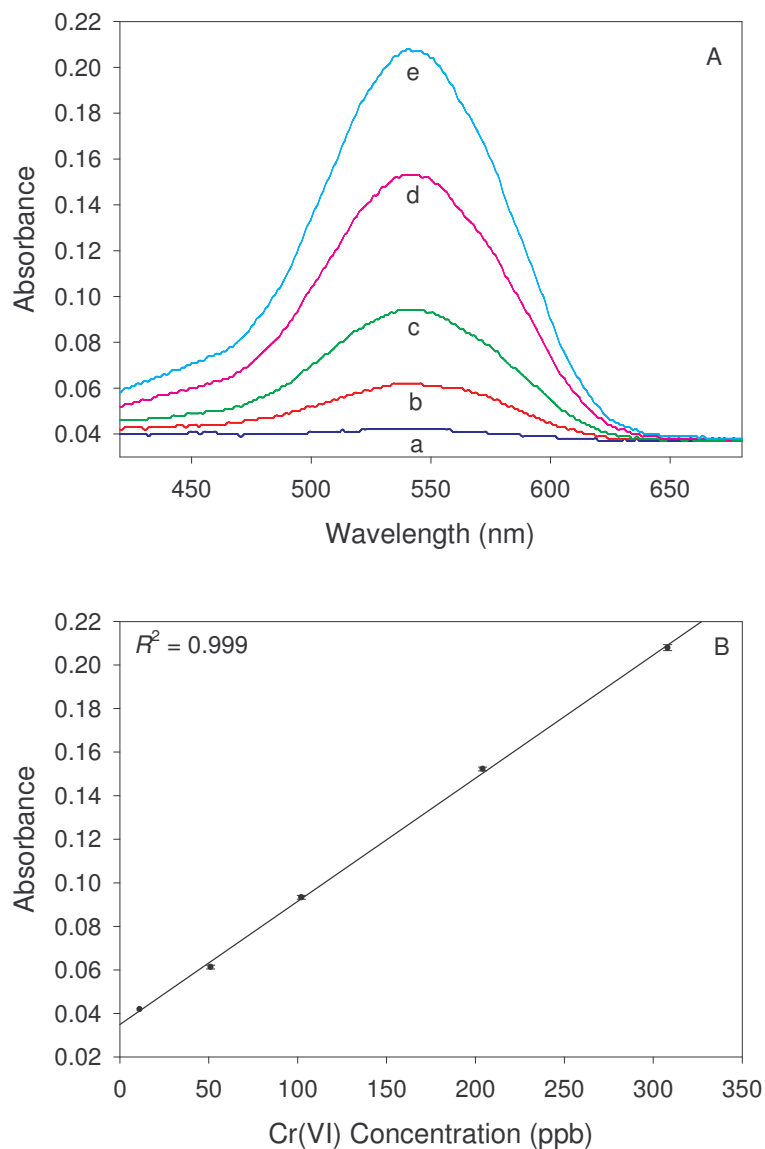
Figure B.6. (A) Spectra of Cr(VI)-containing solutions after exposure to diphenylcarbazide. 5 mL of each solution were exposed to diphenylcarbazide, and the color was allowed to develop for one hour before analyzing in 1 cm path length cuvettes. (a) 0 ppb; (b) 11 ppb; (c) 51 ppb; (d) 102 ppb; (e) 204 ppb; (f) 308 ppb Cr(VI). (B) The corresponding calibration plot. Data points represent an average of measurements from three solutions of the same concentration.

B.7. Based on the average absorbance measurements determined for each set of concentrations and the calibration plot shown in Figure B.6, it was determined that, for the 156 ppb Cr(VI) solutions, 16.8 ppb Cr(VI) remained, and for the 59 ppb Cr(VI) solutions, the amount of Cr(VI) remaining was below the limit of detection for this system. This indicates that, even at the ppb level, Cr(VI) is removed from solution.

B.6. Spectra From Lake Water Study

Figure B.8 shows the spectra discussed in Section 3.3.5. One pyridine-functionalized monolith was exposed to a lake water sample spiked with 85 ppb Cr(VI) while the other was used as a control gel and exposed to an 85 ppb Cr(VI) solution prepared with DI water. The difference between the two measurements, corresponding to 0.002 absorbance units, gives an error of 5.88%.

B.7. Example of a Combined Calibration Plot

Using the two techniques, a calibration plot consisting of two curves, one for ppb-level concentrations using the diphenylcarbazide method and the other for ppm-level concentrations using the standard technique, can be established. Figure B.9 is an example of such a plot.
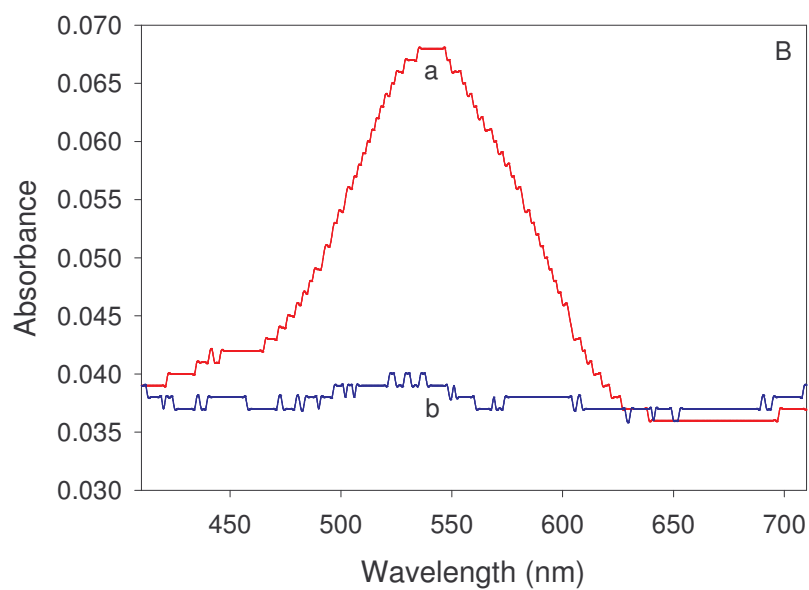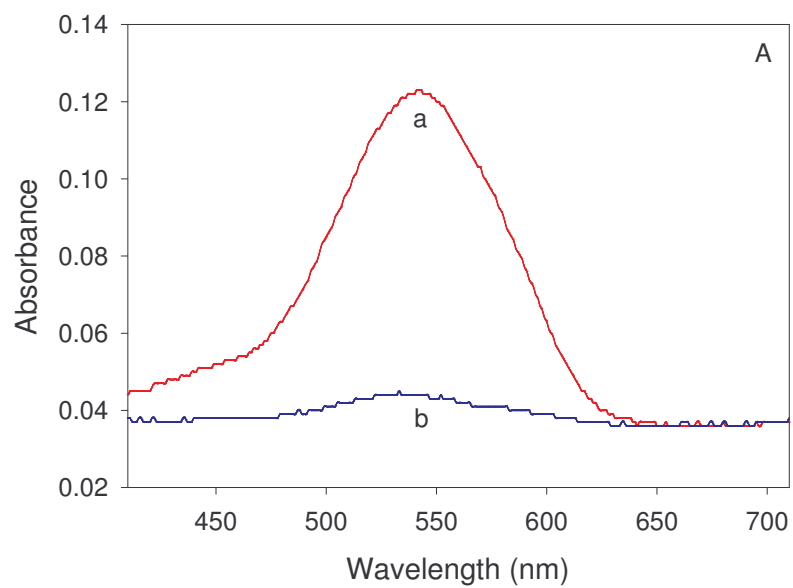
Figure B.7. (A) Spectra of a 156 ppb Cr(VI) solution before (a) and after (b) exposure to a pyridine-functionalized monolith. (B) Spectra of a 59 ppb Cr(VI) solution before (a) and after (b) exposure to a pyridine-functionalized monolith.
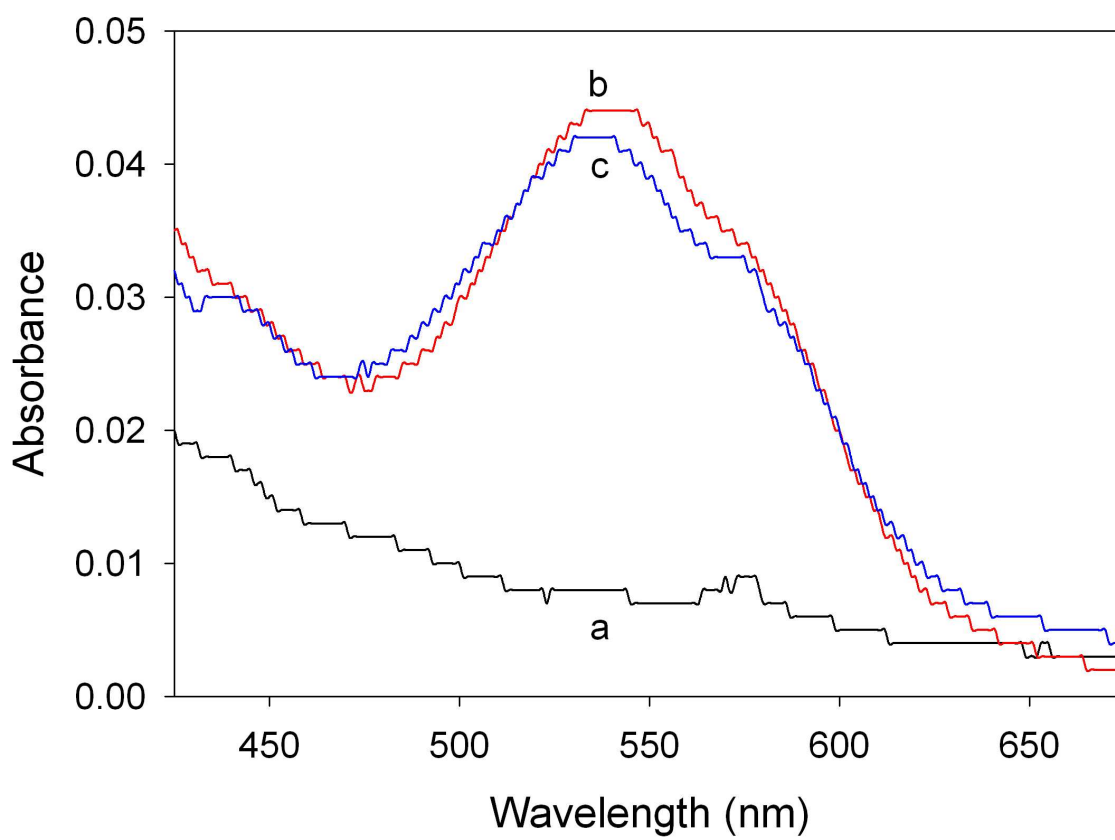
Figure B.8. Spectra of sol-gel monoliths exposed to: (a) 0 ppb Cr(VI); (b) a lake water sample spiked with 85 ppb Cr(VI); (c) a control solution of 85 ppb Cr(VI) prepared with DI water.
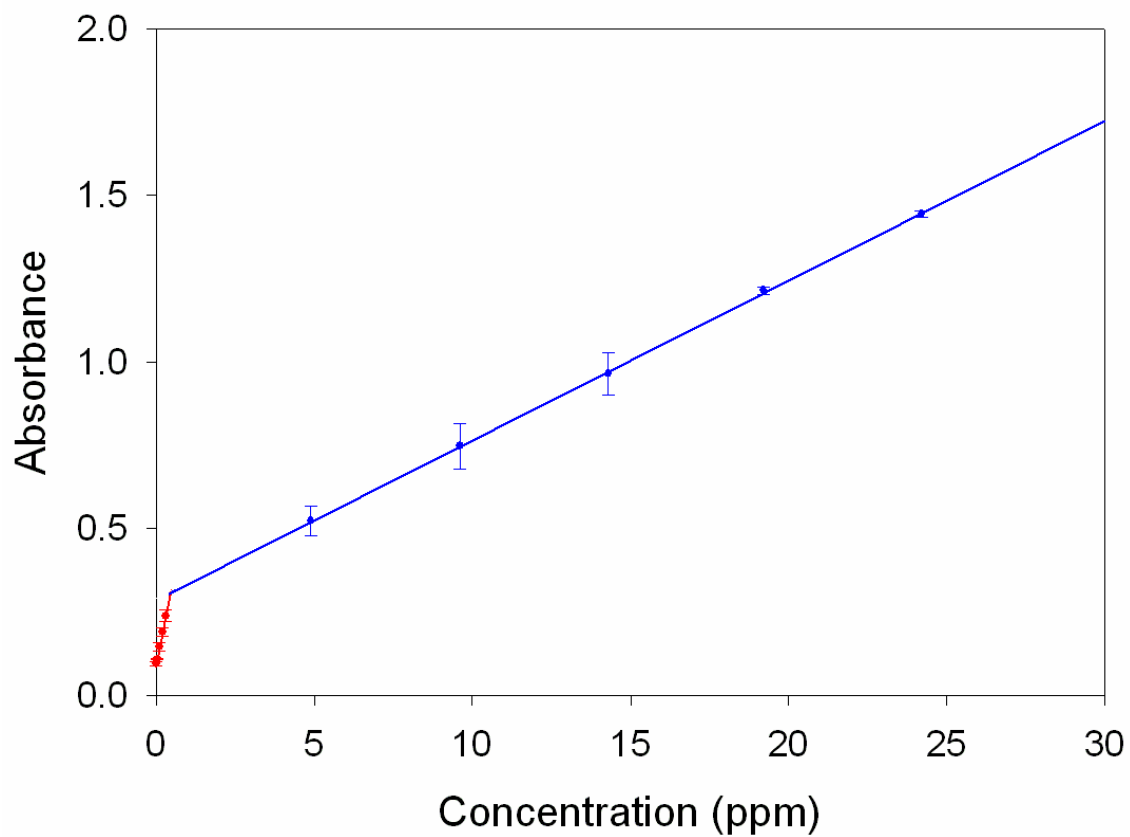
Figure B.9. A combination calibration curve for both ppb-level (red) and ppm-level (blue) Cr(VI) concentrations.

Appendix C

C.1. Calibration Plot Data for Figure 4.4

The data for the calibration plot in Figure 4.4, including the standard deviation, are given in Table C.1 below.

C.2. Reproducibility Measurements

Figure C.1 shows multiple depositions from a 0.0780 Pd^{2+} solution, as discussed in section 4.3.2.

C.3. N,N-dimethyl-4-nitrosoaniline Study

Figure C.2 shows the spectra obtained when Pd^{2+} complexes with N,N-dimethyl-4-nitrosoaniline. A Beer's law linear plot of the absorbance maxima at 496 nm for the standards yields the plot: *Absorbance = 0.02 + 78.8 C_{Pd} (R = 0.997)*. The concentration of this spiked Pd^{2+} sample determined by the N,N-dimethyl-4-nitrosoaniline method is 0.0985 mM.

Table C.1. Data for the calibration plot given in Figure 4.4.

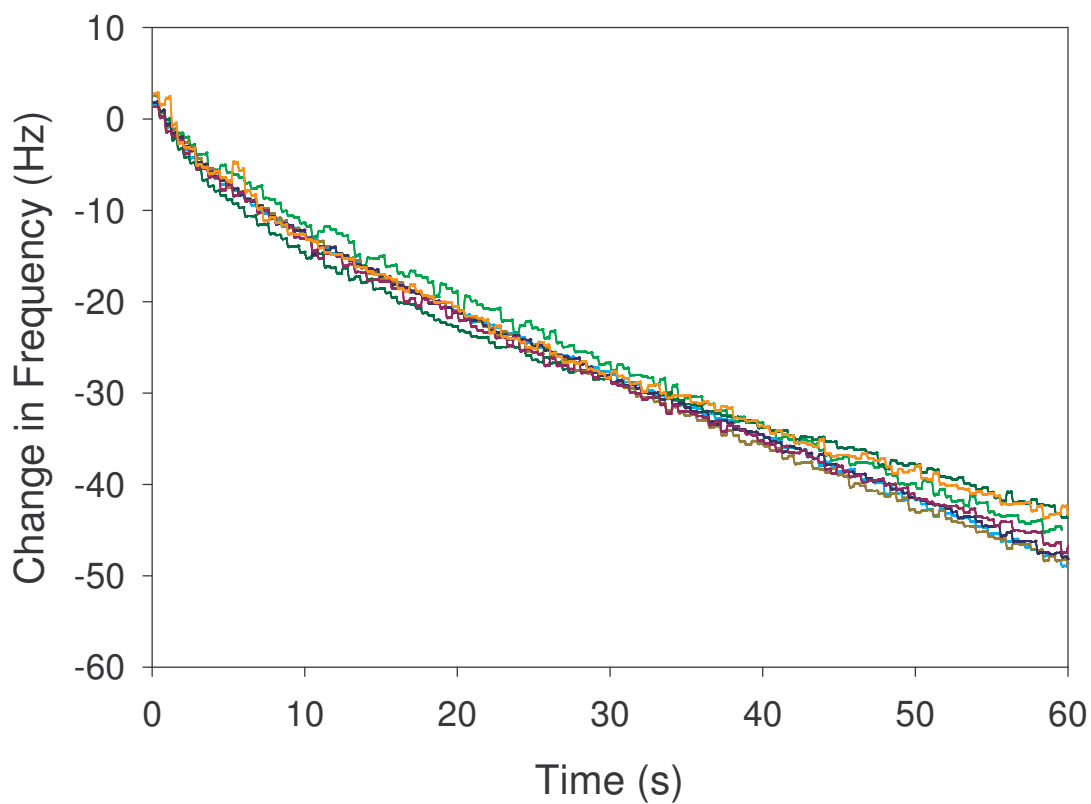| Concentration (mM)	Avg. Frequency Change (Hz)	Average Standard Deviation
0.0156	-19.98	1.7233
0.07802	-54.42	0.52333
0.156	-91.32	1.0333
0.2341	-129.58	0.643
0.3121	-181.8	0.58
0.3901	-206.53	1.55

Figure C.1. Seven deposition measurements carried out involving 0.0780 mM

Pd^{2+} solution. The relative standard deviation for the measurements is 4.15%.
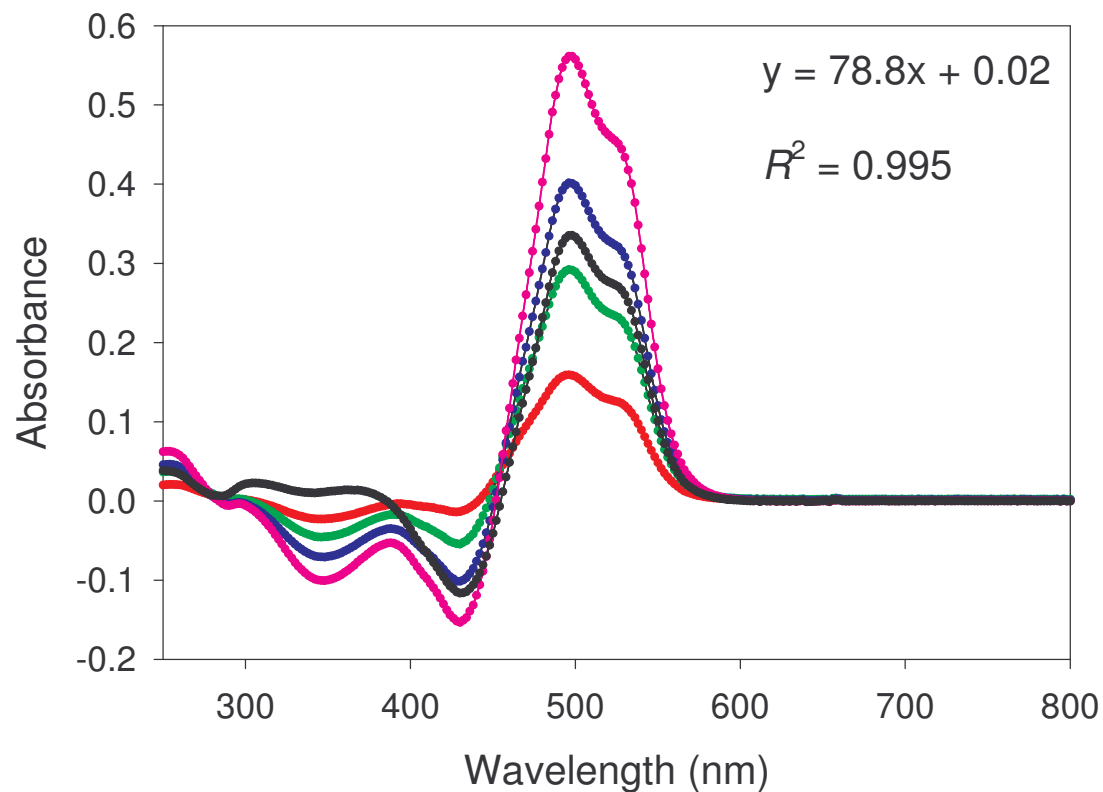
Figure C.2. UV-vis absorption spectra for Pd^{2+} determination using N,N-dimethyl-4-nitrosoaniline. The spectra were obtained from: (●) 0.00167 mM Pd^{2+}; (●) 0.00334 mM Pd^{2+}; (●) 0.00501 mM Pd^{2+}; (●) 0.00668 mM Pd^{2+}; (●) Pd^{2+} sample.

VITA

Nathan Allen Carrington was born on April 8, 1981 in Pittsburgh, PA. He and his family then moved to Charlotte, NC where he spent the majority of his childhood and adolescent years, graduating from Zebulon B. Vance High School in June of 1999. The following fall, Nathan enrolled at Erskine College in Due West, SC. He graduated with honors in the spring of 2003 with a major in chemistry and a minor in business.

Nathan began his graduate studies at the University of Tennessee, Knoxville in the summer of 2003. He joined Dr. Ziling (Ben) Xue's research group in the chemistry department where he studied sol-gel materials, sensor development, electrochemistry, and various other methods related to chemical analysis. Nathan's research resulted in the publication of ten manuscripts in various scientific journals by the time he received his Ph.D in the summer of 2007.